2013-07-24

Ultraviolet Degradation of H2S in Waste Gas: A Comprehensive First–Principles Model

Asili, Vahid

UNIVERSITY OF CALGARY

Ultraviolet Degradation of H_2S in Waste Gas:

A Comprehensive First – Principles Model

by

Vahid Asili

A THESIS

SUBMITTED TO THE FACULTY OF GRADUATE STUDIES

IN PARTIAL FULFILMENT OF THE REQUIREMENTS FOR THE

DEGREE OF MASTER OF SCIENCE

DEPARTMENT OF CHEMICAL AND PETROLEUM ENGINEERING

CALGARY, ALBERTA

JULY, 2013

ABSTRACT

In upstream oil and gas operations, a considerable amount of hydrogen sulfide (H_2S) is being emitted every year. Health issues associated with H_2S that might be very serious vary dependent on the length of exposure. Furthermore, the gas is highly corrosive, which is a concern in the industry. A promising technique that can be used to remove this air pollutant from waste gas is photolysis, which has been successfully used in wastewater treatment processes. However, to the best knowledge of the author, no inclusive model has yet been developed for H_2S gas phase photolysis. In this research study, a sophisticated simulation model was developed successfully to describe ultraviolet degradation of H_2S from waste gas. The photochemical reactor has been modeled with 19 chemical species and a total of 47 chemical and photochemical reactions which includes a light field model, a chemical model, a flow pattern model and a mass transfer model.

Simulation shows that the UV degradation of H_2S in waste gas is a highly efficient process. Simulations were run to investigate the process efficiency is a function of initial concentration, gas flow rate, and relative humidity. The model was also validated with some literature experimental data by applying the model to those experimental conditions, and comparing the results. Comparison of simulation results and the experimental data indicates that the model overestimates the removal efficiency to some extent; however, observing the same trends in two different cases of the effect of initial H_2S concentration and the effect of gas flow rate validates the model with sufficient accuracy to establish the feasibility of the process.

Previously, it was found experimentally that the main photolysis (or photocatalysis) product is SO_4^{2-} (or H_2SO_4) at very low concentration of H_2S. The model also agrees with this result, and furthermore predicts SO_2 as another photolysis product which is predominant at high

concentration of H_2S. Hence altogether, it can be concluded based on the model that the UV degradation technique is effective, and it decomposes H_2S to less harmful products which are also easier to be treated.

Moreover, the capability of the model for modeling the degradation of multiple pollutants at the same time was tested by model extension with NO_x reactions. According to the simulation results, adding H_2S in the NO_x photolysis system has positive effects on the degradation efficiency for both H_2S and NO_x. The extended model indicates that the proposed model can be used as the basis of a modular comprehensive model to predict removal efficiency for each species and moreover product analysis when more than one pollutant is present.

ACKNOWLEDGEMENTS

I would like to express my utter gratitude to my supervisor, Dr. Alex De Visscher, for his continuous support throughout the course of my program. His fruitful advices have always helped and encouraged me through different stages of work. He has remarkably been thoughtful of me and encouraged me during my research. In addition, I am thankful to my co-supervisor, Dr. Jalel Azaiez. His support is greatly acknowledged and appreciated.

I would like to express my sincere appreciation and love for my parents and siblings, whose support has always been with me in life. Moreover, I would like to specially thank my lovely wife, Behnoosh, for her patience, understanding, and invaluable source of unconditional love and support. Also, I thank my dear friends; Kamran, Ehsan and Hashem for being great sources of motivation and encouragement in many respects during the project and over the project in my day to day life.

I am also grateful to my official referees; Dr. Roberts, Dr. Mahinpey, and Dr. Mohamad for their participation in assessment of my thesis.

DEDICATION

To my beloved parents

whose love, guidance, and sacrifices have made me the person I am today.

To my lovely wife

for her constant love, understanding, support and encouragement.

Table of Contents

List of Tables

List of Figures

List of Symbols

Symbol	Definition
A	absorbance [cm^2]
	area [cm^2]
	Arrhenius factor [cm^3/molecules. s]
a	absorption coefficient [1/cm]
C	concentration [molecules/cm^3] or [ppm] or [g/m^3]
$\overline{C}$	average outlet concentration [molecules/cm^3] or [g/m^3]
d	pipe diameter [m]
d_h	hydraulic diameter [m]
D_i	diffusion coefficient [cm^2/s]
E	irradiance [$W.m^{-2}$]
	activation energy [J/mol]
E_p , E_0	fluence rate [photon/cm^2 .s]
$E_{p\lambda}$	energy per photon [photon/s. cm^2. nm]
F	broadening factor [-]
k_i	reaction rate constant [cm^3/molecules. s]
L	radiance [W/m^2. sr]
	length [cm]
l	optical pathlength [cm]
M	molecular weight [g/mol]
P	pressure [Pa] or [atm]
P_λ	transmitted spectral radiant power [W] [J/s. cm^2. nm]
P_λ^0	incident spectral radiant power [W] [J/s. cm^2. nm]
Q	volumetric flow rate [cm^3/s] or [L/min]
r	radial coordinate
R	universal ideal gas constant [J/mol. K]
r_i	reaction rate [molecules/cm^3. s]
S	area [m^2]
T	absolute temperature [K]

	internal transmittance at the defined wavelength [-]
U , u	mean velocity [cm/s]
V	local velocity of gas [cm/s]
z	length coordinate

Greek letters

α	absorption coefficient [cm^{-1}]
θ	angle [degree]
λ	wavelength [nm]
v	kinematic viscosity [cm^2/s]
σ	absorption cross-section [cm^2]
Σ_v	summation of diffusion volumes [cm^3]
τ	shear stress [Pa]
φ	quantum yield [molecules/photon]
Ω	solid angle [steradians]

CHAPTER 1 : INTRODUCTION

Hydrogen sulfide (H_2S) is known as one of the components that occur naturally in natural gas and crude oil. A noteworthy amount of trapped H_2S in oil and gas deposits is released during decomposition of high-sulfur organic matter in sedimentary rocks and about 90 percent of the sources emitting H_2S into the air are natural (EPA, 1993). According to the Canadian Association of Petroleum Producers status report (CAPP, 2005), more than 10,000 tonnes of H_2S is emitted annually by upstream oil and gas operations in Canada. Almost two-thirds of these emissions are from natural gas production and processing and the rest is from oil production. As a dangerous toxic gas, H_2S is extremely harmful; human health effects of exposure to hydrogen sulfide depend of the concentration of the gas and the length of exposure which can even cause death. Besides, the presence of H_2S may result in rapid and extensive corrosion necessitating expensive repairs for industries.

Introducing new H_2S elimination techniques can benefit the industry by achieving present and future emission standards. Since these emissions are coming from thousands of small sources, any technology to reduce these emissions needs to be cheap and easy to operate to accomplish wide use in industry. Using ultraviolet light to break molecules, *Photolysis*, is an effective technique that could fall into this category.

Wavelength has a key role in the application of UV photolysis. Typically photolysis is categorized as near UV, middle UV and far UV. For near UV the characteristic wavelength is 350 nm, which requires a catalyst to be effective. A common catalyst used is titanium dioxide or

TiO_2 (Demeestere et al., 2007). For middle UV, the typical wavelength is 254 nm and it can break ozone and some organic molecules, but not oxygen or water. The representative wavelength for far UV is 185 nm, which can break oxygen molecules and water vapor (Mahmoudkhani, 2012).

Mercury (Hg) lamps irradiate UV light at two wavelengths, 185 nm and 254 nm, in narrow bands (less than 1nm). For photolysis of H_2S, the 185 nm line is used to directly break water vapor molecules to produce OH radicals which are essentially important for H_2S photolysis. In addition, it can also break oxygen molecules to highly reactive oxygen radicals. Likewise, the 254 nm line can directly break reaction products and also breaks produced ozone into reactive species decomposing H_2S.

In this study, the possibility of using photolysis for the removal of H_2S from waste gas originating from the oil and gas industry (or any other usual sources) has been studied. In this regard, the most effective combination of processes and conditions has been explored. A sophisticated model has been developed for a photochemical reactor containing 47 chemical and photochemical reactions and 19 chemical species to eliminate H_2S is being emitted from waste gases. In order to limit the complexity of the model, it is assumed that the H_2S photolysis will happen in pure moist air. Simulation results were also compared with experimental data in representative conditions to validate the model.

Prior to this project, Mahmoudkhani (2012) developed a photochemical reaction model for benzene degradation from waste gas through photolysis. Later on, Atyabi (2013) extended that

model to photocatalytic degradation process for benzene. They both concluded photolysis can be feasible technique to eliminate pollutants form waste gas.

This thesis is organized as follows: a brief introduction and literature review are introduced initially. Then Chapter 3 deals with the model development of the system as the main part of the thesis. In this chapter all mathematical formulation, and reaction rates used in the model are clearly described. Moreover, the feasibility of adding other pollutants such as NO_x to the model is proposed. Afterwards the simulation results and model predictions with some model validation are presented. In the next chapter, the project economy and scale-up considerations are discussed. Lastly, the significant points of this study and some recommendations for future work are emphasized in the conclusion chapter.

CHAPTER 2 : LITERATURE REVIEW

2.1. Definition of Photolysis Terms

Photochemistry, a chemistry subfield, is the study of chemical reactions that conduct with the absorption of light (ultraviolet, visible or infrared) by atoms or molecules (Braslavsky, 2007).

Absorbance, *A* (λ), is logarithm to the base 10 (linear absorbance) of the incident spectral radiant power, P_λ^0, divided by the transmitted spectral radiant power, P_λ: (Braslavsky, 2007)

$$A(\lambda) = \log(\frac{P_\lambda^0}{P_\lambda}) = -\log T(\lambda) \qquad \text{Eq. 2.1}$$

T (λ) is the transmittance at the particular wavelength (λ).

Absorption coefficient, *a* (λ), for a molecule is absorbance divided by the optical path-length: (Braslavsky, 2007)

$$a(\lambda) = \frac{A(\lambda)}{l} = \frac{1}{l}\log(\frac{P_\lambda^0}{P_\lambda}) \qquad \text{Eq. 2.2a}$$

If the natural logarithm (logarithm to the base e) is used, the absorption coefficient is defined as:

$$\alpha(\lambda) = a(\lambda)\ln(10) = \frac{1}{l}\ln(\frac{P_\lambda^0}{P_\lambda}) \qquad \text{Eq. 2.2b}$$

Absorption cross-section, σ (λ), has been defined as linear napierian absorption coefficient, α (λ), divided by the number of existing molecules in a volume of the absorbing medium along the light radiation path typically with the unit of cm^2: (Braslavsky, 2007)

$$\sigma(\lambda) = \frac{\alpha(\lambda)}{C}$$ Eq. 2.3

Where C is the number concentration of molecular entities (number of molecules per volume); which is usually expressed as molecule/cm^3 specifically in photochemistry.

Quantum yield, $\varphi(\lambda)$, is the number of certain events occurring per photon absorbed by the system. The integral quantum yield is: (Braslavsky, 2007)

$$\varphi(\lambda) = \frac{\text{number of events}}{\text{number of photons absorbed}}$$ Eq. 2.4a

For a photochemical reaction, the quantum yield is defined as:

$$\varphi(\lambda) = \frac{\text{amount of reactant consumed or product formed}}{\text{amount of photons absorbed}}$$ Eq. 2.4b

Irradiance, E, (at a point of a surface) has been defined as radiant power, *P*, of all wavelengths coming toward the surface from all directions on a small element of surface (d*S*) divided by the area of the element: (Braslavsky, 2007)

$$E = \mathrm{d}P \big/ \mathrm{d}S$$ Eq. 2.5a

If the radiant power is constant over the surface area considered:

$$E = P \big/ S$$ Eq. 2.5b

There is an alternative definition which is integrating over the hemisphere observable from the certain point, of the expression $L \cdot \cos\theta \cdot \mathrm{d}\Omega$, where L is the radiance at the certain point in the

several directions of the incident elementary rays of solid angle Ω, and θ is the angle between any of the rays and the normal to the surface at the certain point: (Braslavsky, 2007)

$$E = \int_{2\pi} L \cdot \cos\theta \cdot \mathrm{d}\Omega \qquad \text{Eq. 2.5c}$$

Fluence rate, E_0, (radiant energy fluence rate) has been defined as total radiant power, P, occurrence from all directions onto a small sphere divided by the cross-sectional area of that sphere which has unit of $W.m^{-2}$ in SI: (Braslavsky, 2007)

$$E_0 = \mathrm{d}P \big/ \mathrm{d}S \qquad \text{Eq. 2.6a}$$

If the radiant power is constant over the area S:

$$E_0 = P \big/ S \qquad \text{Eq. 2.6b}$$

Also, there is an alternative definition for E_0:

$$E_0 = \int_{4\pi} L \cdot \mathrm{d}\Omega \qquad \text{Eq. 2.6c}$$

With Ω the solid angle of each light ray passing through the specific point on the surface and L the radiance of the beam at that point.

According to the above defined terms, an equivalent for photochemical reaction rate can be derived as follows.

Based on Eq. 2.2b,

$$l \cdot \alpha(\lambda) = \ln\left(\frac{P_\lambda^0}{P_\lambda}\right) \qquad \text{Eq. 2.7}$$

Consequently:

$$\exp(l \cdot \alpha(\lambda)) = \frac{P_\lambda^0}{P_\lambda} \qquad \text{Eq. 2.8a}$$

So:

$$P_\lambda = P_\lambda^0 \cdot \exp(-l \cdot \alpha(\lambda)) \qquad \text{Eq. 2.8b}$$

Differentiating of both sides of Eq. 2.8b results in:

$$\frac{\mathrm{d}P_\lambda}{\mathrm{d}l} = P_\lambda^0 \cdot (-\alpha(\lambda)) \cdot \exp(-l \cdot \alpha(\lambda)) \qquad \text{Eq. 2.9}$$

Replacing Eq. 2.8b to Eq. 2.9 yields:

$$\frac{\mathrm{d}P_\lambda}{\mathrm{d}l} = -\alpha(\lambda) \cdot P_\lambda \qquad \text{Eq. 2.10}$$

Now, taking a cylindrical element in the reactor and applying energy balance over that:

Figure 2-1: Energy balance on a cylindrical element

Energy rate consumed = Incoming energy rate – Outgoing energy rate Eq. 2.11

Energy consumed = $A \cdot P_\lambda - A \cdot (P_\lambda + \mathrm{d}P_\lambda)$ Eq. 2.12

In both Eq. 2.11 and Eq. 2.12 it is assumed that all light energy is dissipated as heat, or consumed in energy of reaction.

Dividing Eq. 2.12 by the volume of the element and substituting Eq. 2.10 results in:

$$\frac{\text{Energy consumed}}{\text{Volume}} = \frac{-A \cdot \mathrm{d}P_\lambda}{A \cdot \mathrm{d}l} = -\frac{\mathrm{d}P_\lambda}{\mathrm{d}l} = \alpha(\lambda) \cdot P_\lambda \qquad \text{Eq. 2.13}$$

Photon irradiance for each wavelength is defined as:

$$E_{P\lambda} = \frac{P_\lambda}{E_{photon,\lambda}} \qquad \text{Eq. 2.14}$$

Where P_λ is spectral radiant power, (J/s cm^2 nm) and $E_{photon,\lambda}$ is energy per photon in the wavelength of λ, (J/photon). So $E_{P\lambda}$ has a unit of (photon/s cm^2 nm) and integrating over wavelength λ removes nm from units.

Merging Eq. 2.13 and Eq. 2.14 yields to:

$$\frac{\text{Photons consumed}}{\text{Volume}} = \alpha(\lambda) \cdot \frac{P_\lambda}{E_{\text{photon}}} = \alpha(\lambda) \cdot E_P \qquad \text{Eq. 2.15}$$

Substituting absorption coefficient, α (λ), from Eq. 2.3 gives:

$$\frac{\text{Photons consumed}}{\text{Volume}} = C \cdot \sigma \cdot E_P \qquad \text{Eq. 2.16}$$

Based on the definition of quantum yield,

$$r = \varphi \cdot \frac{\text{Photons consumed}}{\text{Volume}} \qquad \text{Eq. 2.17}$$

Therefore:

$$r = \varphi \cdot C \cdot \sigma \cdot E_P \qquad \text{Eq. 2.18}$$

This can be written for each component *i* as:

$$-r_i = \varphi_i \cdot C_i \cdot \sigma_i \cdot E_P \qquad \text{Eq. 2.19}$$

If the value of quantum yields, the concentration of component *i*, the absorption cross section and the fluence rate are determined, the photochemical reaction rate of component *i* can be calculated.

2.2. Hydrogen Sulfide (H_2S)

2.2.1. General Properties:

Table 2-1 shows the general physical and chemical properties of H_2S according to the information adapted from the Canadian Centre for Occupational Health and Safety (CCOHS) website.

Table 2-1: Physical and Chemical Properties of H_2S

Appearance	Colorless gas
Odor	Faint rotten egg
Molar mass	34.08 g mol^{-1}
Melting point	-85.5 ^oC
Boiling point	-63.3 ^oC
Density	1.393 g L^{-1} (STP)
Solubility in Water	Slightly soluble (398 mg/100 g at 20 ^oC)
Solubility in Other Liquids	Soluble in ethanol, methanol, acetone, diethyl ether, glycerol, glycol ethers, N-methylpyrrolidone, propylene carbonate, gasoline, kerosene, carbon disulfide and crude oil
Vapor pressure	3553.3 kPa at 50 ^oC
Critical Temperature	100.4 ^oC
Critical Pressure	9008 kPa

Corrosivity to Metals	Corrosive to some metals (e.g. copper, brass, bronze, cast iron, carbon steel; under moisture)
Corrosivity to Non-Metals	- Dry H_2S can attack plastics, elastomers, chlorinated polyethylene, hard rubber, polyacrylate and silicone. - Wet H_2S can attack plastics, elastomers, natural rubber, soft rubber, styrene-butadiene (SBR), polyacrylate, polyurethane and silicone

2.2.2. Health effects of H_2S

Human health effects of exposure to hydrogen sulfide depend of the concentration of the gas and the length of exposure. According to Occupational Health and Safety (OHS) of Alberta, H_2S can be detected by smell at concentrations ranging from 0.01 to 0.3 ppm (OHS, 2010); however, some people can detect the gas by its odor at concentrations as low as 0.5 ppb by its rotten egg odor characteristics (Skrtic, 2006).

Based on information from OHS (2010) and Skrtic (2006), health effects associated with H_2S are listed in the Table 2-2.

Table 2-2: Health Effects Associated with H_2S

Concentration (ppm)	**Effects**
0.0057	Eye and nasal symptoms, coughs, headaches and/or migraines
0.003 – 0.02	Detectable odor
0.1 – 1	Abnormal balance with closed eyes, delayed verbal recall, impaired color discrimination, decreased grip strength
1 – 20	Offensive odor, tearing of the eyes or headaches with prolonged exposure

Concentration (ppm)	Effects
20 – 50	Nose, throat and lung irritation; digestive upset and loss of appetite; sense of smell starts to become fatigued; acute conjunctivitis may occur (pain, tearing and light sensitivity)
50 – 100	Eye irritation (painful conjunctivitis, sensitivity to light, tearing, clouding of vision) and serious eye injury (permanent scarring of the cornea)
100 – 200	Severe nose, throat and lung irritation; complete disappearance of ability to smell odor
200 – 500	Pulmonary edema (build-up of fluid in the lungs)
500 – 1000	Respiratory paralysis, irregular heartbeat, collapse and death without rescue
1000 – 2000	Immediate collapse with paralysis of respiration
5000	Immediate death

It is also worth mentioning that the symptoms of pulmonary edema (buildup of fluid in the lungs), such as chest pain or shortness of breath, can be delayed for up to 72 hours after exposure (OHS, 2010).

According to the specific legislation of Alberta Occupational Health and Safety, the 8-hour exposure limit is 10 ppm (OHS, 2010).

2.2.3. H_2S in Oil and Gas industries

Hydrogen sulfide (H_2S) is known as one of the components that occur naturally in natural gas and crude oil. A significant amount of H_2S is trapped in oil and gas deposits. High-sulfur kerogens[1] release H_2S during decomposition (EPA, 1993).

Based on EPA (1993) classification, natural gas is called *sour* when the amount of H_2S is greater than 5.7 milligrams per normal cubic meter (mg/Nm^3) or 0.25 grains per 100 standard cubic feet. Around one-fifth of natural gas produced in Alberta and British Columbia is sour (Bott, 2007). As a matter of fact, H_2S is the predominant impurity of natural gas (EPA, 1993). H_2S may be emitted from oil and gas operations, routinely or accidentally, during the extraction, storage, transport, or processing stage (Oilfield Glossary). Throughout extraction, hydrogen sulfide might be released into the atmosphere at pumps, wellheads, piping, oil storage tanks, separation devices, water storage vessels, and during flaring processes (EPA, 1993). As a waste gas treatment method, H_2S is flared routinely. As a safety measure, flares burn gases that cannot be sold, along with the gases at points in the system where operational problems may happen. Sulfur dioxide (SO_2) is the combustion product of hydrogen sulfide, but at incomplete combusting, H_2S may be emitted into the atmosphere (Bott, 2007).

2.2.4. H_2S Emission

Around 90 percent of the sources that release hydrogen sulfide into the air are natural (EPA, 1993). Although current regulations generally prevent the release of H_2S to the atmosphere, some emissions still occur due to fugitive equipment leaks (45.7 percent), emitting of waste gas

[1] Kerogen is a mixture of organic chemical compounds that make up a portion of the organic matter in sedimentary rocks (Oilfield Glossary).

streams containing low concentrations of H_2S (e.g., less than 10 ppm) (29.4 percent), incomplete combustion of fuels containing H_2S (24.2 percent), and evaporation losses during product storage and handling (0.7 percent). Approximately two-thirds of these emissions are from natural gas production and processing and the rest is from oil production (CAPP, 2005). Statistical data showed that more than 10,000 tons of H_2S is emitted by upstream oil and gas operations; in Alberta alone, more than 90% of this considerable amount has been produced. The following table shows the amount of H_2S release from oil and gas industries in Canada and Alberta as comparison. All these data were obtained in the year 2000.

Table 2-3: H_2S Emission from Oil and Gas Operations in 2000 (CAPP, 2005)

Sector	**H_2S emission (Tonnes/Year)**	
	Canada	Alberta
Fuel Combustion	35.4	19.9
Flaring	2,445.6	2,124.0
Oil and Gas Well Drilling	3.2	2.6
Natural Gas Production	3,515.4	3,276.6
Conventional Oil Production	1,328.5	1,269.7
Heavy Oil/Cold Bitumen Production	1,226.6	1,206.7
Thermal Operations	17.6	15.7
Natural Gas Processing	1,683.3	1,501.3
Total	**10,255.7**	**9,416.5**

Also, Environment Canada recently updated the amount of H_2S emissions from all sources to the environment through NPRI (National Pollutant Release Inventory) for the year 2010, which was revised in June 2012. According to the NPRI (2012) the emission of H_2S has decreased since the past decade, but still a significant amount of H_2S is emitted every year. Likewise in Alberta the

H_2S emissions decrease, nevertheless Alberta is the largest contributor H_2S emissions to the environment across Canada. Data in the following table indicate H_2S emissions from all reported sources.

Table 2-4: H_2S Emission from All Sources in 2010 (NPRI, 2012)

Release	**H_2S emission (Tonnes/Year)**	
	Canada	Alberta
Air Emission[§]	2,707	1,538
Water Release [§§]	92	16
Disposal [§§§]	613,188	252,661
Total	**615,987**	**254,212**

[§] includes all direct emissions to air such as *Stack, Fugitive, Storage/Leak, etc*.

[§§] includes direct releases such as *Direct discharge, Spill and Leaks* to water resources.

[§§§] includes *Onsite disposal* (such as *Landfill, Underground injection, Tailing, Waste rock, etc.*) and *Offsite disposal* (such as *Landfill, Underground injection, Storage, Waste rock, etc.*) to Air or Water resources.

2.2.5. Corrosive Effects

The presence of H_2S may cause rapid and extensive damage to metals used in industry. H_2S corrosion necessitates costly repairs for industries. As an example, for wastewater treatment plants, sewers fail after 10 to 20 years because of H_2S corrosion while their design is based on 50 to 100 years. Also, electrical and mechanical equipment with 20 years of life, have to be replaced after 5 years due to corrosion of H_2S (EPA, 1991).

H_2S corrosion can happen by two main mechanisms. First, acid attack resulting from biological conversion of H_2S to sulfuric acid in the presence of moisture; Second, direct chemical reaction

of H_2S with metals such as silver, iron and copper (EPA, 1991). The first mechanism generally happens in wastewater treatment plants (EPA, 1991) and the second one can occur everywhere especially in oil and gas production (ASM, 1994).

In oil and gas production, two types of damage can happen in systems containing H_2S; Normal weight loss corrosion and Hydrogen-induced damage. Iron sulfide (which is called *Black Scale*) on a steel surface is indicative of H_2S attack. The typical reaction of H_2S with iron or steel is: (Allen and Roberts, 2000)

$$Fe_{(s)} + H_2S \rightarrow FeS + H_2$$

In the H_2S environment many types of iron sulfide may form like amorphous ferrous sulfide, mackinawite[1], cubic ferrous sulfide, smythite[2], greigte[3], pyrrhotite[4], troilite[5] and pyrite, among which mackinawite is considered to form initially on the steel surface (Koteeswaran, 2010). The poorly known mechanism of H_2S corrosion makes it difficult to quantify the kinetics of iron dissolution in aqueous solutions containing H_2S based on the formation of a mackinawite film; also, the understanding of the effect of H_2S corrosion is still limited because the nature of the interaction with carbon steel is complicated (Obuka et al. 2012).

2.3. Waste Water Photolysis

There are several studies on wastewater photolysis, which has been successfully used in wastewater treatment. In any UV process, the energy of the photon emitted should be higher

[1] An iron nickel sulfide mineral with formula $(Fe,Ni)_{1+x}S$ (where x = 0 to 0.11)
[2] An iron sulfide mineral with the formula of $Fe_{(3+x)}S_4$ (x = 0 to 0.3)
[3] Greigite is an iron sulfide mineral with formula Fe_3S_4 (Iron(II,III) sulfide)
[4] An unusual iron sulfide mineral with a variable iron content: $Fe_{(1-x)}S$ (x = 0 to 0.2)
[5] A rare iron sulfide mineral with the formula of $Fe_{(1-x)}S$ (x = 0 to 0.2)

than the bond dissociation energy (Luo, 2007). UV radiation alone is not sufficient to degrade recalcitrant compounds such as polymers or VOC's in water. Hence, it has to be combined with auxiliary oxidants in order to produce more powerful oxidants like hydroxyl (·OH) radicals (Barrera, 2011). According to EPA (1998) one mole of photons emitted at 254 nm release 471 kJ, while one mole of photons, at 185 nm contains 647 kJ based on the Planck's relation which is defined as $E = h \cdot \frac{c}{\lambda}$, where E (J) is the energy of one photon at the given λ (m), c is the universal constant for light speed in vacuum with the value of 299,792,458 m/s and h is Planck's constant with the value of 6.626×10^{-34} (J s). Oppenländer (2003) clarified that the water molecule starts absorbing radiation from 498 kJ and higher which corresponds to 240 nm. However, hydroxyl (·OH) and hydrogen (H·) radicals are mainly generated at wavelength of 190 nm or shorter (EPA, 1998) as primary species because the light absorption is low at higher wavelengths. These species are necessary for wastewater UV process reactions.

Yue (1993) investigated a kinetic model for reactor design of a water purification system consisting of UV/H_2O_2 and UV/O_3 to eliminate low levels of organics in water production plants. He theoretically derived the concentration equations, kinetics reactions and used energy and mass balances to conclude that the design of photoreactor for water purification requires several considerations such as reactor geometry, selection of UV lamp, proper residence time, size, reactants rate constant and eventually required energy. Pereira et al. (2007) studied kinetics and modeling of pharmaceutical compounds in laboratory grade and surface water. Their model includes direct and indirect photolysis which can predict the experimental UV waste water treatment very well but somehow underestimates the effect of UV/H_2O_2. Sanches et al. (2011)

studied direct photolysis of polycyclic aromatic hydrocarbons in drinking water sources listed as priority pollutants by the European Water Framework Directive and EPA. They concluded that pollutant species were efficiently degraded since 83-93% efficiency was observed for groundwater samples they studied; however, there might be formation of photolysis by-products which are dependent on water resources.

Sellami et al. (2003) modeled a radiation field inside a photochemical reactor designed for waste water disinfection; they considered the effect of light intensity and wavelength, and also the effect of annular space on the degradation process. Then they validated their model which was based on independent reaction rates with experiments in the same conditions showing maximum 10 % difference between their model and experimental data. Kralik et al. (2010) developed a detailed mathematical model for degradation of chlorinated hydrocarbon pollutants in water by the UV/H_2O_2 process; they also tested their model with some experimental design methods and found that their model can be accurate and useful for maximizing the efficiency of the wastewater treatment processes.

It is worth mentioning that since H_2S has very low solubility in water, no study was found for photolysis in aqueous phase.

2.4. Waste gas photolysis

2.4.1. Background

As a promising technique, photolysis has been used widely in industry for removing several pollutants in aqueous phase, but in waste gas treatment this method is not used as much; specifically only a few papers proposed simulation models for waste gas photolysis.

Kinetics of gas phase photo-dissociation of VOC's has been evaluated by Wang and Ray (2000) using a low pressure mercury UV lamp. They achieved almost complete degradation for all VOCs after 20 minutes and a light intensity of 80 W/m^2 in their work. Based on their work, photolysis at 185 nm and 254 nm, followed by oxidation, is a dominant way for degradation. It has been confirmed that coupling UV photolysis and biofiltration effectively degraded aromatic air pollutants (Mohseni and Zhao, 2006). Zhang and Anderson (2013) examined the destruction of chlorobenzene (C_6H_5Cl) as a chlorinated aromatic compound by UV photolysis with and without the presence of O_3 for potential use in air emissions treatment. Their model estimated the quantum yield and photonic efficiency for the photochemical decomposition of chlorobenzene (C_6H_5Cl) in air. They found out the photo-reactor is more efficient at high concentrations of the target organic pollutant. They also concluded that ozone increased the degradation efficiency as well as humidity and oxygen; however, ozone decreased quantum yield of chlorobenzene since this value is strongly dependent on chain reactions caused by other chemicals present in the reactor.

A reactor model has been developed for CCl_4 and $CHCl_3$ photolysis in gas phase by Chen et al. (2004). Their model consists of a kinetic model of UV photo-oxidation of chloroform and carbon tetrachloride using a low pressure mercury UV lamp. They included 14 reactions in their model in order to predict the outlet concentration of the pollutant, and they were able to predict a simple equation for the outlet concentration when the initial concentration of VOCs was low. They concluded, based on a good agreement between the simulated and experimental data, that a sound basis for the design of large-scale reactors had been established. However, they were aware that their approach would be difficult to accomplish for complex photochemical processes

involving multiple reactions. Later on, Mahmoudkhani (2012) developed a very complete model on BTEX photochemical degradation including 59 reactions and 47 species. Her model included all independent reaction rates, photochemical reaction data, and also covered model validation for benzene degradation in waste gas. Her model predicted that the ozone premixing can greatly increase the efficiency of UV degradation of BTEX removal from waste gas. In addition, it was confirmed that a combination of condensation, ozone pre-mixing and UV photolysis is economically feasible.

The feasibility of the use of short-wavelength UV (254 + 185 nm) coupled with a TiO_2 catalyst for photodegradation of toluene in gas phase was evaluated by Jeong et al. (2004). They concluded that using TiO_2 under 185+254 nm UV irritation considerably raised the photo-degradation of VOCs (such as toluene) compared with using UV only. They also tested three light sources and suggested that applying 254 + 185 nm UV light can be useful to remove a wide range of VOCs in polluted air, particularly with high reactivity with OH radical or ozone. On the contrary, Shen and Ku (2002) verified that the degradation efficiency of trichloroethane reduced by the UV/TiO_2 process in the presence of ozone compared with UV/TiO_2 alone. Recently, Atyabi (2013) developed a comprehensive model for BTEX photo-dissociation from waste gas based on the model of Mahmoudkhani (2012). She also included both photolysis and photo-catalysis in her model, and collected experimental data for toluene, benzene and xylene proving photolysis as a feasible method. In her work, based on the low value predicted for the quantum yield of the catalytic process, it was concluded that photolysis is a feasible alternative to photocatalysis. Although her model overestimated the degradation efficiency to some extent, her experimental results confirmed that adding ozone increased the process efficiency for BTEX

removal form waste gas. Moreover, it was predicted coupling ozone premixing and condensation pretreatment would cause the lowest energy consumption for UV photolysis.

2.4.2. H_2S Removal

There are only a few research published papers on H_2S removal from waste gas and specifically for photolysis. As a principle of sulfur compound photolysis there are some strong experimental supports from some kinetics studies such as CH_3SH (Methanethiol) and H_2S at 243.1 nm in the near-UV black light region (330–400 nm) by Rogers et al. (1996), photodissociation of H_2S at 157.6 nm with laser light (193–252 nm) by Liu et al. (1999) and photodissociation of H_2S at 242 and 248 nm in a deuterium light beam (190–400 nm) by Koda et al. (2001). Earlier, Wine et al. (1981) employed photolysis to study the kinetics of hydroxyl (·OH) reaction with H_2S at 185 nm and also proposed a rate constant for this reaction as a function of temperature. Later on, Weiner et al. (1989) examined photolysis of H_2S at 193, 222 and 248 nm. They successfully measured the transition state energy for each excitation level at all three wavelengths.

Xia et al. (2008) studied comprehensively the photolysis of low concentration H_2S with a microwave discharge electrodeless lamp (MDEL) like microwave UV mercury lamp (emitting light at 185 and 253.7 nm). Their study was showing a highly efficient process for H_2S removal from waste gas with UV light precisely for low H_2S inlet concentration. Their work verified that by increasing the initial inlet concentration of H_2S and also increasing the gas flow rate the process efficiency would decrease dramatically; beside, increasing the amount of light intensity could increase the removal efficiency. Their experiments confirmed that the product of H_2S photolysis will be SO_4^{2-} at very low concentration of H_2S. They also repeated the experiments with a $Kr+I_2$ (Krypton Iodine) lamp and the same trend of efficiency was observed.

There are also some research studies on a photocatalytic approach for H_2S removal from waste gas. Canela et al. (1998) conducted TiO_2/UV-VIS for H_2S destruction in the gas phase. Their experimental results showed high efficiency of H_2S destruction (99 % efficiency for 33 to 855 ppm_v of H_2S inlet concentration). The product observed on the surface of the catalyst and also in the reactor outlet was confirmed to be the sulfate ion. Kataoka et al. (2005) used a batch reactor coated with TiO_2 and a medium pressure Hg UV lamp with a light intensity of 6 mW/cm^2. Although they injected only H_2S (with N_2 1% in volume) and observed the formation of SO_2 at the beginning of the reaction, they concluded that SO_4^{2-} is a predominant product accumulated on the surface of the catalyst.

Li et al. (2012) compared ozone photolytic and photocatalytic degradation of H_2S with a continuous flow mode. They studied several effects such as UV wavelength, oxygen content, relative humidity (RH) etc. They emphasized that irritation at 185 nm gave the highest degradation efficiency compared with 254 nm. Irradiation at 365 nm (black light) had the lowest efficiency at these conditions. They also stated at 21% oxygen content (which is very close to the ambient air) the highest process efficiency was observed; meanwhile, the removal efficiency with using TiO_2 catalyst was slightly higher than UV alone. Moreover, increasing relative humidity (RH) increased the process efficiency significantly, and 80% RH was the optimum humidity for their experimental data.

Recently, Huang et al. (2012) introduced a new method for H_2S removal from a gas stream using a combined plasma photolysis technique at atmospheric pressure. In their research, they used a reactor which works based on a Combination of a Dielectric Barrier Discharge (CDBD) plasma

with photolysis. Their results indicated the degradation efficiency in this case is considerably higher compared with UV alone.

CHAPTER 3 : MODEL DEVELOPMENT

A sophisticated mathematical model is proposed for ultraviolet degradation of H_2S in waste gas. The developed model contains four major parts which contribute to the simulation, such as the velocity profile, a chemical kinetics model, material balances, and a UV radiation field. In order to develop a comprehensive model for the first time simulating UV degradation of H_2S in gas phase, all these four modeling parts should be considered.

3.1. Flow Pattern Model (Velocity Profile)

The UV reactor for modeling is assumed tubular (based on the actual reactor). The UV lamp is assumed in the reactor and along with the reactor axis. Therefore, it can be assumed the waste gas flows between two nested concentric pipes.

Knowing the mean flow velocity (U), kinematic viscosity (ν), and pipe diameter (d), Reynold's number can be obtained by: (White, 2003)

$$Re = \frac{U \cdot d}{\nu} \qquad \text{Eq. 3.1}$$

In case of pipes that do not have a circular cross-section, the hydraulic diameter (d_h) is used, defined as: (Bansal, 2005)

$$d_h = \frac{4A}{P} = \frac{4 \times \text{area}}{\text{wetted perimeter}} \qquad \text{Eq. 3.2}$$

For the assumed tubular reactor with R_0 = 1.25 cm (outer lamp diameter) and R_1 = 2.1 cm (inner reactor wall diameter), d_h is calculated 1.7 cm. With variable volumetric flow rate 500 – 5000

cm^3/min (based on assumed flow rate in the model) and assuming pure air with kinematic viscosity, v = 0.15 cm^2/s (Bansal, 2005), the Reynolds number is calculated to be 10.5 – 105 respectively. Since the Reynolds number below 2100 is known as laminar flow (White, 2003), a laminar flow velocity profile is a sensible assumption for this model.

With a force balance and Newton's viscosity law, the laminar velocity profile in an annular space can be derived. Since the gas mixture contains over 99 % air and water vapor, the rest being gas phase pollutant, Newtonian fluid is assumed.

In order to derive an equation for the velocity profile, a force balance was applied on a thin cylindrical element (Figure 3-1).

Force = (Pressure or stress) × Area Eq. 3.3a

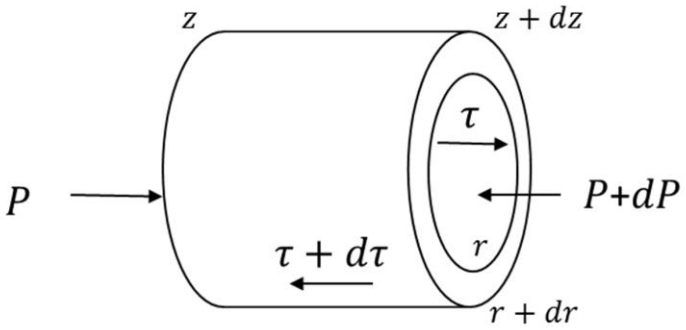

Figure 3-1: Force balance on an annular element

Writing the force balance:

Pressure + Shear stress forward = Pressure + Shear stress backward Eq. 3.3b

The variables in Figure 3-1 are P (pressure), τ (shear stress), z (the length coordinate), and r (the radial coordinate). Based on Bird et al. (2002) and Mahmoudkhani (2012)'s model, solving the second-order differential equation resulting from the force balance equation an annular space by

integration between the radius of the lamp (R_0) and the inside radius of the reactor (R_1) yields to a general formulation for that specific annular space. So, the local gas velocity for any r for an annular space was derived as: (Bird et al. (2002) and Mahmoudkhani (2012))

$$V = \frac{\frac{2U(R_1^2 - R_0^2)}{\ln \frac{R_1}{R_0}} \ln \frac{r}{R_0} - 2U(r^2 - R_0^2)}{R_1^2 + R_0^2 - \frac{R_1^2 - R_0^2}{\ln \frac{R_1}{R_0}}} \qquad \text{Eq. 3.4}$$

Where U is the mean flow velocity defined as the volumetric flow rate divided by the cross-sectional area and r is the radial coordinate, which has a value between R_0 and R_1 in the annular space.

This equation used in the model to calculate local gas velocity. Mahmoudkhani (2012) compared model predictions with the plug flow velocity profile, $V=U$, and the laminar flow velocity profile and the differences were negligible. While choosing velocity is not critical in the calculation, hereafter all of modeling calculations and simulations are consistent to the laminar velocity profile.

The model assumes that laminar flow is established immediately at the reactor entrance. However, because the effect of flow regime on the model results is small, the model is not sensitive to this assumption. Furthermore, calculating the Hydrodynamic Entrance Length (L_{hy}) with the formulation of $\frac{L_{hy}}{d_h} = 0.59 + 0.056Re$ (Atkinson et al., 1969) and knowing the value of

hydraulic diameter (d_h = 1.7 cm) and maximum Reynolds number at worst case scenario (Re = 105), yields to L_{hy} = 11.0 cm; which is less than 20% of the total reactor length.

3.2. Material Balance

As an important consideration, the diffusivity of the H_2S-Air mixture should be calculated. For this purpose, the Fuller et al. (1969) empirical formulation is used to calculate the diffusion coefficient:

$$D_{AB} = \frac{0.00143\ T^{1.75}}{PM_{AB}^{1/2}[(\sum_V)_A^{1/3} + (\sum_V)_B^{1/3}]^2} \qquad \text{Eq. 3.5a}$$

Where D_{AB} is in cm^2/s, P is in atm, T is in kelvin, Σ_v is summation of aromatic and structural diffusion volumes. Also, M_{AB} is defined based on each molecular weight:

$$M_{AB} = \frac{2}{(1/M_A) + (1/M_B)} \qquad \text{Eq. 3.5b}$$

Using some of Seader et al. (2010)'s information, $(\Sigma_v)_{Air}$ = 19.7 cm^3, $(\Sigma_v)_{H2S}$ = 27.52 cm^3, M_{H2S} = 34.08 g/mol, M_{Air} = 28.97 g/mol. Substituting these values yields an equation for diffusion coefficient of H_2S-Air mixture parametrically related to P and T:

$$D_{H_2S-Air} = 0.7914\frac{T^{1.75}}{P(Pa)} \qquad \text{Eq. 3.6}$$

Now taking T = 310 K and P = 89000 Pa, yields D = 0.204 cm^2/s.

Furthermore, the Peclet number, Pe_L, which is flow velocity divided by diffusion velocity, has a determining role in the mass transfer mechanism: (Cussler, 2009)

$$Pe_L = \frac{U \cdot L}{D} \qquad \text{Eq. 3.7}$$

When the Peclet number is greater than 40, the dominant mass transfer mechanism in the flow direction is advection (Froment and Bischoff, 1993).

In the assumed system, L is the length of the reactor; U is the mean gas velocity which is volumetric flow rate divided by cross-sectional area, $U = \frac{Q}{\pi(R_1^2 - R_0^2)}$, and D is diffusivity. Now applying Q = 500 cm^3/min, L = 56 cm, and D = 0.2 cm^2/s yields Pe_L = 260.82. So, as an assumption, advection is the dominant mass transfer mechanism in the direction of the flow in this study. On the contrary, flow regime was assumed laminar previously; hence, diffusion is the dominant mass transfer mechanism in radial direction. Therefore, in the proposed model, radial diffusion of all species is included. Species are produced or consumed through reactions occurring in the element.

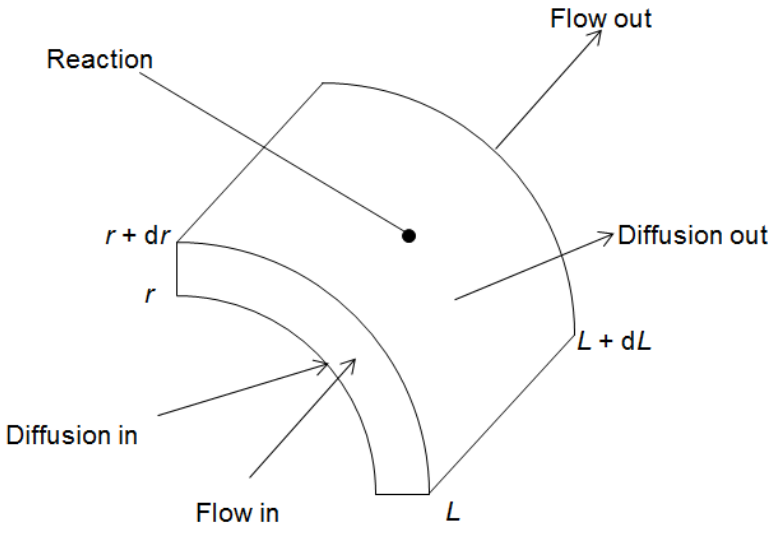

Figure 3-2: Material balance on an annular element

Figure 3-2 shows a material balance on an annular element. The terms on the figure are defined as follow:

$$Flow\ in = C_i \cdot V \cdot 2\pi r \cdot \mathrm{d}r \qquad \text{Eq. 3.8a}$$

$$Flow\ out = (C_i + \frac{\partial C_i}{\partial L}\mathrm{d}L) \cdot V \cdot 2\pi r \cdot \mathrm{d}r \qquad \text{Eq. 3.8b}$$

$$Diffusion\ in = -D_i \left.\frac{\partial C_i}{\partial r}\right|_r \cdot 2\pi r \cdot \mathrm{d}L \qquad \text{Eq. 3.8c}$$

$$Diffusion\ out = -D_i \left.\frac{\partial C_i}{\partial r}\right|_{r+\mathrm{d}r} \cdot 2\pi(r + \mathrm{d}r) \cdot \mathrm{d}L \qquad \text{Eq. 3.8d}$$

$$reaction = r_i \cdot 2\pi r \cdot \mathrm{d}r \cdot \mathrm{d}L \qquad \text{Eq. 3.8e}$$

Where:

C_i is the concentration of compound *i* (molecules/cm^3),

D_i is the molecular diffusivity of compound *i* (cm^2/s),

r_i is the reaction rate of *i* (molecules/cm^3 s) and

V is the local gas velocity (cm/s).

Considering that there are no mechanical dispersion effects, since the flow is laminar, the material balance equation can be written as:

Flow in + Diffusion in +Reaction = Flow out + Diffusion out Eq. 3.9

Substituting all the above terms to the material balance equation, and dividing all of the terms by $2\pi r \cdot \mathrm{d}r \cdot \mathrm{d}L$ leads to:

$$r_i = V \cdot \frac{\partial C_i}{\partial L} - \frac{D_i}{\mathrm{d}r}\left(\left.\frac{\partial C_i}{\partial r}\right|_{r+\mathrm{d}r} - \left.\frac{\partial C_i}{\partial r}\right|_r\right) - \frac{D_i}{r} \cdot \left.\frac{\partial C_i}{\partial r}\right|_{r+\mathrm{d}r} \qquad \text{Eq. 3.10}$$

At the limit to $\mathrm{d}r \rightarrow 0$, the terms between brackets divided by d*r* form a second partial derivative. All in all:

$$V \cdot \frac{\partial C_i}{\partial L} = D_i \cdot \frac{\partial^2 C_i}{\partial r^2} + \frac{D_i}{r} \cdot \frac{\partial C_i}{\partial r} + r_i \qquad \text{Eq. 3.11}$$

There is one material balance partial differential equation per compound. In principle, a different value of D_i should be used for all chemical species. To simplify, the H_2S-Air gas mixture diffusivity equation (Eq. 3.6) was used for all species. Simulation results indicate that the model is not sensitive to the value of diffusivity.

The boundary condition of the concentration at the reactor inlet is assumed to be a known concentration of the feed stream. For the radial derivatives, boundary conditions at $r = R_0$ (UV lamp outer radius) and $r = R_1$ (reactor wall inner radius) are needed. The no-flux condition is assumed, which means:

$$\frac{\partial C_i}{\partial r} = 0 \qquad @ \qquad r = R_0 \quad \text{and} \quad r = R_1 \qquad \text{Eq. 3.12}$$

3.3. Radiation Field

The proposed model approximately assumes that the lamp is a line source of light that sends out light rays perpendicular to the lamp. Because it considers only the light with the shortest path length, it would underestimate the real light absorption. In practice, a more complicated condition will exist, similar to the below figure.

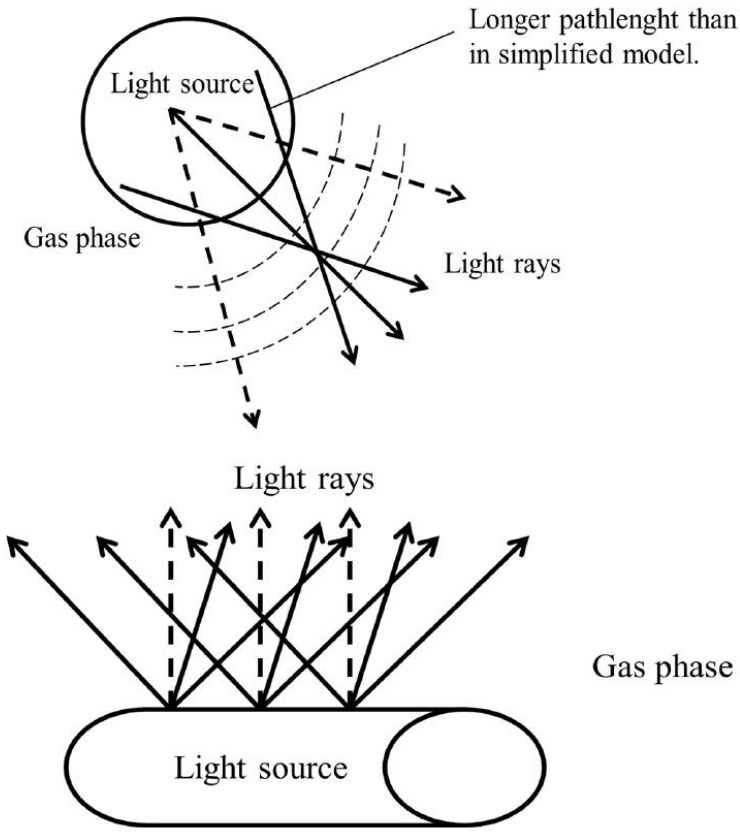

Figure 3-3: Light rays in the simplified model (dashed lines) and in the detailed model (solid lines)

Due to the reflection level of the light back and forth between the lamp and the outside cylinder, it is probable that path length does not play a significant role in the system, which means that the approximate model and the detailed model are in close agreement (Mahmoudkhani, 2012). In contrast, photolysis in the aqueous phase, where absorption is much stronger, and the reaction is more limited to a region near by the lamp (Atyabi, 2013), the path length becomes more important.

Mahmoudkhani (2012) developed two versions of light field model. The first version made an initial estimate of the light intensity in the reactor, while the second one calculated light rays moving at different angles and within a plane that contains the lamp axis, in an iterative

procedure in cylindrical symmetry. The summation of the irradiance of the outgoing light and the reflected light is presumed to be equal to the fluence rate in the simplified model. Mahmoudkhani (2012) found that the predictions of the simplified model differed by only 2% from the iterative model. However, the iterative model had a run time about 20 times longer (up to an hour for each single run) than the simplified model. For these reasons, the first approximation version (first guess initial estimate) has been selected for this study.

In order to calculate the values of the light intensity at each location in the reactor, an annular element of the reactor is considered for the photon balance, as shown in Figure 3-4.

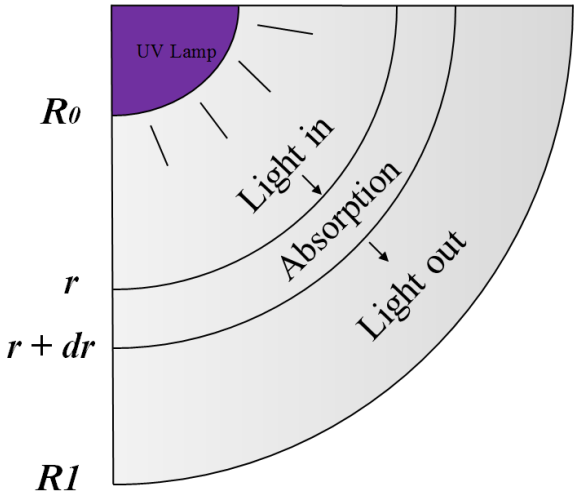

Figure 3-4: Photon balance

The terms of Figure 3-4 are defined as follow:

$$Light\,in = E_p \cdot 2\pi r \cdot L \qquad \text{Eq. 3.13a}$$

$$Light\,out = (E_p + \mathrm{d}E_p) \cdot 2\pi \cdot (r + \mathrm{d}r) \cdot L \qquad \text{Eq. 3.13b}$$

$$Absorption = \sum_i \alpha_i E_p \cdot 2\pi r \mathrm{d}r \cdot L \qquad \text{Eq. 3.13c}$$

Where the extinction coefficient α_i is given by:

$$\alpha_i = C_i\,\sigma_i \qquad \text{Eq. 3.13d}$$

Here:

E_p is irradiance (photons/cm^2 s),

C_i is the concentration of compound i (molecules/cm^3) and

σ_i is the absorption cross-section of compound i (cm^2)

The general photon balance equation is:

Light out = Light in – Absorption Eq. 3.14

In the above equation, the light scattering is neglected, since it has a value of 5.1×10^{-27} cm^2 at 532 nm, and its wavelength dependence is proportional to λ^{-4} (Sneep and Ubachs, 2005). By a quick calculation, the scattering wavelength is found to be at least 5 orders of magnitude lower than the absorption cross-section for 185 nm in the system studied.

Now, substituting all the above terms to the photon balance (Eq. 3.14) equation yields:

$$(E_p + \mathrm{d}E_p)\cdot 2\pi.(r+\mathrm{d}r)\cdot L = E_p\cdot 2\pi r\cdot L - \sum_i \alpha_i E_p\cdot 2\pi r\mathrm{d}r\cdot L \qquad \text{Eq. 3.15a}$$

Where the summation is over all chemical species i. Expanding the terms between brackets, and dividing by $2\pi L$ leads to:

$$E_p\cdot r + \mathrm{d}E_p\cdot r + E_p\cdot \mathrm{d}r + \mathrm{d}E_p\cdot \mathrm{d}r = E_p\cdot r - \sum_i \alpha_i\cdot E_p\cdot r\cdot \mathrm{d}r \qquad \text{Eq. 3.15b}$$

In Eq. 3.15b, $\mathrm{d}E_p\cdot\mathrm{d}r$ has two differentials while the other terms have only one. At the limit to $\mathrm{d}E_p \to 0$ and $\mathrm{d}r \to 0$ this term becomes negligible. Consequently:

$$\mathrm{d}E_p\cdot r + E_p\cdot \mathrm{d}r = -\sum_i \alpha_i\cdot E_p\cdot r\cdot \mathrm{d}r \qquad \text{Eq. 3.16}$$

Replacing $\alpha_i = C_i\,\sigma_i$, dividing by $r \cdot dr$ and reordering terms:

$$\frac{dE_p}{dr} = -\frac{E_p}{r} - \sum_i C_i \sigma_i E_p \qquad \text{Eq. 3.17}$$

This equation stands for one differential equation for each wavelength, at each location along the length of the reactor. To obtain photon irradiance, E_p, the emitted light power of the lamp should be divided by the surface area of the lamp and then divided by the energy of one photon; and can be used as a boundary condition for the above equation.

In order to implement the above reaction in other radial points, 9 concentric, equally spaced cylinders were assumed in the space between the lamp and the outside reactor wall as the grid points. The results were around 1% different when the model was tested with 19 concentric cylinders (Mahmoudkhani, 2012).

The UV reactor provider pointed out that 99 % of the photons reaching the reactor outer wall is reflected; however, no information was available on the fraction of the photons reaching the lamp that are re-emitted. Through comparing the light irradiance at the wall by model predictions with experimental measurements this fraction can be established. As an instance, for pure air, good agreement was observed (55 mW/cm^2) when it was assumed that 64 % of the light returning to the lamp is re-emitted (i.e. not absorbed by the lamp), (Mahmoudkhani, 2012). However, a new lamp generates as much as 65 mW/cm^2 of light irradiance corresponding with 70% re-emission. In the current study, 70 % of lamp reflection is assumed.

3.4. Chemical Model

A comprehensive chemical model was developed, including 47 reactions (39 chemical reactions and 8 photochemical reactions) involving 19 chemical species. In current model, the main degradation pathways are considered and all the relevant chemical and radical reactions which contain oxygen, water, ozone, hydrogen sulfide and their reaction products are included.

3.4.1. Chemical Reactions

The rate of reaction, $-r_i$, is "the number of moles of *i* reacting per unit time, per unit volume" (Fogler, 2005). For a typical reaction ($A+B \rightarrow Products$), the reaction kinetics is usually described as: (De Visscher, 2013)

$$-r_i = k_i C_A^{n_{i,A}} C_B^{n_{i,B}} \qquad \text{Eq. 3.18a}$$

Where k_i is the reaction rate constant, C represents concentration of reactant and the power, n, represents the order of the reaction for its particular reactant.

The reaction rate constant in gas phase, k_i, is expressed by the Arrhenius equation as follows:

$$k_i = A\exp(-\frac{E}{RT}) \qquad \text{Eq. 3.18b}$$

Where A is known as the frequency factor, E is the activation energy, and R is universal gas constant. For simplicity, very often in the literature E/R is presented instead of E. Not necessarily, all rate constants should be a function of temperature; in some cases they are presented only as a constant number. However, combining the above equations yield to general reaction rate for a typical chemical reaction ($A+B \rightarrow Products$) in gaseous phase:

$$-r_i = A\exp(-\frac{E}{RT})\, C_A^{n_{i,A}} C_B^{n_{i,B}} \qquad \text{Eq. 3.19}$$

Mostly, there is no pressure dependence for gas phase reaction kinetics. Nevertheless, some combination reactions have an order of three at low pressure, and two at high pressure. Hence, there is an intermediate pressure range to describe kinetics which is known as falloff (Troe, 1979). Typically, the mechanism of these reactions is shown as follows: (Sander, 2011)

$A + B \leftrightarrow AB^*$ Eq. 3.20a

$AB^* + M \rightarrow AB + M$ Eq. 3.20b

In this case, AB* decomposes at low pressure, and the overall reaction rate is proportional to the concentration of M which can be either N_2 or O_2; at high pressure, the concentration of M is sufficiently high that every produced intermediate reacts to AB, irrespective of the actual concentration of M (De Visscher, 2013).

For the reactions extracted from Atkinson et al. (2004), the rate constant for the falloff range is calculated by Troe (1979)'s model with the equation of:

$$k_i = \frac{k_0 k_\infty}{k_0 + k_\infty} F \qquad \text{Eq. 3.21}$$

$$\log F = \frac{\log F_c}{1 + \left(\frac{\log(k_0 / k_\infty)}{0.75 - 1.27 \log F_c} \right)^2} \qquad \text{Eq. 3.22}$$

In which, k_0 is the second order rate constant in the low pressure limit (which is actually a third order constant as multiplied by the concentration of M), k_∞ expressed as rate constant at high pressure limit, and F_c is a broadening factor which is an empirical parameter for that specific reaction.

For the reactions obtained from Sander et al. (2011), the rate constant for the falloff range is calculated by their own method with the equation of:

$$k_i = \left(\frac{k_0}{1 + \frac{k_0}{k_\infty}} \right) 0.6^{\left\{ 1 + \left[\frac{k_0}{k_\infty} \right]^2 \right\}^{-1}} \qquad \text{Eq. 3.23}$$

For the chemical reactions in this study, it has been properly assumed that all reaction rates are first-order to each component (second-order or maximum third-order in total) and beside, each component participates to the reaction according to its stoichiometry number, unless it was specified otherwise by any particular reference.

All components that participate in the model (either in chemical or in photochemical reactions) are listed in Table 3-1.

Table 3-1: List of Components in the model

Component Number	Component
1	H_2S
2	O_2
3	N_2 + Ar
4	H_2O
5	O(^{3}P) Radical
6	OH Radical
7	HO_2 Radical
8	O(^{1}D) Radical
9	O_3
10	H_2O_2
11	HS Radical

Component Number	Component
12	S Radical
13	SO radical
14	SO_2
15	SO_3
16	HSO_3 Radical
17	HSO_2 Radical
18	HSO Radical
19	H_2SO_4

In the Table 3-2, the reaction scheme used in this model is shown. Reaction rate constants are also given. Only the overall reactions are given in the table.

Table 3-2: Chemical reactions in the model and their rate constants

#	Reaction	Rate Constant (cm^3/molecules s)	Reference
1	$O(^3P) + OH\cdot \rightarrow H\cdot + O_2$	$2.3 \times 10^{-11} \exp(110/T)$	De Visscher et al. (2008)
2	$O(^3P) + HO_2\cdot \rightarrow OH\cdot + O_2$	$2.7 \times 10^{-11} \exp(224/T)$	De Visscher et al. (2008)
3	$O(^3P) + H_2O_2 \rightarrow OH\cdot + HO_2\cdot$	$1.4 \times 10^{-12} \exp(-2000/T)$	De Visscher et al. (2008)
4	$O(^3P) + O_2 + M \rightarrow O_3 + M$	$k_0 = 6 \times 10^{-34} (T/300)^{-2.8} [O_2] + 5.6 \times 10^{-34} (T/300)^{-2.8} [N_2]$	De Visscher et al. (2008)
5	$2\ O(^3P) + M \rightarrow O_2 + M$	$2.7 \times 10^{-34} T^{-0.41} ([N_2 + O_2])$	De Visscher et al. (2008)
6	$O(^3P) + O_3 \rightarrow 2\ O_2$	$8 \times 10^{-12} \exp(-2060/T)$	De Visscher et al. (2008)

#	Reaction	Rate Constant (cm^3/molecules s)	Reference
7	$2\ OH\cdot \rightarrow O(^3P) + H_2O$	$7.9 \times 10^{-14}\ (T/298)^{2.6}\ \exp(945/T)$	De Visscher et al. (2008)
8	$O(^1D) + H_2O \rightarrow 2\ OH\cdot$	2.2×10^{-10}	Atkinson et al. (2004)
9	$O(^1D) + O_2 \rightarrow O(^3P) + O_2$	$3.2 \times 10^{-11}\ \exp(67/T)$	Atkinson et al. (2004)
10	$O(^1D) + N_2 \rightarrow O(^3P) + N_2$	$2.15 \times 10^{-11}\ \exp(110/T)$	Sander et al. (2011)
11	$OH\cdot + H_2O_2 \rightarrow HO_2\cdot + H_2O$	$2.9 \times 10^{-12}\ \exp(-160/T)$	De Visscher et al. (2008)
12	$OH\cdot + O_3 \rightarrow HO_2\cdot + O_2$	$1.9 \times 10^{-12}\ \exp(-1000/T)$	De Visscher et al. (2008)
13	$HO_2\cdot + O_3 \rightarrow OH\cdot + 2\ O_2$	$1.4 \times 10^{-14}\ \exp(-600/T)$	De Visscher et al. (2008)
14	$OH\cdot + HO_2\cdot \rightarrow H_2O + O_2$	$4.8 \times 10^{-11}\ \exp(250/T)$	De Visscher et al. (2008)
15	$2\ HO_2\cdot + M \rightarrow H_2O_2 + O_2 + M$	$2.2 \times 10^{-13}\ \exp(600/T) +$ $1.9 \times 10^{-33}\ \exp(980/T)\ [N_2] +$ $\{1.6 \times 10^{-33}\ \exp(980/T)\ [O_2] \times$ $(1 + 1.4\times10^{-21}\ \exp(980/T)\ [H_2O])\}$	De Visscher et al. (2008)
16	$2\ OH\cdot + M \rightarrow H_2O_2 + M$	$k_0 = 6.9 \times 10^{-31}\ (T/300)^{\wedge -0.8}\ [N_2]$ $k_\infty = 2.6 \times 10^{-11}$ $F_c = 0.5$	De Visscher et al. (2008)
17	$HO\cdot + H_2S \rightarrow H_2O + HS\cdot$	$6.1 \times 10^{-12}\ \exp(-80/T)$	Atkinson et al. (2004)
18	$S\cdot + O_2 \rightarrow SO + O(^3P)$	$2.3 \times 10^{-12}\ \exp(0/T)$	Atkinson et al. (2004)

#	Reaction	Rate Constant (cm^3/molecules s)	Reference
19	$O(^3P) + SH\cdot \rightarrow SO\cdot + H\cdot$	1.6×10^{-10} §	Sander et al. (2011)
20	$O(^3P) + H_2S \rightarrow HO\cdot + SH\cdot$	$9.2 \times 10^{-12} \exp(-1800/T)$	Sander et al. (2011)
21	$O(^3P) + SO_2 + M \rightarrow SO_3 + M$	$k_0 = 1.8 \times 10^{-33} (T/300)^2 [N_2+O_2]$ $k_\infty = 4.2 \times 10^{-14} (T/300)^{1.8}$	Sander et al. (2011)
22	$O_3 + SO_2 \rightarrow SO_3 + O_2$	$3.0 \times 10^{-12} \exp(-7000/T)$	Sander et al. (2011)
23	$OH\cdot + S\cdot \rightarrow H\cdot + SO\cdot$	6.6×10^{-11} §	Sander et al. (2011)
23	$OH\cdot + SO\cdot \rightarrow H\cdot + SO_2$	$2.7\times10^{-11} \exp(335/T)$	Sander et al. (2011)
25	$S\cdot + O_3 \rightarrow SO\cdot + O_2$	1.2×10^{-11} §	Atkinson et al. (2004)
26	$SO\cdot + O_2 + M\rightarrow SO_2 + O(^3P) + M$	$1.6 \times10^{-13} \exp(-2280/T)$	Atkinson et al. (2004)
27	$SO\cdot + O_3 \rightarrow SO_2 + O_2$	$4.5 \times 10^{-12} \exp(-1170/T)$	Atkinson et al. (2004)
28	$HO\cdot + SO_2 + M \rightarrow HSO_3\cdot + M$	$k_0 = 4.5 \times 10^{-31} (T/300)^{-3.9}[N_2]$ $k_\infty = 1.3 \times 10^{-12} (T/300)^{-0.7}$ $F_c = 0.525$	Atkinson et al. (2004)
29	$HSO_3\cdot + O_2 \rightarrow SO_3 + \cdot HO_2$	$1.3 \times 10^{-12} \exp(-330/T)$	Atkinson et al. (2004)
30	$SO_3 + H_2O \rightarrow H_2SO_4$ $\{SO_3 + 2\ H_2O \rightarrow H_2SO_4 + H_2O\}$	$8.5 \times 10^{-41} \exp(6540/T)\ [H_2O]^2$ §§§	Sander et al. (2011)
31	$\cdot HO_2 + H_2S \rightarrow H_2O_2 + HS\cdot$ §§	1.5×10^{-15} §	Atkinson et al. (2004)

#	Reaction	Rate Constant (cm^3/molecules s)	Reference
32	$\cdot HO_2 + SO_2 \rightarrow O_2 + \cdot HSO_2$ §§	5.0×10^{-19} §	Atkinson et al. (2004)
33	$\cdot HS + O_2 \rightarrow \cdot HO + SO\cdot$	2.0×10^{-19} §	Atkinson et al. (2004)
34	$\cdot HS + O_3 \rightarrow \cdot HSO + O_2$	$9.5 \times 10^{-12} \exp(-280/T)$	Atkinson et al. (2004)
35	$\cdot HS + H_2O_2 \rightarrow \cdot HO_2 + H_2S$ §§	2.5×10^{-15} §	Sander et al. (2011)
36	$\cdot HSO + O_2 \rightarrow \cdot SO + \cdot HO_2$ §§	1.0×10^{-17} §	Atkinson et al. (2004)
37	$\cdot HSO + O_3 \rightarrow SH\cdot + 2O_2$	6×10^{-14} §	Atkinson et al. (2004)
38	$\cdot HSO + O_3 \rightarrow O_2 + \cdot HSO_2$	5×10^{-14} §	Atkinson et al. (2004)
39	$\cdot HSO_2 + O_2 \rightarrow \cdot HO_2 + SO_2$	3×10^{-13} §	Atkinson et al. (2004)

§ For rate constants which have a certain value at 298 K, the exact values are used; for those that are reported as an upper limit, half of the upper values are assumed.

§§ Assumed reaction products.

§§§ The whole value of rate constant has the unit of s^{-1}.

The main reaction in this study is Reaction Number 17, which is the degradation of H_2S at the presence of OH radical.

3.4.2. Photochemical Reactions

As shown before, the rate of a photochemical reaction (a reaction caused by adsorption of a photon), r_i, (molecules/cm^3 s) can be described as:

$$-r_i = \varphi_i \cdot C_i \cdot \sigma_i \cdot E_p \qquad \text{Eq. 3.24}$$

Here:

φ_i is the quantum yield of molecule *i* (molecule/photon),

C_i is the concentration of the component *i* (molecule/cm^3),

σ_i is the absorption cross-section of molecule *i* (cm^2/molecule) and

E_p is the fluence rate, (photons/cm^2 s).

The photochemical reactions considered in this study are shown Table 3-3.

Table 3-3: Photochemical Reactions in the model

Reaction Number	Reaction
1	$H_2S + h\nu \rightarrow \cdot HS + H\cdot$
2	$H_2O + h\nu \rightarrow \cdot H + \cdot OH$
3	$O_3 + h\nu \rightarrow O(^1D) + O_2$ $\rightarrow O(^3P) + O_2$
4	$\cdot HO_2 + h\nu \rightarrow \cdot OH + O(^3P)$
5	$H_2O_2 + h\nu \rightarrow \cdot OH + \cdot OH$
6	$H_2O_2 + h\nu \rightarrow H_2O + O(^3P)$
7	$SO_2 + h\nu \rightarrow SO\cdot + O(^3P)$
8	$SO_3 + h\nu \rightarrow SO_2 + O(^3P)$

Tables 3-4 and 3-5 show the absorption cross-section and the quantum yield values for each reaction scheme in Table 3-3 consecutively based on its reaction number.

Table 3-4: Adsorption Cross-Section of each photochemical reaction component at 185 and 254 nm wavelengths

Reaction Number	Adsorption Cross-Section (σ) (cm^2)			
	185 nm	Reference	254 nm	Reference
1	3.82×10^{-18}	Sander et al. (2011)	7.457×10^{-21}	Wu and Chen (1998)
2	5.50×10^{-20}	Sander et al. (2011)	------[§]	-------
3	6.61×10^{-19}	Sander et al. (2011)	1.148×10^{-17}	Sander et al. (2011)
4	3.25×10^{-18}	Sander et al. (2011)	2.99×10^{-19}	Sander et al. (2011)
5	8.01×10^{-19}	Sander et al. (2011)	6.99×10^{-20}	Sander et al. (2011)
7	3.65×10^{-18}	Danielache et al. (2008)	1.35×10^{-19}	Vandaele et al. (2009)
8	9.95×10^{-19}	Sander et al. (2011)	1.34×10^{-20}	Burkholder and McKeen (1997)

[§] Since the value is low, and its corresponding quantum yield is zero, this value no longer matters.

Table 3-5: Quantum Yield of each photochemical reaction component at 185 and 254 nm wavelengths

Reaction Number	Quantum yield (φ)			
	185 nm	Reference	254 nm	Reference
1	1[§]	----------	1[§]	----------
2	1	Sander et al. (2011)	0	Sander et al. (2011)
3	$O(^1D)$:0.9 $O(^3P)$: 0.1	Sander et al. (2011)	$O(^1D)$:0.9 $O(^3P)$: 0.1	Sander et al. (2011)
4	1	Sander et al. (2011)	1	Sander et al. (2011)
5	0.75	Sander et al. (2011)	1	Sander et al. (2011)
6	0.16	Sander et al. (2011)	0	Sander et al. (2011)
7	0.27	Driscoll and Arneck (1968)	0[§]	----------
8	1[§]	----------	1[§]	----------

[§] Assumed values based on calculation of the corresponding wavelengths according to the value of bond dissociation energy in Table 3-6.

For H_2S, SO_2 and SO_3 quantum yields, no studies were found; hence, on the one hand, it can be assumed that H_2S, which is expected to have a lower bond strength (single bond), has a value of one for its quantum yield. For SO_2 and SO_3, which are expected to have a higher bond strength (double bond) a value of zero can be assumed for them. On the other hand, calculating the wavelength corresponding with the bond dissociation energy for each compound (Table 3-6) based on an assumed direct photolysis mechanism specifies that a reasonable assumption was made for SO_2 at 254 nm since it needs more energy than a 254 nm photon to react.

These calculations for H_2S and SO_3, which are also confirmed by Sander et al. (2011), indicate that they can react upon absorption of light at 185 and 254 nm. However, doing a sensitivity analysis of H_2S and SO_3 quantum yields shows that the simulation results and estimated reactor outlet concentrations are not affected by the value of the quantum yields; especially for SO_3, which has very low concentration during this photolysis process. This means direct photolysis is not the main dissociation mechanism for these species. Therefore, on the whole, assuming unity quantum yield for both H_2S and SO_3 would be a reasonable assumption.

Table 3-6: Bond Dissociation Energy and their corresponding wavelength

Bond Type	**Bond Dissociation Energy (kJ/mol) data from Dean (1999)**	**Calculated corresponding wavelength (nm)**
H – SH	381	314
OS – O	551.4	217
O_2S – O	348.1	343.7

3.5. Summary of the Model Equations

For the calculation of the concentration for each component at the end of the reactor, the average concentration in outlet has to be defined. In this regard, the integration of mass flow rate for a specific component across the reactor radius should be divided by the integration of its volumetric flow rate, which means:

$$\overline{C_i} = \frac{\int_{R_0}^{R_1} C_i \cdot V \cdot 2\pi r \cdot \mathrm{d}r}{\int_{R_0}^{R_1} V \cdot 2\pi r \cdot \mathrm{d}r} \qquad \text{Eq. 3.25}$$

Here:

C_i is the concentration of component *i* at each location of the reactor (molecules/cm^3),

V is the local gas velocity at any radius of reactor (cm/s),

R_0 and R_1 are the lamp radius (cm) and inner reactor radius (cm) respectively.

Table 3-7 is the summary of all equations used in the model. The purpose of each equation is explained in this chapter. After placing constant values to their particular equations, all these reactions should be solved simultaneously to obtain final results.

Table 3-7: Summary of Equations in the model

Equation Number	Equation	Description
Eq. 3.4	$V = \dfrac{\dfrac{2U(R_1^2 - R_0^2)}{\ln\dfrac{R_1}{R_0}} \ln\dfrac{r}{R_0} - 2U(r^2 - R_0^2)}{R_1^2 + R_0^2 - \dfrac{R_1^2 - R_0^2}{\ln\dfrac{R_1}{R_0}}}$	Velocity profile; local gas velocity for any *r* for an annular space
Eq. 3.11	$V \cdot \dfrac{\partial C_i}{\partial L} = D_i \cdot \dfrac{\partial^2 C_i}{\partial r^2} + \dfrac{D_i}{r} \cdot \dfrac{\partial C_i}{\partial r} + r_i$	Material balance; one partial differential equation for each compound
Eq. 3.17	$\dfrac{\mathrm{d}E_p}{\mathrm{d}r} = -\dfrac{E_p}{r} - \sum_i C_i \sigma_i E_p$	Radiation field; one differential equation for each wavelength, at each location in the reactor
Eq. 3.19	$-r_i = A\exp(-\dfrac{E}{RT})\, C_A^{n_{i,A}} C_B^{n_{i,B}}$	General chemical reaction rate for a binary reaction
Eq. 3.24	$-r_i = \varphi_i \cdot C_i \cdot \sigma_i \cdot E_p$	Photochemical reaction rate for each component participating in a photochemical reaction
Eq. 3.25	$\overline{C_i} = \dfrac{\int_{R_0}^{R_1} C_i \cdot V \cdot 2\pi r \cdot \mathrm{d}r}{\int_{R_0}^{R_1} V \cdot 2\pi r \cdot \mathrm{d}r}$	Concentration of each species in the outlet of the reactor

In order to solve the partial differential equations (PDEs) resulting from the material balance, they are converted to series of ordinary differential equations (ODEs) using the finite difference method on the grid defined by the cylindrical element. Then the sets of ODEs have been solved by "ode15s", a function in MATLAB© which is a variable order and multistep solver based on

the numerical differentiation formulas (NDFs). Optionally, it uses the backward differentiation formulas (BDFs, also known as Gear's method) that are usually less efficient except for stiff sets of equations (MATLAB© help). “s” in ode15s indicates “stiffness” which is practically appropriate for the proposed model since the rates of the reactions are not at the same order of magnitude and some of them are fast while some are not. Moreover, the accuracy of the numerical solver was established since changing the absolute tolerance and relative tolerance by an order of magnitude does not change the simulation results.

The following is an overview of the model assumptions with justification:

- Steady state condition
- Laminar flow: $Re < 2{,}100$
- Negligible hydrodynamic entrance length: Negligible influence of flow regime on the model results
- Newtonian fluid: over 99% pure moist air and the rest gas phase pollutants
- Same diffusivity equation ($D_{H2S\text{-}Air}$) for all species: model results are not sensitive to the value of diffusivity
- No mechanical dispersion: fully developed laminar flow
- Emitting UV light just perpendicular to the lamp with the shortest path length: Not important effects for path length in gas phase based on previous studies
- Negligible light scattering: the effect is at least 5 orders of magnitude lower than absorption
- Negligible heat transfer mechanism: temperature insensitivity analysis of model

3.6. Model Extension (Adding NO_x reactions)

The term "NO_x" denotes all known oxides of nitrogen containing NO, NO_2, NO_3, N_2O_3, N_2O_4 and N_2O_5. Because of large quantities of emissions, NO and NO_2 are the most important air pollutants (Cooper and Alley, 2010). According to EPA (2000), the emission of NO_x can be either from mobile sources (such as automobiles, trucks and so forth) or stationary sources (for instance fuel combustion and utility furnaces). Formation of NO_x from a stationary combustion source is coming from either ***Thermal NO_x*** which is oxygen and nitrogen in the air used for combustion at flame temperature; or ***Fuel NO_x*** which is caused by combustion of fuel containing organic nitrogen and oxygen (Cooper and Alley, 2010).

The background concentrations of NO_x in the atmosphere are quite small, so it cannot have an effect on the model results and therefore they are not considered in the model. However, as an extension, all of the chemical and photochemical reactions resulting from NO_x, either as reactants or products, with the H_2S-Air mixture are studied and presented in this section. In this case, 30 species are present (11 more added), 75 chemical reactions (36 more added) and 16 photochemical reactions (8 more added).

3.6.1. Chemical Reactions Added

Again in the extended model, it has been properly assumed that all the chemical reaction rates are first-order to each component (second-order or maximum third-order in total) and beside, each component participates in the reaction according to its stoichiometry number, unless it was specified otherwise by any particular reference.

All additional components which participate in the extended model (either in chemical or in photochemical reactions) are listed in Table 3-8 below.

Table 3-8: List of added components in the extended model

Component Number (Added)	Component
20	N_2O
21	NO
22	NO_2
23	NO_3
24	N_2O_4
25	HNO_2
26	HNO_3
27	HO_2NO_2
28	N_2O_3
29	N_2O_5
30	HSNO

Table 3-9 shows the general scheme of additional chemical reactions for degradation of H_2S in waste gas stream (air) when NO_x species are included. Chemical reactions rate constants for these reactions are also stated. Likewise, for falloff reactions, all rate constants obtained from Atkinson et al. (2004) are calculated by Eq. 3.21 and Eq. 3.22, and also from Sander et al. (2011) by Eq. 3.23.

Table 3-9: Chemical reactions in the extended model and their rate constants

#	Reaction	Rate Constant (cm^3/molecules s)	Reference
1	$O(^1D) + N_2 + M \rightarrow N_2O + M$	$k_0 = 2.8 \times 10^{-36} (T/300)^{-0.9} [N_2]$	Sander et al. (2011)
2	$O(^1D) + N_2O \rightarrow O(^3P) + N_2O$	5.0×10^{-13}	Atkinson et al. (2004)
3	$O(^1D) + N_2O \rightarrow O(^3P) + N_2O$	$4.64 \times 10^{-11} \exp(20/T)$	Sander et al. (2011)
4	$O(^1D) + N_2O \rightarrow NO + NO$	$7.25 \times 10^{-11} \exp(20/T)$	Sander et al. (2011)
5	$O(^3P) + NO + M \rightarrow NO_2 + M$	$k_0 = 9.0 \times 10^{-32} (T/300)^{-1.5} [N_2]$ $k_\infty = 3 \times 10^{-11}$	Sander et al. (2011)
6	$O(^3P) + NO_2 \rightarrow NO + O_2$	$5.15 \times 10^{-12} \exp(210/T)$	Sander et al. (2011)
7	$O(^3P) + NO_2 + M \rightarrow NO_3 + M$	$k_0 = 1.3 \times 10^{-31} (T/300)^{-1.5} [N_2]$ $k_\infty = 2.3 \times 10^{-11} (T/300)^{0.24}$ $F_c = 0.6$	Atkinson et al. (2004)
8	$O(^3P) + NO_3 \rightarrow O_2 + NO_2$	$1.0 \times 10^{-11} \exp(0/T)$	Sander et al. (2011)
9	$NO_2 + NO_2 + M \rightarrow N_2O_4 + M$	$k_0 = 1.4 \times 10^{-33} (T/300)^{-3.8} [N_2]$ $k_\infty = 1.0 \times 10^{-12}$ $F_c = 0.4$	Atkinson et al. (2004)
10	$N_2O_4 + M \rightarrow NO_2 + NO_2 + M$	$k_0 = 1.3 \times 10^{-5} (T/300)^{-3.8} \exp(-6400/T)[N_2]$ $k_\infty = 1.15 \times 10^{16} \exp(-6460/T)$ $F_c = 0.4$	Atkinson et al. (2004)
11	$\cdot H + NO_2 \rightarrow \cdot OH + NO$	$4 \times 10^{-10} \exp(-340/T)$	Sander et al. (2011)

#	Reaction	Rate Constant (cm^3/molecules s)	Reference
12	$OH\cdot + NO + M \rightarrow HNO_2 + M$	$k_0 = 7.4 \times 10^{-31} (T/300)^{-2.4} [N_2]$ $k_\infty = 3.3 \times 10^{-11} (T/300)^{-0.3}$ $F_c = \exp(-T/1420)$	Atkinson et al. (2004)
13	$OH\cdot + NO_2 + M \rightarrow HNO_3 + M$	$k_0 = 3.3 \times 10^{-30} (T/300)^{-3} [N_2]$ $k_\infty = 4.1 \times 10^{-11}$ $F_c = 0.4$	Atkinson et al. (2004)
14	$OH\cdot + NO_3 \rightarrow \cdot HO_2 + NO_2$	2.0×10^{-11} §	Atkinson et al. (2004)
15	$OH\cdot + HNO_2 \rightarrow H_2O + NO_2$	$1.8 \times 10^{-11} \exp(-390/T)$	Atkinson et al. (2004)
16	$OH\cdot + HNO_3 \rightarrow H_2O + NO_3$	$8.3 \times 10^{-15} \exp(850/T)$	Sander et al. (2011)
17	$OH\cdot + HO_2NO_2 \rightarrow H_2O + O_2 + NO_2$	$1.3 \times 10^{-12} \exp(380/T)$	Atkinson et al. (2004)
18	$\cdot HO_2 + NO \rightarrow NO_2 + OH\cdot$	$3.3 \times 10^{-12} \exp(270/T)$	Atkinson et al. (2004)
19	$\cdot HO_2 + NO_2 + M \rightarrow HO_2NO_2 + M$	$k_0 = 1.8 \times 10^{-31} (T/300)^{-3.2} [N_2]$ $k_\infty = 4.7 \times 10^{-12}$ $F_c = 0.6$	Atkinson et al. (2004)
20	$HO_2NO_2 + M \rightarrow \cdot HO_2 + NO_2 + M$	$k_0 = 4.1 \times 10^{-5} \exp(-10650/T) [N_2]$ $k_\infty = 4.8 \times 10^{15} \exp(-11070/T)$ $F_c = 0.6$	Atkinson et al. (2004)
21	$\cdot HO_2 + NO_3 \rightarrow \cdot HO + NO_2 + O_2$	$2.3 \times 10^{-12} \exp(170/T)$	Atkinson et al. (2004)
22	$NO + O_3 \rightarrow NO_2 + O_2$	$3.0 \times 10^{-12} \exp(-1500/T)$	Sander et al. (2011)

#	Reaction	Rate Constant (cm^3/molecules s)	Reference
23	$2NO + O_2 \rightarrow 2\ NO_2$	$3.3 \times 10^{-39}\ \exp(530/T)$	Atkinson et al. (2004)
24	$NO + NO_3 \rightarrow 2NO_2$	$1.5 \times 10^{-11}\ \exp(170/T)$	Sander et al. (2011)
25	$NO + NO_2 + M \rightarrow N_2O_3 + M$	$k_0 = 3.1 \times 10^{-34}\ (T/300)^{-7.7}\ [N_2]$ $k_\infty = 7.9 \times 10^{-12}\ (T/300)^{1.4}$ $F_c = 0.6$	Atkinson et al. (2004)
26	$N_2O_3 + M \rightarrow NO + NO_2 + M$	$k_0=1.9\times10^{-7}(T/300)^{-8.7}\exp(-4880/T)[N_2]$ $k_\infty = 4.7 \times 10^{15}\ (T/300)^{0.4}\ \exp(-4880/T)$ $F_c = 0.6$	Atkinson et al. (2004)
27	$NO_2 + NO_3 + M\rightarrow N_2O_5 + M$	$k_0 = 3.6 \times 10^{-30}\ (T/300)^{-4.1}\ [N_2]$ $k_\infty = 1.9 \times 10^{-12}\ (T/300)^{0.2}$ $F_c= 0.35$	Atkinson et al. (2004)
28	$N_2O_5 + M \rightarrow NO_2 + NO_3 + M$	$k_0=1.3\times10^{-3}(T/300)^{-3.5}\exp(-11000/T)[N_2]$ $k_\infty = 9.7 \times 10^{14}\ (T/300)^{0.1}$ $\exp(-11080/T)$ $F_c= 0.35$	Atkinson et al. (2004)
29	$N_2O_5 + H_2O \rightarrow\ 2\ HNO_3$	2.5×10^{-22} §	Atkinson et al. (2004)
30	$NO_2 + O_3 \rightarrow NO_3 + O_2$	$1.2 \times 10^{-13}\ \exp(-2450/T)$	Sander et al. (2011)
31	$O_3 + HNO_2 \rightarrow O_2 + HNO_3$	2.5×10^{-19} §	Sander et al. (2011)
32	$SO + NO_2 \rightarrow SO_2 + NO$	$1.4\times10^{-11}\ \exp(0/T)$	Sander et al. (2011)
33	$\cdot HS + NO + M\rightarrow HSNO + M$	$k_0 = 2.4 \times 10^{-31}\ (T/300)^{-2.5}\ [N_2]$ $k_\infty = 2.7 \times 10^{-11}$	Sander et al. (2011)

#	Reaction	Rate Constant (cm^3/molecules s)	Reference
34	$\cdot HS + NO_2 \rightarrow \cdot HSO + NO$	$3.0 \times 10^{-11} \exp(250/T)$	Sander et al. (2011)
35	$\cdot HS + N_2O \rightarrow \cdot HSO + N_2$	2.5×10^{-16} §	Sander et al. (2011)
36	$\cdot HSO + NO_2 \rightarrow HSO_2 + NO$	9.6×10^{-12} §	Sander et al. (2011)

§ For rate constants which have a certain value at 298 K, the exact values are used; for those that are reported as an upper limit, half of the upper values are assumed.

3.6.2. Photochemical Reactions Added

Many nitrogen oxide molecules are decomposed in appropriate photolysis conditions. Added photochemical reactions considered in the extended model shown in Table 3-10.

Table 3-10: Photochemical Reactions in extended the model

Reaction Number	Reaction
1	$NO_2 + h\nu \rightarrow NO + O(^3P)$
2	$N_2O + h\nu \rightarrow N_2 + O(^1D)$
3	$N_2O_5 + h\nu \rightarrow NO_3 + NO_2$
4	$N_2O_5 + h\nu \rightarrow NO_3 + NO + O(^3P)$
5	$HNO_2 + h\nu \rightarrow \cdot OH + NO$
6	$HNO_3 + h\nu \rightarrow \cdot OH + NO_2$
7	$HO_2NO_2 + h\nu \rightarrow \cdot HO_2 + NO_2$
8	$HO_2NO_2 + h\nu \rightarrow \cdot OH + NO_3$

Tables 3-11 and 3-12 below show reaction rate constant for each reaction scheme in Table 3-10 consecutively based on its reaction number.

Table 3-11: Adsorption Cross-Section of each photochemical reaction component in the extended model at 185 and 254 nm wavelengths

Reaction Number	Adsorption Cross-Section (σ) (cm^2)			
	185 nm	Reference	254 nm	Reference
1	6.88×10^{-18}	Bass et al. (1976)	1.16×10^{-20}	Atkinson et al. (2004)
2	1.43×10^{-19}	Sander et al. (2011)	0	Sander et al. (2011)
3	1.85×10^{-17}	Osborne et al. (2000)	3.26×10^{-19}	Sander et al. (2011)
4	1.85×10^{-17}	Osborne et al. (2000)	3.26×10^{-19}	Sander et al. (2011)
5	9.0×10^{-19}	Sander et al. (2011)	1.45×10^{-19}	Sander et al. (2011)
6	1.63×10^{-17}	Burkholder et al. (1993)	1.95×10^{-20}	Sander et al. (2011)
7	1.24×10^{-17}	Sander et al. (2011)	3.63×10^{-19}	Sander et al. (2011)
8	1.24×10^{-17}	Sander et al. (2011)	3.63×10^{-19}	Sander et al. (2011)

Table 3-12: Quantum Yield of each photochemical reaction component in the extended model at 185 and 254 nm wavelengths

Reaction Number	Quantum yield (φ)			
	185 nm	Reference	254 nm	Reference
1	1	Sander et al. (2011)	1	Sander et al. (2011)
2	1	Atkinson et al. (2004)	------[§]	------
3	0	Atkinson et al. (2004)	0.08	Atkinson et al. (2004)
4	1	Atkinson et al. (2004)	0.72	Atkinson et al. (2004)
5	1	Atkinson et al. (2004)	1	Atkinson et al. (2004)
6	1	Johnston and Graham (1974)	0.97	Atkinson et al. (2004)
7	0.7	Sander et al. (2011)	0.8	Sander et al. (2011)
8	0.3	Sander et al. (2011)	0.2	Sander et al. (2011)

[§] Since its corresponding quantum yield is zero, this value no longer matters.

NO_x species reactions do not have impact on simulation results and removal efficiency when NO_x is present at background concentrations since their concentration is very low in the proposed model and they just form or disappear with their background concentrations. However, it is worth mentioning that the model can predict the removal efficiency and outlet concentration of any species for a waste air stream polluted by H_2S combined with NO_x and also NO_x alone. In addition, through only some partial changes in the fixed parameters of the model, the current model can be used for prediction of photolysis of NO_x alone from waste gas. For instance, taking nitrogen monoxide, NO, which is around 95 % of all NO_x emitting from combustion sources (Cooper and Alley, 2010), as a pollutant in an air waste stream, knowing inlet concentration and operational condition, photolysis efficiency and other product outlet concentration can be predicted through the developed model.

CHAPTER 4 : SIMULATION RESULTS AND DISCUSSIONS

The simulation results in this chapter are obtained based on the actual photoreactor for which the set up was described by De Visscher et al. (2010). The ultraviolet reactor (UV Sciences, San Diego, CA) is cylindrical with continuous flow mode, the length is 56 cm and the inside diameter is 4.2 cm, with the lamp (40 W amalgam emitting at 185 nm and 254 nm wavelengths) at the horizontal axis. All the reactions happen in an 8.5 mm gap between the UV lamp and the reactor wall. This reactor has been used experimentally for benzene and toluene degradation (De Visscher et al., 2010) and m-xylene (Atyabi, 2013). Table 4-1 shows the simulated operating conditions for this reactor. All of the simulation results are obtained according to these conditions unless they are specified otherwise.

Table 4-1: Simulation operation conditions

Electrical Power	40 W
Irradiation Power	185 nm, 3.2 W 254 nm, 12 W
Reactor Length	56 cm
Reactor Radius (R_1)	2.1 cm
Lamp Radius (R_0)	1.25 cm
Pressure (barometric)	89 kPa
Temperature	310 K
Relative Humidity (RH)	28 %
H_2S Concentration	1 – 10 g/m^3
Volumetric Flow Rate	0.5 – 5 L/min

4.1. Product Analysis and Mechanisms

Atmospheric chemical degradation of H_2S is assumed to be initiated by reaction with hydroxyl radical: (Wine et al., 1981)

$$HO\cdot + H_2S \rightarrow H_2O + \cdot HS \qquad \text{(R. 4.1)}$$

All other reactions are chain reactions, and are happening with producing or consuming H_2S, oxygen, water vapor and their formed species which are presented in Table 3-2 and Table 3-3.

Hydrogen sulfide is oxidized to SO_2 with the overall reaction of: (Steijns et al., 1976)

$$H_2S + 1.5\ O_2 \rightarrow H_2O + SO_2 \qquad \text{(R. 4.2)}$$

This reaction also was confirmed as a dominant pathway with excess oxygen in the gas phase at temperatures below the sulfur dew point and almost all entering H_2S converted to SO_2 (Kovalenko et al., 2001). Furthermore, the formation of SO_2 in photolysis and photocatalysis of H_2S can be either from the above reaction (R. 4.2) or some radical reactions which are already shown in Table 3-2. Canela et al. (1998), Kataoka et al. (2005), Portela et al. (2007) and Portela et al. (2012) confirmed the observation of initial SO_2 formation. It is also worth mentioning that all of their experimental studies were carried out at a very low inlet concentration of H_2S.

On the other hand, among the few studies on either photolysis or photocatalysis of H_2S, it is believed that H_2SO_4 or SO_4^{2-} is the main product of this process. Canela et al. (1998), Xia et al. (2008), and Huang et al. (2012) confirmed that SO_4^{2-} is the predominant product of H_2S photolysis or photocatalysis. All these studies used low concentration of H_2S. The reaction pathway can be expressed as follows: (Stockwell and Calvert, 1983)

$SO_2 + \cdot OH + M \rightarrow \cdot HSO_3 + M$ (R. 4.3)

$\cdot HSO_3 + O_2 \rightarrow SO_3 + \cdot HO_2$ (R. 4.4)

$SO_3 + H_2O \rightarrow H_2SO_4$ (R. 4.5)

According to the rate constants of (R. 4.4) and (R. 4.5), formation and consumption of SO_3 is very fast, so immediately after forming SO_3 it will react with water vapor, and H_2SO_4 will be formed quickly (Lovejoy et al., 1996). From reaction rate point of view, SO_3 in these reactions can react as a free radical and intermediate species since the time constant for these two reactions is in the order of 10^{-6} second (Jayne et al., 1997). Moreover, according to Lovejoy et al. (1996) and Jayne et al., (1997), because the reaction rate of (R. 4.5) is second order to the water concentration ($k_i \, \alpha \, [H_2O]^2$), sufficient water vapor is required to produce H_2SO_4 or sulfate ion (SO_4^{2-}).

Therefore, two main products can be predicted for H_2S photolysis from waste gas. Table 4-2 shows simulation results for predicting the outlet concentration of products at different inlet H_2S concentration at a fixed flow rate of 1 L/min.

Table 4-2: Product analysis of model

	Initial concentration of H_2S ($g.m^{-3}$)	**Products concentration ($g.m^{-3}$)**
SO_2	0.1	0.006
	1.0	0.970
	10	13.402

	Initial concentration of H_2S ($g.m^{-3}$)	Products concentration ($g.m^{-3}$)
H_2SO_4	0.1	0.278
	1.0	1.391
	10	1.754

Figure 4-1 shows outlet concentration of products as a function of inlet H_2S concentration at a fixed flow rate of 1 L/min based on simulation results.

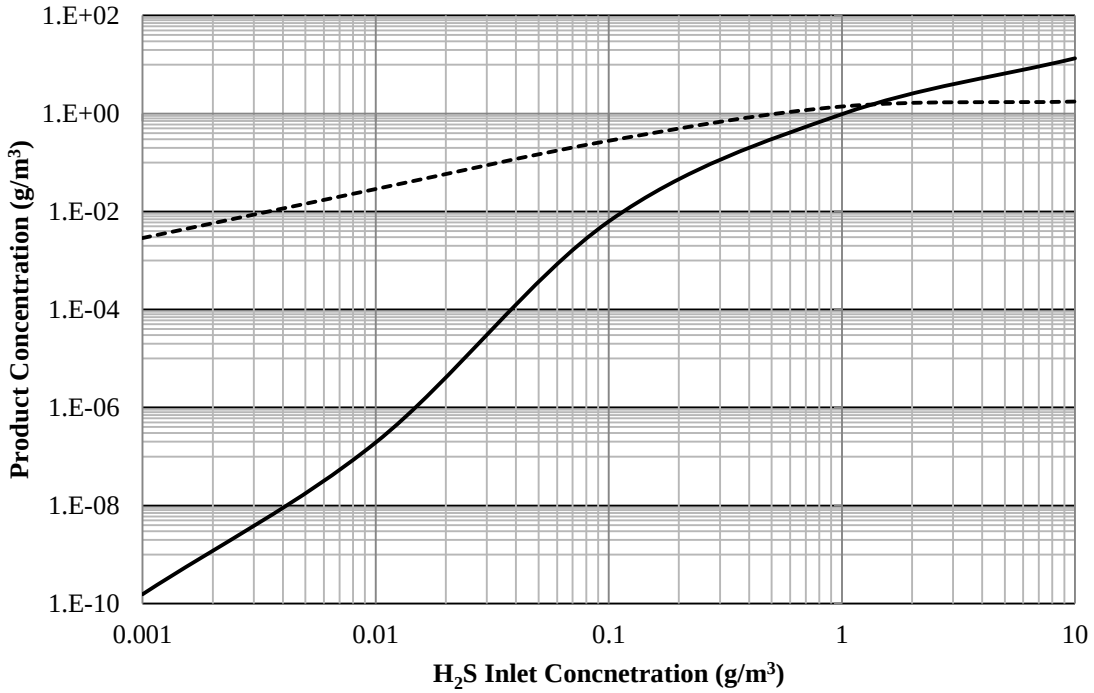

Figure 4-1: Product analysis of model at volumetric flow rate 1 L/min (Dashed line represents H_2SO_4 and solid line represents SO_2)

Simulation results clearly demonstrate that at a very low concentration of H_2S, the predominant product of this photolysis process would be only H_2SO_4. By increasing the inlet H_2S concentration, the relative amount of H_2SO_4 as a product would decrease and so SO_2 would be the dominant photolysis product. The model predicts that as long as a sufficient amount of

hydroxyl radical is present in the system, H_2S will be degraded completely and the SO_2 formed during this process will convert to H_2SO_4 through reactions (R. 4.3) to (R. 4.5) by remaining OH radical. Due to the decreasing OH radical concentration resulting from the reaction with enhanced H_2S concentration or other reactions, these reactions will not occur as significantly and consequently SO_2 will remain as the main product.

4.2. Parameters of H_2S Degradation

4.2.1. Effect of H_2S inlet concentration

Figure 4-2 shows the simulation results of the photolysis efficiency of a fixed volumetric gas flow rate of 1 L/min, as a function of H_2S inlet concentration. A highly efficient process was observed since the efficiency decreases from 99.97 % to 77.44 % as the inlet H_2S concentration increases from 1 g/m^3 to 10 g/m^3.

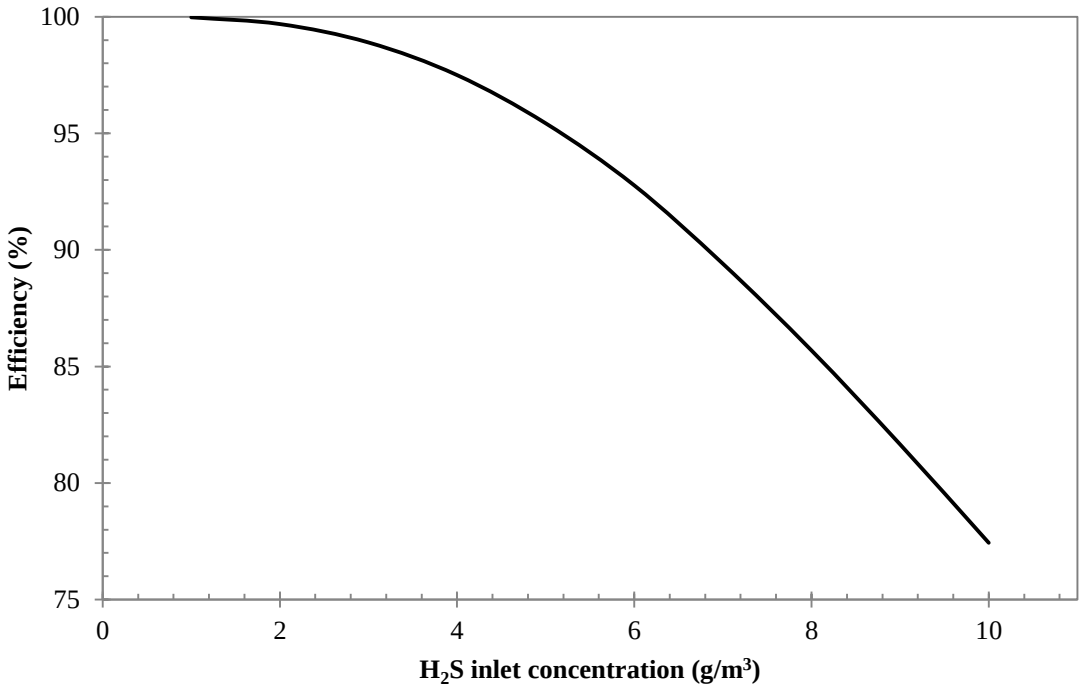

Figure 4-2: Simulation result for degradation efficiency as a function of initial H_2S concentration at fixed gas flow rate (1 L/min)

At a fixed UV lamp power, the energy and number of photons and active radicals in the reaction area do not change; hence, with constant gas flow rate, by increasing inlet H_2S concentration, H_2S molecules obtain less energy, which results in a lower removal efficiency. This effect was experimentally observed in a few studies that worked on H_2S photolysis or photocatalysis. The model predicts a high efficiency for H_2S removal in waste gas accomplished by dealing with the variation in feed gas concentration.

4.2.2. Effect of gas flow rate

Figure 4-3 displays the removal efficiency of H_2S as a function of gas flow rate at fixed inlet concentration of H_2S of 1 g/m^3. The efficiency decreases from 100 % to 62.56 % as gas flow rate increases from 0.5 L/min to 5 L/min. The smaller gas flow rate which leads to longer gas

residence time, provides both longer collision time and higher collision probability with photons and OH radicals, which increases the degradation efficiency of H_2S.

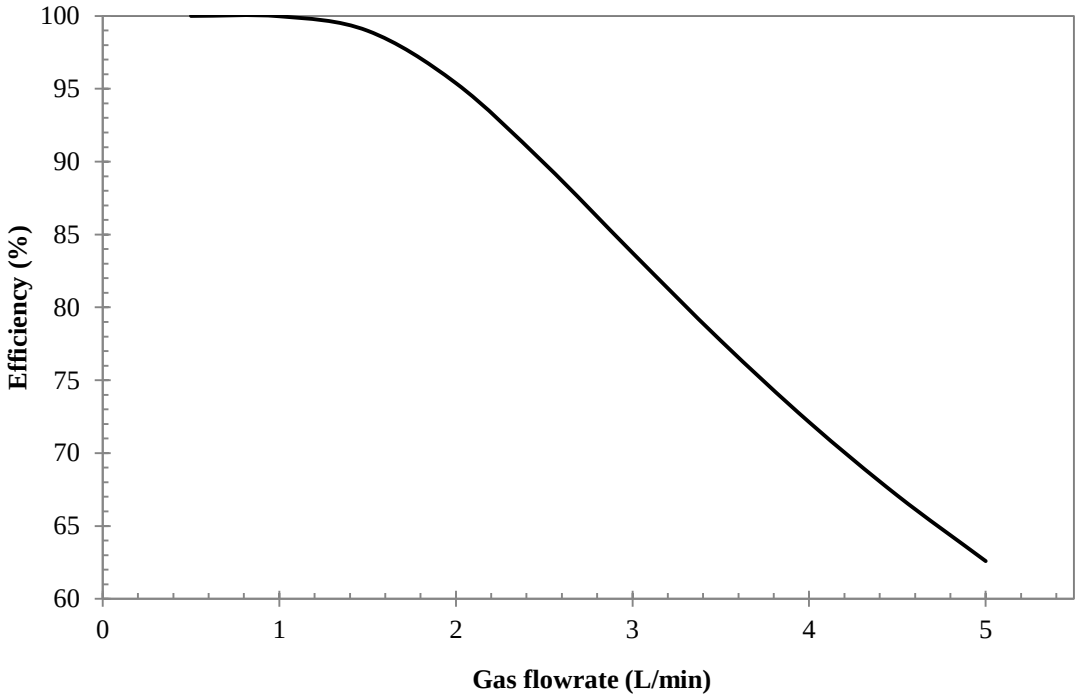

Figure 4-3: Simulation result for degradation efficiency as a function of gas flow rate at fixed initial H_2S concentration (1 g/m^3)

Moreover, the simulated outlet concentrations indicated that by increasing gas flow rate, the concentration of H_2SO_4 in the reactor outlet is decreased since has the same trend with changing efficiency as discussed in the previous section. For SO_2 also, increasing outlet concentration along with increasing gas flow rate is observed due to the decreasing of the removal efficiency. In some points, the concentration of SO_2 is decreasing since at those points condition H_2S does not decompose completely and would be one of outlet components; however, an increasing SO_2 trend is noticeably seen. Figure 4-4 shows simulation results.

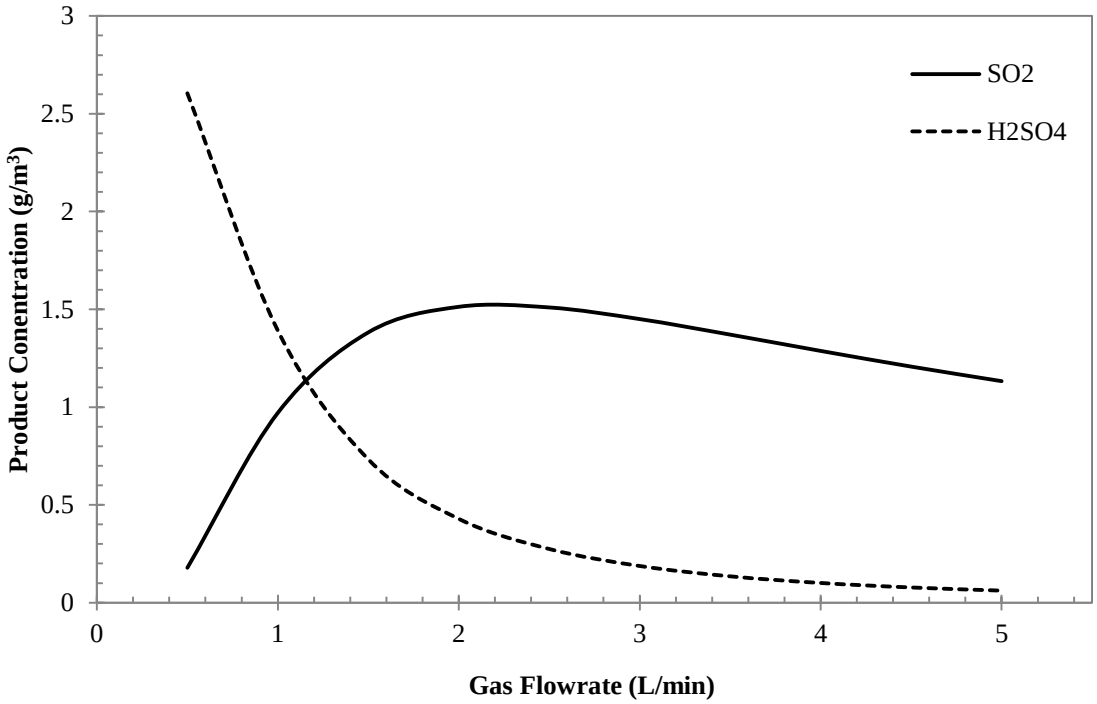

Figure 4-4: Simulation result for products analysis as a function of gas flow rate at a fixed initial H_2S concentration (1 g/m^3)

4.2.3. Effect of water content (Relative Humidity)

Humidity, or water content in the system, has a key role in photolysis of H_2S. As discussed before, degradation of H_2S will be initiated by OH radicals. The main source for OH radicals in the system is water vapor. Li et al. (2012) experimentally showed that the relative humidity caused increasing degradation efficiency, especially when it is close to 80%. Figure 4-5 shows simulation results for the case of 1.5 L/min volumetric flow rate and 2.5 g/m^3 of initial H_2S concentration. Although the removal efficiency does not change significantly, a completely ascending trend is observed.

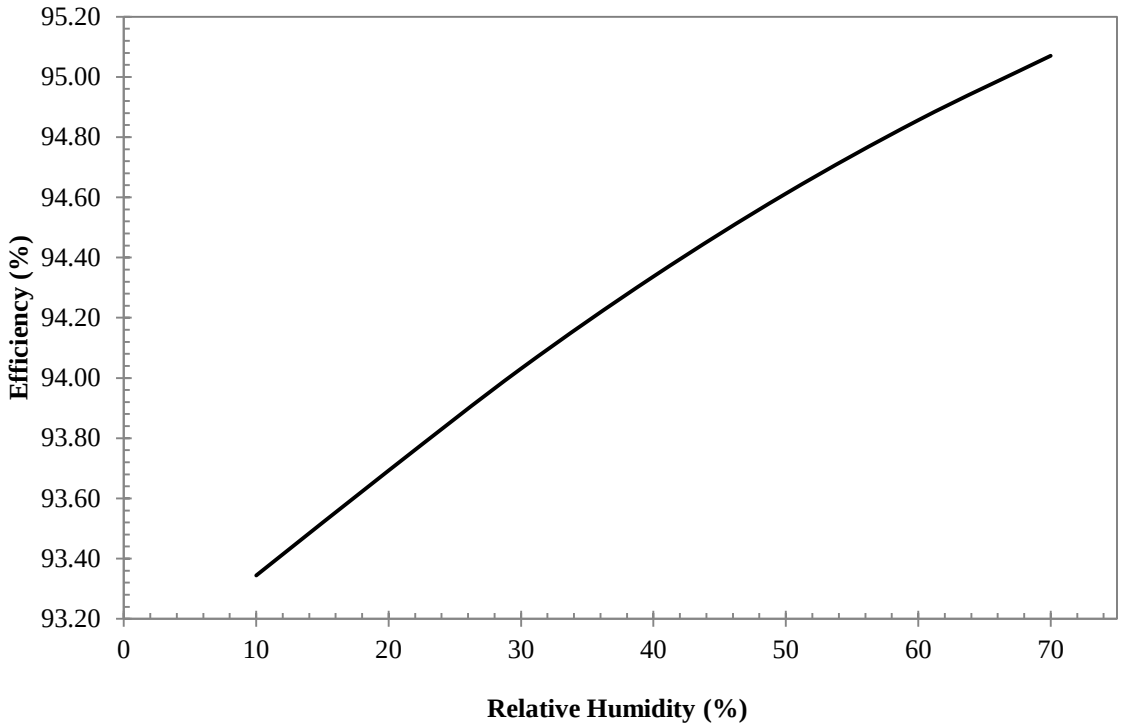

Figure 4-5: Simulation result for degradation efficiency as a function of humidity at fixed mass flow rate (3.75 mg/min)

In order to see this effect more clearly, simulation results are compared at three different relative humidity levels. Figure 4-6 shows removal efficiency as a function of mass flow rate at three different humidity levels. Results are obtained at a fixed inlet concentration of H_2S of 2 g/m^3 and a variable gas flow rate of 0.5 to 5 L/min. The curves are close together but the effect of humidity is apparent.

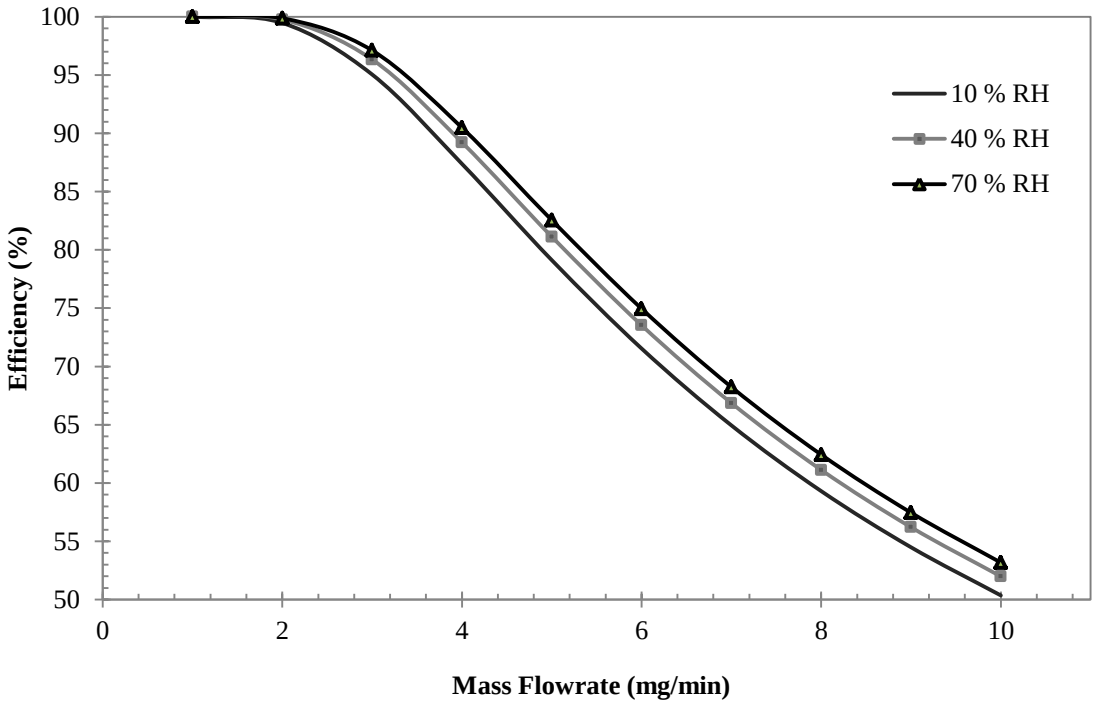

Figure 4-6: Simulation result for degradation efficiency as a function of mass flow rate at three water content levels

Water content can also affect products concentration. By increasing relative humidity in the system, it can be expected since the efficiency of process increases, more SO_2 forms. However, due to increasing amounts of OH radicals in the system, more H_2SO_4 is formed based on reactions (R. 4.3) to (R. 4.5) and the photochemical production of OH radical from water. Consequently, the concentration of SO_2 will decrease slightly. Figure 4-7 evidently shows this phenomenon. Here again, fixed volumetric gas flow rate (1.5 L/min) and initial H_2S concentration (2.5 g/m^3) have been chosen.

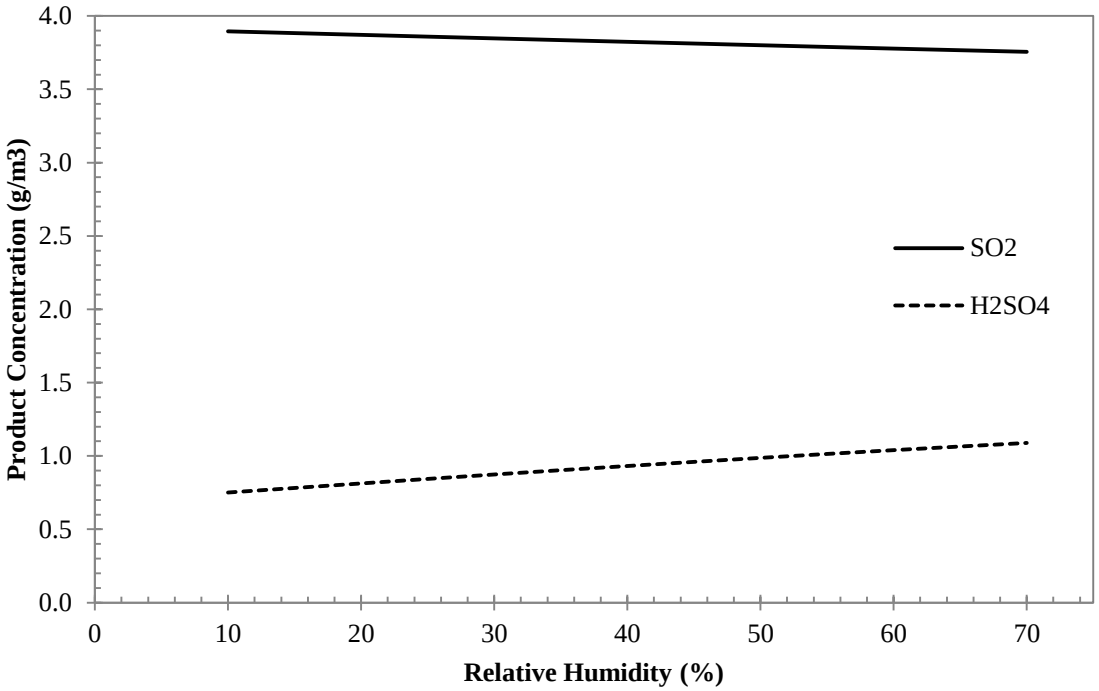

Figure 4-7: Simulation result for products analysis as a function of humidity at fixed initial H_2S concentration (2.5 g/m^3) and fixed gas flow rate (1.5 L/min)

4.2.4. Effect of Temperature

As with every process, temperature can have an impact on the process efficiency. In order to see this effect, all of the dependent variables with temperature should be considered.

- Diffusivity ($D_{H_2S\text{-}Air}$): This value has a functionality of temperature and pressure as shown in Eq. 3.6. By increasing T, this value will increase and potentially increase mass transfer. For instance, rising temperature from 300 K to 450 K, the diffusivity doubles. However, since radial mass transfer occurs only in an 8.5 mm gap, the difference is negligible.

- Absorption Cross-Section (σ): This value is a function of wavelength and can have an important temperature variation. For the species included in the model, the effect of temperature on their absorption cross section was studied. Wu and Chen (1998) found out

this value for H_2S is not sensitive to temperature at the given wavelength. For H_2O, Chung et al. (2001) observed this value is not practically dependent in temperature. The same effect was found for O_2 (Youshino et al., 2005) and O_3 (Ashtolz et al. 1982). For SO_2, this value might be temperature sensitive, but in the region reflected in the model negligible difference was observed (Wu et al., 2000). Therefore, keeping a fixed adsorption cross-section at varying temperature in the model is a realistic assumption.

- Water Content or Relative Humidity: According to the Psychometric Chart (e.g. Perry et al., 1997) by increasing the temperature of a system and maintaining relative humidity, the water content of that system increases. However for simplicity, the following results are obtained at a fixed water content ($y_{H_2O} = 0.02$) since as discussed in previous section, its effect is substantial for forming H_2SO_4 and less for process efficiency.

- Reaction rate constants (k_i): These values have a functionality of temperature as shown in Eq. 3.18b. This effect can contribute to the process efficiency, as many of the chemical reactions in the model are temperature sensitive.

Figure 4-8 shows effect of temperature variation on simulation results for a case of 1.5 L/min volumetric flow rate and 2.5 g/m^3 of initial H_2S concentration (3.75 mg/min of mass flow rate). Although the removal efficiency is increasing slightly, temperature distinction does not have significant impact on the degradation efficiency. Therefore, it can be concluded the model results are not temperature dependent.

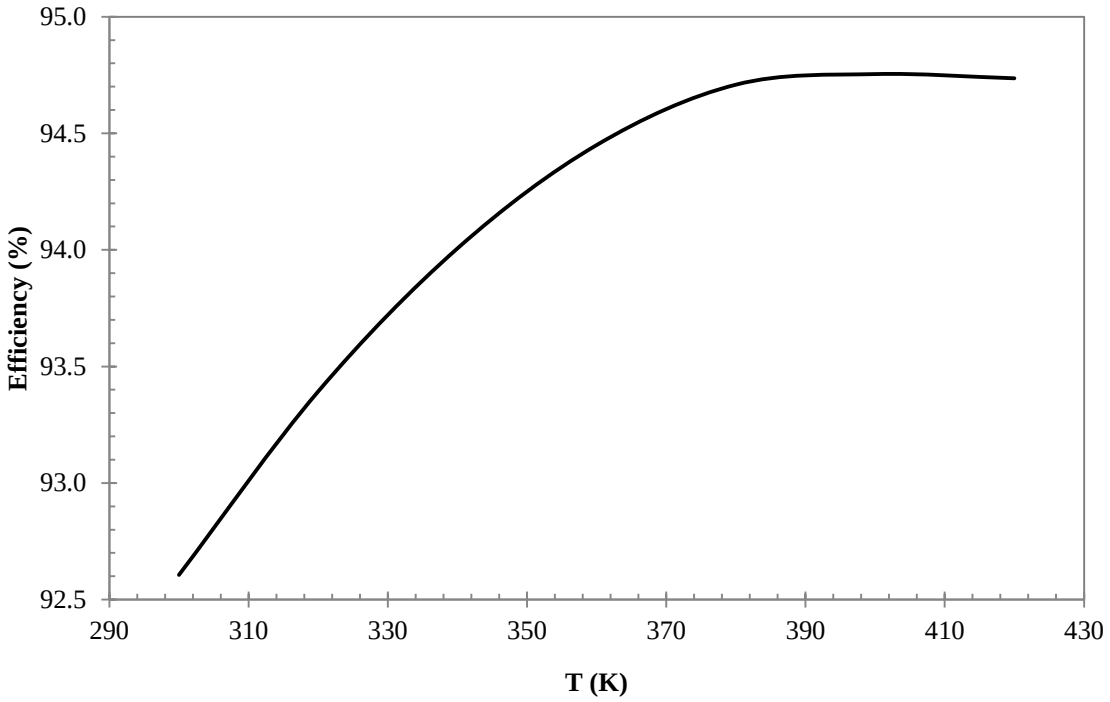

Figure 4-8: Simulation result for degradation efficiency as a function of temperature at fixed mass flow rate (3.75 mg/min)

4.3. Model Validation

For safety reasons, the H_2S concentration in experiments is limited to 10 ppm in the available laboratory space, which is the 8-hour exposure limit in the Alberta occupational health and safety regulation (OHS, 2010). Therefore, doing some experiments at different initial concentration of H_2S was quite impossible. So, in order to validate the proposed model, an experimental journal paper, which described data in conditions similar to the proposed model, was selected for this regard.

Xia et al. (2008) studied "photolysis of low concentration H_2S under UV/VUV irradiation emitted from microwave discharge electrodeless lamp". They investigated two different light sources, Hg-Ar and Kr-I_2. Only Hg-Ar lamp is compatible with this work since it only emitted

UV light at 185 nm and 253.7 nm which is the UV emission spectrum of mercury (Hg). They used quartz tubes as a reaction area, so around 1% UV reflection was assumed compared with 99% reflection in the proposed model that was used in the previous sections. Overall input electricity power for their work was 200 W which created 80 W of total output microwave in their research. The emission spectrum of Hg-Ar lamp that they used indicated that the lamp is 12% efficient at 185 nm and 84% at 254 nm. However, according to Gutierrez et al. (2006) the maximum efficiency of a UV microwave lamp in terms of its total input electrical power is 20%. In order to see the effects of gas residence time and radial UV radiation diffusion, they used two different reaction tubes, Tube-A with 36 mm diameter and Tube-B with diameter of 46 mm, at two different residence time 1.5 s and 4.5 s at two different reaction volumes of 633 cm^3 and 1213 cm^3 for Tube-A and Tube-B, respectively.

Table 4-3 summarizes their experimental effective parameters that are incorporated into the proposed model for comparing results.

Table 4-3: Parameters of Xia et al. (2008) conducted into the model

Electrical Input Power	200 W
Microwave Output Power	80 W
Irradiation Power	185 nm, 4.8 W 254 nm, 33.6 W
Reactor Length	90 cm
Reactor Radius (R_1)	1.8 cm (Tube-A) 2.3 cm (Tube-B)
Lamp Radius (R_0)	1.0 cm
Pressure	1 atm
Temperature	25 °C

Relative Humidity (RH)	40 %
H_2S Concentration	0 – 25 mg/m^3
Volumetric Flow Rate	140 – 420 cm^3/s (Tube-A) 269 – 808 cm^3/s (Tube-B)

4.3.1. Effect of H_2S inlet concentration

Experimental data of Xia et al. (2008) indicates the process efficiency of H_2S degradation decreased from 96.43% to 62.62% when the initial concentration of H_2S increased from 1.4 to 21.9 mg/m^3 at a fixed gas flow rate of 140 cm^3/s of Tube-A. The model predicts that the removal efficiency would decrease from 99.22 to 60.97% at the same conditions. It can be concluded that there is a good agreement between the experimental data and the proposed model. Although the model overestimates results in some points, the same trend is observed with less than 10% difference. Figure 4-9 shows a comparison of model and experimental data. The deviation between the model results and the experimental data is less than 10%.

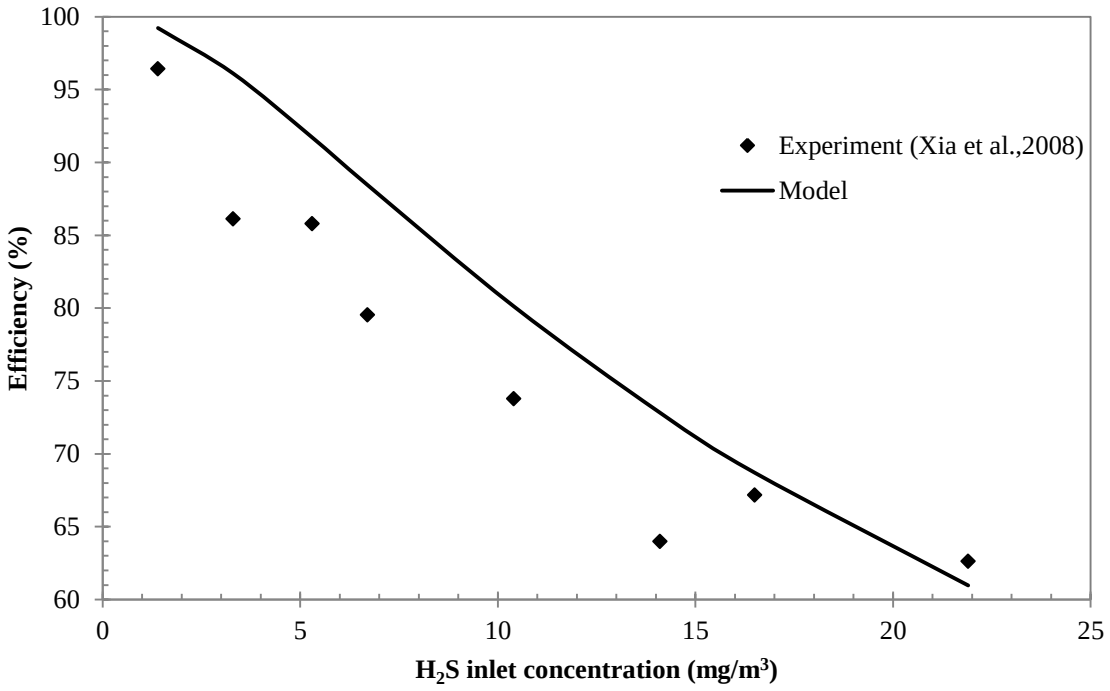

Figure 4-9: Comparison of Modeling results and Experimental data at fixed gas flow rate (140 cm^3/s)

Moreover, Xia et al. (2008) used another reaction volume with different reaction diameter (Tube-B) at different gas flow rate (808 cm^3/s) and the same trend was achieved. By increasing initial concentration of H_2S from 0.6 to 17.3 mg/m^3 the experimental data of process efficiency decreased from 61.83% to 10.15%. The model predicts the removal efficiency values from 80.17% to 20.67% at the same conditions, with slight overestimate to some extent. The Figure 4-10 below shows a comparison of the model and the experimental data. The deviation between the model results and the experimental data is less than 20%.

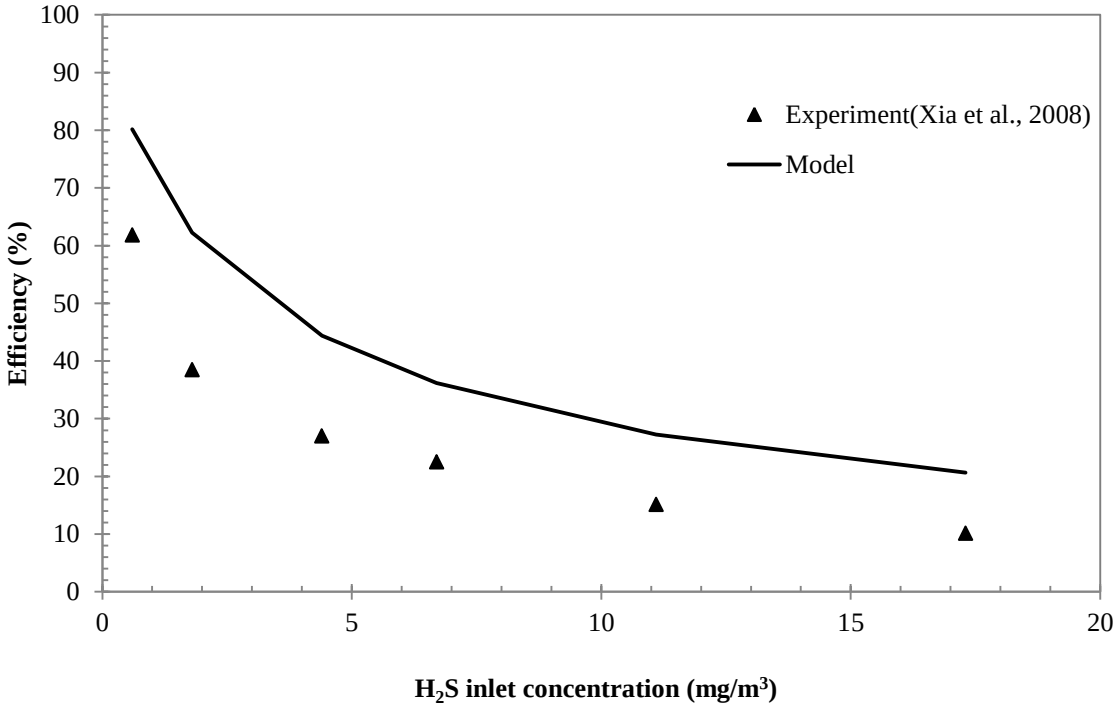

Figure 4-10: Comparison of Modeling results and Experimental data at fixed gas flow rate (808 cm^3/s) and different reactor diameter (Tube-B)

4.3.2. Effect of gas flow rate

As discussed in the previous section, by increasing gas flow rate, degradation efficiency decreases at a fixed concentration of H_2S. In order to validate the model for this effect, two sets of data for each reaction volume (Tube-A and Tube-B) with different gas flow rates were selected from Xia et al. (2008). A comparison between experimental data and model prediction can be used as model validation. Figures 4-11 and 4-12 show these comparisons. As clearly shown in both figures, at the same initial concentration, the removal efficiency is lower at higher value of gas flow rate for both experiments and model.

In Figure 4-11, the deviation between the model results and the experimental data is less than 10% for a flow rate of 0.14 L/s, and less than 20% for a flow rate of 0.42 L/s.

Also, in Figure 4-12, the values of the model results and the experimental data are apart less than 15% for a gas flow rate of 0.296 L/s, and less than 20% for a gas flow rate of 0.808 L/s.

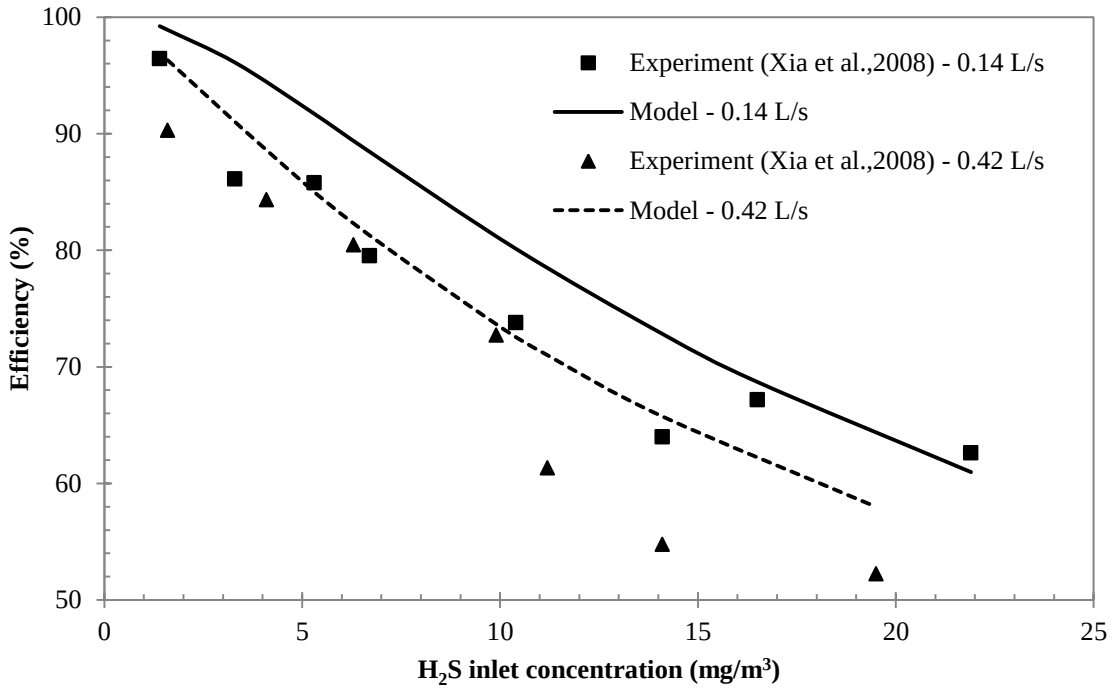

Figure 4-11: Comparison of Modeling results and Experimental data at different gas flow rate and the same reactor diameter (Tube-A)

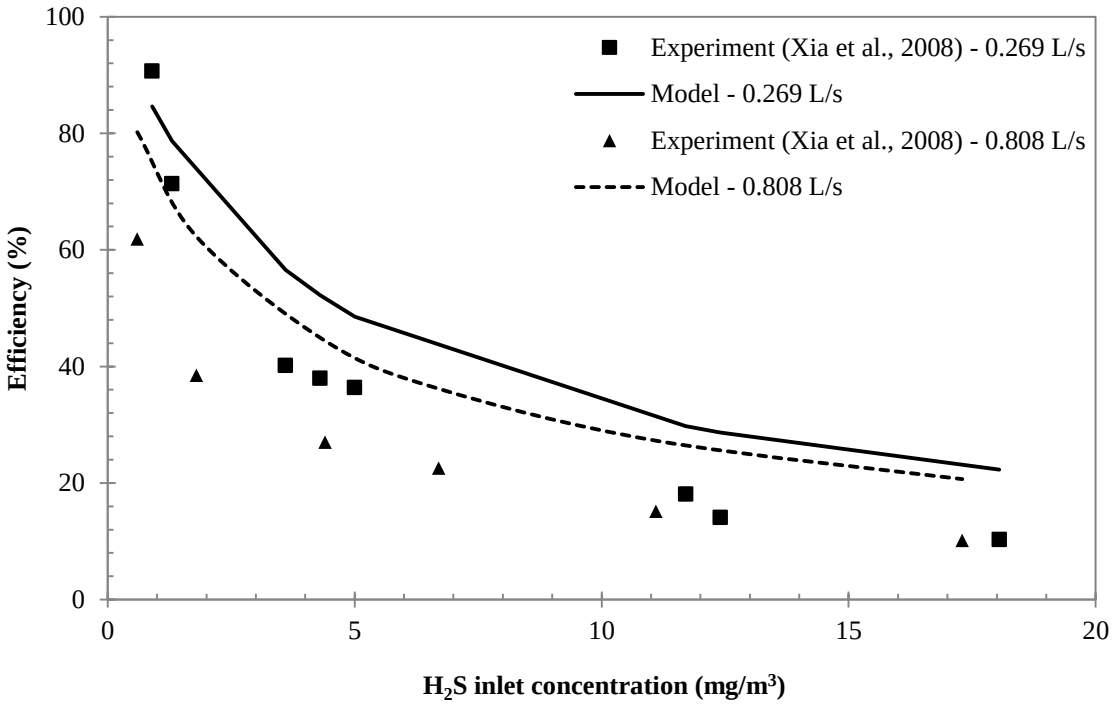

Figure 4-12: Comparison of Modeling results and Experimental data at different gas flow rate and the same reactor diameter (Tube-B)

4.4. Simulation results for extended model (Adding NO_x reactions)

In order to see the capability of the model to add other pollutants, some simulation results have been provided at two different conditions. The first case is the condition of H_2S molecules introduced to the reactor combined with NO molecules while the second one is a completely new case when only NO molecules are entering to the reactor.

4.4.1. Degradation of H_2S combined with NO

Simulation results indicate the degradation efficiency is quite high for both pollutants since at a fixed inlet concentration of NO (1 g/m^3) efficiency of H_2S decreases from 99.5% to 74.5% when its inlet concentration increases from 1 to 10 g/m^3 at a fixed volumetric flow rate of 1.5 L/min.

The process for NO in this case is almost completely efficient. Obviously, taking a higher concentration of NO may show its efficiency pattern more clearly; however predicting a pattern is not possible when both concentrations are changing at the same time, since these two pollutants have some interactions. Figure 4-13 shows both efficiencies in the case of fixed NO (1 g/m^3).

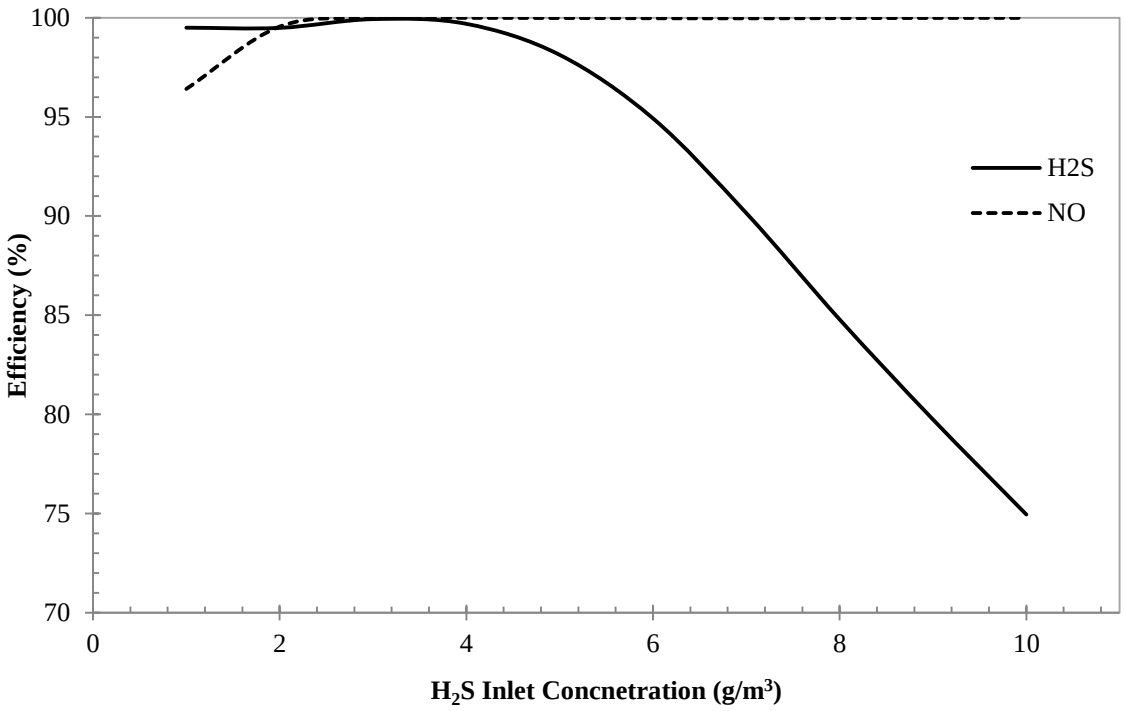

Figure 4-13: Simulation results for degradation efficiency of H_2S when combined with a fixed initial concentration of NO (1 g/m^3) and fixed gas flow rate (1.5 L/min)

When a combination of H_2S and NO enters to the reactor, as long as H_2S is the highly concentrated pollutant introduced to the reactor, SO_2 and H_2SO_4 are still the main reaction products in the reactor outlet. In case of low concentration of both pollutants, NO_2 might form and would decrease by increasing H_2S concentration; nevertheless, its amount is not at a level of concern. Moreover, one of the interactions between these two pollutants can produce a species

which is HSNO. This molecule is called “thionitrous acid”, “nitrosomercaptan” or “S-nitrosothiol”. It seems to be less hazardous rather than H_2S and NO alone. Nonetheless, the concentration of this species formed in the reactor is too low to be a concern. Figure 4-14 below shows simulation results for product analysis at fixed inlet NO concentration (1 g/m^3) and fixed gas flow rate (1.5 L/min) as a function of H_2S inlet concentration.

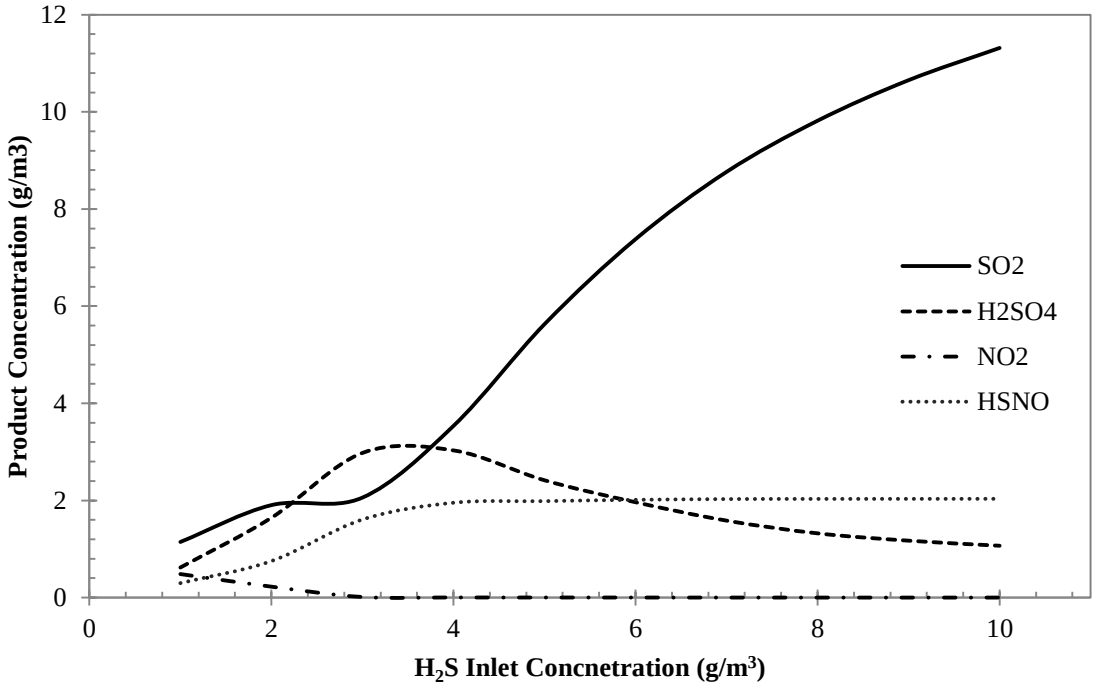

Figure 4-14: Simulation results for production analysis of H_2S when combined with a fixed initial concentration of NO (1 g/m^3) and fixed gas flow rate (1.5 L/min)

4.4.2. Degradation of NO alone

In this part, simulation results are provided for the extended model when NO is the only pollutant mixed with air and treated with UV photolysis. Simulation results indicate that this process might lead to lower conversions as H_2S alone or mixing H_2S and NO do. As shown in

Figure 4-15, removal efficiency decreases sharply from 99.22 to 31.13% when initial concentration of NO is varied from 0.5 to 5 g/m^3 at a fixed gas flow rate of 1 L/min.

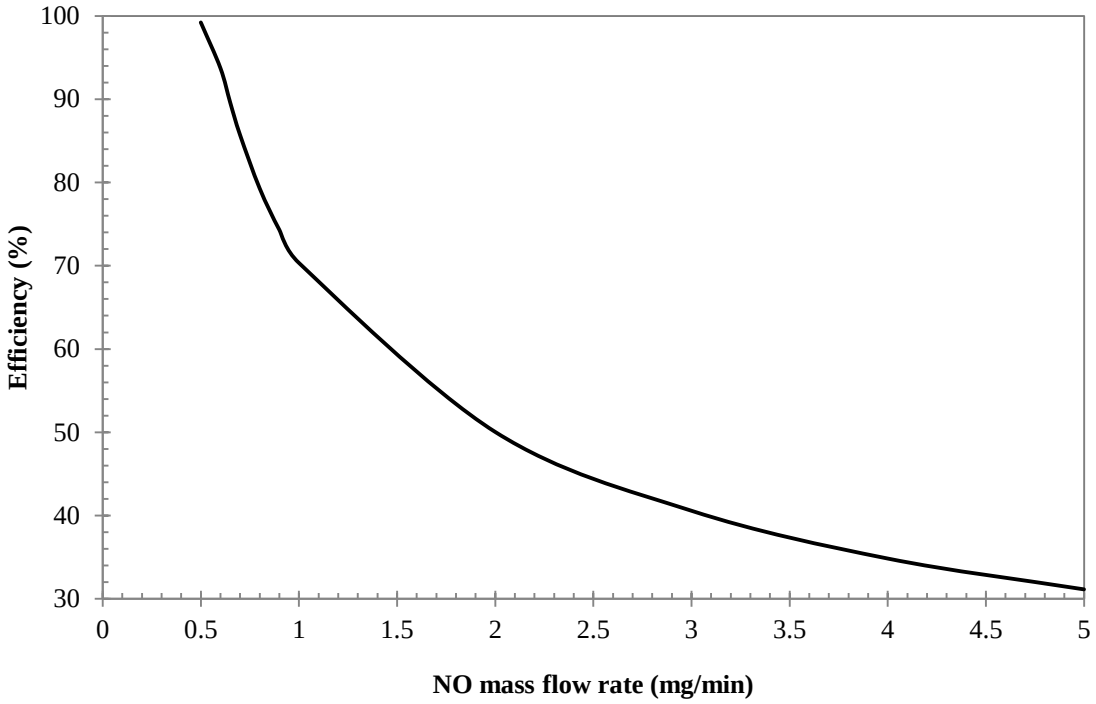

Figure 4-15: Simulation result for NO degradation efficiency as a function of mass flow rate

According to simulation results, it is expected that HNO_3 would be the main product of this process at low inlet concentration of NO. However, by increasing inlet concentration of NO and decreasing efficiency, this species will consume to form HNO_2. On the other hand, although NO_2 will be another product of this process at high NO concentration, the formation of NO_2 is not considered degradation, because NO oxidized to NO_2 rapidly in the atmosphere. Figure 4-16 shows these products distinctively as a function of NO inlet concentration.

It is notable that although the photolysis process of NO alone is not efficient as H_2S photolysis, the photolysis products, which are mainly HNO_3 and HNO_2 in this case, are soluble in water

which is indicating that the photolysis of NO degrade to the molecules which are less harmful and also easier to treat.

In case of photolysis of H_2S combined with NO, according to the simulation results, the concentrations of formed HNO_3 and HNO_2 are negligible compared with other photolysis products in this particular case, since a significant amount of OH radicals is consumed by other reactions based on their reaction mechanisms, therefor these species will be less formed.

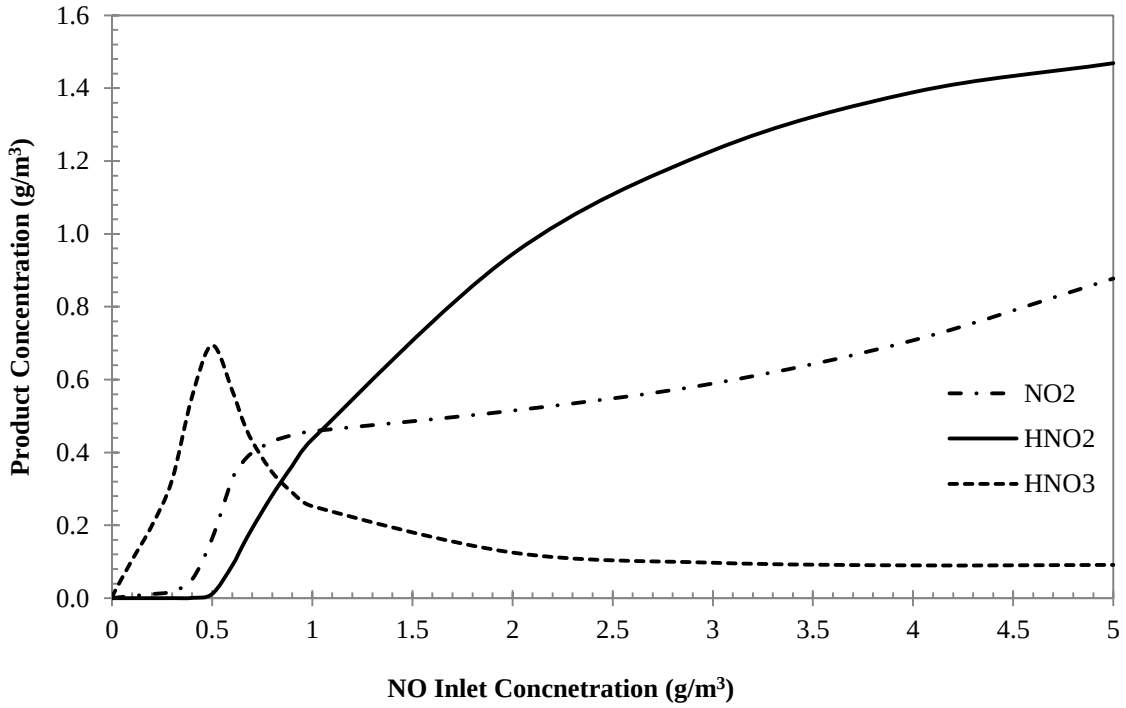

Figure 4-16: Simulation results for product analysis of NO photolysis at fixed volumetric flow rate (1 L/min)

CHAPTER 5 : PROCESS DESIGN AND FEASIBILITY STUDY

5.1. Process Feasibility

The energy cost is usually the main cost of photolysis processes. Thus, in feasibility studies it can be an appropriate parameter. The energy requirement followed by cost estimation was calculated in the current chapter. For all calculations a 40 W UV lamp has been assumed.

5.1.1. H_2S degradation

The basis of the calculation is a system treating 1 tonne per year of H_2S emitted from waste gas. Based on the model simulation, taking a fixed volumetric waste gas flow rate of 1 L/min, and assuming 90 % removal efficiency for each lamp, it is found that the required inlet concentration of H_2S is 6.88 g/m^3. In this case, the H_2S mass flow rate treated was calculated as below.

H_2S mass flow rate with 90 % efficiency with 1 L/min of volumetric flow rate is:

$$6.83\frac{\text{g}}{\text{m}^3}\cdot\frac{10^3 mg}{1g}\cdot 1\frac{\text{L}}{\text{min}}\cdot\frac{1\text{m}^3}{10^3 L}=6.83\frac{\text{mg}}{\text{min}}$$

In terms of total H_2S mass flow rate treated for a year it is determined as:

$$6.83\frac{\text{mg}}{\text{min}}\cdot\frac{60\,\text{min}}{1\,\text{hr}}\cdot\frac{24\text{hr}}{1\,\text{day}}\cdot\frac{365\text{day}}{1\text{year}}\cdot\frac{1\text{kg}}{10^6\,\text{mg}}=3.56\frac{\text{kg}}{\text{year}}$$

$$\text{Number of lamps required} = \frac{\text{Total } H_2S \text{ treated}}{H_2S \text{ mass flow rate per lamp}} = \frac{1000\ (\text{kg}/\text{year})}{3.56\ (\text{kg}/\text{year})} \cong 279$$

So, the annual energy consumption for this system is:

$$279\ \text{lamps} \times \frac{40\text{W}}{\text{lamp}} \times \frac{1\text{kW}}{10^3\text{W}} \times \frac{365\text{day}}{1\text{year}} \times \frac{24\text{hr}}{1\text{day}} = 97{,}762\ \text{kWh}$$

Considering $ 0.1 per kWh, the approximate annual electricity cost is $ 9,776.

Obviously, using larger and brighter lamps would reduce the capital cost practically; nevertheless, it would not have a pronounced impact on the energy sustainability. In addition, optimization of reactor effective diameter and volumetric flow rate can lessen the energy cost for this kind of processes. This will be discussed in Section 5.2.

5.1.2. Degradation of H_2S combined with NO

Since there are some interactions between species formed from H_2S and NO degradation, the inlet concentration of both to the reactor significantly contribute to the degradation of efficiency of each of these two pollutants. Based on simulation results, taking a fixed volumetric flow rate of gas stream at 1 L/min, a reasonable combined removal efficiency is found when the initial concentration is 10.9 g/m^3 and 5.5 g/m^3 for H_2S and NO respectively. In this situation the degradation efficiency for both H_2S and NO (on the other word, overall efficiency of the reactor) was 90 % (± 2%). The values of concentration of H_2S and NO were obtained by an iterative process on the developed code of the proposed model to find the unknown initial concentration of pollutants when the efficiency is known.

Converting NO to NO_2 is an obvious process, so it does not count as degradation process. For the above particular conditions, when approximately 90% of NO is converted, the degradation efficiency of NO_x (NO + NO_2) is around 70%, which is still good be a feasible process. However, in the following calculations, the corresponding concentration for approximately 90% conversion of NO is considered.

Now, assuming a system treating a combined amount of 1 tonne per year for of H_2S and NO (assuming equal treated quantities for both) emitted in the form of waste gas, the required lamps and energy cost estimation can be calculated as follows.

The mass flow rate of each H_2S and NO when mixed entering to the reactor with approximately 90 % efficiency with 1 L/min of volumetric flow rate is:

For H_2S: $10.9\frac{\text{g}}{\text{m}^3}\cdot\frac{10^3\text{mg}}{1\text{g}}\cdot 1\frac{\text{L}}{\text{min}}\cdot\frac{1\text{m}^3}{10^3\text{L}}=10.9\frac{\text{mg}}{\text{min}}$

For NO: $5.5\frac{\text{g}}{\text{m}^3}\cdot\frac{10^3\text{mg}}{1\text{g}}\cdot 1\frac{\text{L}}{\text{min}}\cdot\frac{1\text{m}^3}{10^3\text{L}}=5.5\frac{\text{mg}}{\text{min}}$

In terms of total mass flow rate treated for a year they are determined as follow:

For H_2S: $10.9\frac{mg}{\text{min}}.\frac{60\,\text{min}}{1hr}.\frac{24hr}{1day}.\frac{365day}{1year}.\frac{1kg}{10^6 mg}=5.73\frac{kg}{year}$

For NO: $5.5\frac{mg}{\text{min}}.\frac{60\,\text{min}}{1hr}.\frac{24hr}{1day}.\frac{365day}{1year}.\frac{1kg}{10^6 mg}=2.89\frac{kg}{year}$

So total numbers of lamps for each of these pollutants at the above conditions are calculated as:

Number of lamps required for H_2S = $\frac{\text{Total } H_2S \text{ treated}}{H_2S \text{ mass flow rate per lamp}}=\frac{500\,(^{\text{kg}}/_{\text{year}})}{5.73\,(^{\text{kg}}/_{\text{year}})}\cong 87$

Number of lamps required for NO = $\frac{\text{Total NO treated}}{\text{NO mass flow rate per lamp}}=\frac{500\,(^{\text{kg}}/_{\text{year}})}{2.89\,(^{\text{kg}}/_{\text{year}})}\cong 173$

So, taking total 173 lamps would be a sensible conservative assumption for the degradation of both H_2S and NO together with a high efficient process.

Hence, the annual energy consumption for this system is:

$$173\ \text{lamps} \times \frac{40\text{W}}{\text{lamp}} \times \frac{1\text{kW}}{10^3\text{W}} \times \frac{365\text{day}}{1\text{year}} \times \frac{24\text{hr}}{1\text{day}} = 60{,}620\ \text{kWh}$$

Considering $ 0.1 per kWh, the approximate annual electricity cost is $ 6,062.

Obviously, in this case NO mass flow rate would be limiting condition and has a demonstrative role to specify the total number of lamps. Therefore, number of required lamps should be calculated based on NO mass flow rate and the difference between two calculated above sets can be considered as an overdesign condition for the process.

5.1.3. Degradation of NO alone

In this case, the only air pollutant introduced to the reactor is NO. Taking the model simulation results and assuming a system treating 1 tonne per year of NO releasing form waste gas, taking a fixed volumetric flow rate of gas stream at 1 L/min, and assuming 90 % removal efficiency for each lamp, the corresponding inlet concentration of NO is found to be 0.645 g/m^3. The NO mass flow rate treated and was calculated as below.

NO mass flow rate with 90 % efficiency with unity volumetric flow rate is:

$$0.645\frac{\text{g}}{\text{m}^3} \cdot \frac{10^3\text{mg}}{1\text{g}} \cdot 1\frac{\text{L}}{\text{min}} \cdot \frac{1\text{m}^3}{10^3\text{L}} = 0.645\frac{\text{mg}}{\text{min}}$$

So, total NO mass flow rate treated for a year it is determined as:

$$0.645\frac{mg}{min}\cdot\frac{60min}{1hr}\cdot\frac{24hr}{1day}\cdot\frac{365day}{1year}\cdot\frac{1kg}{10^6 mg}=0.339\frac{kg}{year}$$

$$\text{Number of lamps required} = \frac{\text{Total NO treated}}{\text{NO mass flow rate per lamp}} = \frac{1000\ (^{kg}/_{year})}{0.339\ (^{kg}/_{year})} \cong 2950$$

Subsequently, the annual energy consumption for this system is:

$$2950\ \text{lamps}\times\frac{40W}{lamp}\times\frac{1kW}{10^3 W}\times\frac{365day}{1year}\frac{24hr}{1day}=1{,}033{,}680\ \text{kWh}$$

Considering $ 0.1 per kWh, the approximate annual electricity cost is $ 103,368.

It seems that the photolysis for NO alone is not as feasible as H_2S mixed with NO, or even H_2S alone, since it requires both higher capital investment and energy cost. If taking 70 % efficiency for NO degradation can be assumed acceptable, total number of required lamps and energy cost can be decreased 37%; however, electricity cost is still considerable to some extent as this value would be around $ 64,965 annually.

5.2. Degradation Efficiency Sensitivity Analysis

In order to evaluate the degradation efficiency sensitivity analysis, some important process conditions have to be changed, and then the simulation results should be compared at those different cases. Concerning this, the effect of changing process conditions on degradation efficiency was studied for different types of processes.

5.2.1. H_2S degradation

The results of reactor optimization of H_2S degradation are summarized in Table 5-1. In each step, all of the base case conditions have been kept fixed except the changing condition in the table. The base case was selected as a flow rate of 1.5 L/min and initial H_2S concentration of 5 g/m^3.

Table 5-1: Effect of process condition on H_2S degradation

Changing Condition	**H_2S degradation efficiency %**
Base case	82.25
Halving O_2 content (compared with regular air)	73.16
Halving relative humidity	82.09
Doubling relative humidity	82.32
Doubling reactor diameter (R_1× 2)	98.97
Tripling reactor diameter (R_1× 3)	99.92

Results clearly indicate that the main influencing factor is the reactor diameter. Increasing reactor diameter can increase the removal efficiency since it provides longer residence time, and better utilization of the light. Besides, as discussed in previous chapters, increasing the water content of the gas can enhance efficiency as it provides OH radical which is essentially important to decompose H_2S. Increasing oxygen increases the removal efficiency which is probably due to reaction of oxygen radicals to produce OH radicals.

5.2.2. Degradation of H_2S combined with NO

In this section, the influence of varying process conditions on degradation efficiency when both H_2S and NO are entering to the reactor was studied. Again, the base case was chosen as flow rate

of 1.5 L/min and initial concentration of 5 g/m^3 for both H_2S and NO. Simulation results are presented in Table 5-2 below.

Table 5-2: Effect of process condition on the degradation of H_2S and NO at the same time

Changing Condition	**H_2S degradation efficiency %**	**NO degradation efficiency %**
Base case	83.73	72.16
Halving O_2 content (compared with regular air)	83.40	71.98
Halving relative humidity	83.59	71.42
Doubling relative humidity	84.04	73.53
Doubling reactor diameter (R_1× 2)	88.07	71.50
Tripling reactor diameter (R_1× 3)	86.37	74.55
Halving initial concentration of NO	95.96	94.17
Doubling initial concentration of NO	67.54	56.06

Due to a number of interactions between species formed during H_2S and NO degradation, the efficiency trends are not easy to predict while efficiency variations are apparent for all changing conditions. However, increasing relative humidity and reactor diameter could increase the removal efficiency for both pollutants to some extent.

5.2.3. Degradation of NO alone

In order to see the effects of reactor process conditions on the degradation efficiency of NO in the absence of H_2S, an initial NO concentration of 5 g/m^3 and a flow rate of 1.5 L/min were selected as the base case. Table 5-3 shows the optimization results for the reactor in this case.

Table 5-3: Effect of process condition on the degradation of NO alone

Changing Condition	**NO degradation efficiency %**
Base case	27.02
Halving O_2 content (compared with regular air)	25.40
Halving relative humidity	19.69
Doubling relative humidity	37.41
Doubling reactor diameter (R_1× 2)	38.06
Tripling reactor diameter (R_1× 3)	48.90

As long as only one pollutant mixed with air is introduced to the reactor, the trend of process efficiency can be predicted by changing conditions. Similar to H_2S, increasing oxygen content and humidity of stream remarkably increase the removal efficiency. The effect of increasing reactor diameter by three times increases the efficiency around 45% as a major inducing factor. This effect is more pronounced in comparison with photolysis of H_2S alone.

CHAPTER 6 : CONCLUSIONS AND RECOMMENDATIONS

6.1. Concluding Remarks

A sophisticated simulation model was developed successfully to describe ultraviolet degradation of H_2S in waste gas. The photochemical reactor has been modeled with 19 chemical species and 47 chemical and photochemical reactions in total. Chemical and photochemical reactions, material balance and flow pattern have been completely considered for each species in the model. For the simulation of the light field, it is assumed that light rays are emitted perpendicular to the lamp, as Mahmoudkhani (2012) showed considering different light rays angles did not change the degradation efficiency significantly.

In order to validate the proposed model, the simulation results were compared with a photolysis experimental data set among few studies on H_2S photolysis or photocatalysis. In this regard, the experimental data of Xia et al. (2008) were taken and compared with model predictions obtained in the same conditions. Comparing simulation results with experimental data indicates that the model overestimates the process efficiency to some extent; however, trends observed in the actual data were very similar to the trends observed in the simulations in two different reactors, confirming that the model is sound, and can be used for feasibility studies.

In previous experimental works on either photolysis or photocatalysis of H_2S, all carried out at low initial concentration level of H_2S, it was found that SO_4^{2-} (or H_2SO_4) is the main product. The simulation results also confirm the formation of H_2SO_4 when low concentration of H_2S is being treated. In contrast, by increasing H_2S concentration in the system, since all hydroxyl

radicals (·OH) are consumed to degrade H_2S based on its reaction mechanism, H_2SO_4 production would decrease and SO_2 formed instead. Therefore, it can be concluded based on the model that the UV degradation technique is effective, and it decomposes H_2S to less harmful products which are also easier to be treated.

To date, this is the first mechanistic model developed for H_2S photochemical waste gas treatment. Simulation results indicated that annual electricity cost of treating one tonne per year of H_2S using photolysis to remove around 90% pollutant is about $ 9,776. Actual energy cost requirements may be higher than this value since it is thought that the model overestimates the process efficiency slightly. On the other hand, based on experimental data in laboratory scale, adding ozone, catalyst, and increasing the water content (Li et al., 2012) and using a different type of reactor (Huang et al., 2012) can increase degradation efficiency so these effects might offset the possible overestimate and might cause lower energy consumption.

In addition, model predictions for degradation of H_2S combined with NO and also degradation of NO alone were included. Simulation results indicated that the efficiency of the H_2S photolysis process when NO is present in the system is higher than the process efficiency of H_2S or NO alone. Alternatively, when two waste gas streams, one polluted with H_2S and the other with NO, are introduced to the photoreactor, the degradation efficiency can be higher than two systems treating each of those of pollutants separately because of their interactions. It is believed that Sulfanyl radical (·HS) has similar role in degradation of NO_x species as OH radical has in the H_2S photolysis.

6.2. Future Work and Recommendations

Although the model was validated with some experimental data, it would be of value to compare it with new experimental data, to ensure that the reactor configuration conforms to the model assumptions. Results should be obtained in other different conditions to further validate the model.

One of the other areas of future research might be to test the effect of adding more pollutant species to see the predicted effects of interactions between molecules for each pollutant. As shown, by extending the model with all of the NO_x species reactions, the proposed model allows to add other pollutants and is able to predict degradation efficiency for each species and moreover product analysis when of more than one pollutant is present.

In the current model, all reaction terms are entered into the chemical kinetics model manually; even for the extended model. Now, since it is established that the model is capable of handling more than one pollutant, it is proposed for the future to have all the reaction information, both chemical and photochemical, in a data bank to recall them automatically by the model when they are present as pollutants. In other words, it may be planned for the future to have a comprehensive and sophisticated general model for any kind of pollutant and any type of photoreactor which can be used either for any specific pollutant or combining more than one (such as hydrocarbons) and then see the efficiency and product predictions; which means a general modular comprehensive model.

Obviously, in all cases discussed above, pilot scale studies are required to examine the practical feasibility of the process.

REFERENCES

Allen, T.O., and Roberts, A.P., "*Production Operation: Well Completions, Worker and Stimulation*", 4th Ed., Oil & Gas Consultants International (OGCI), **2000**.

Ashtolz, D.C., Crose, A.E., and Troe, J., "Temperature dependence of the ozone absorption coefficient in the Hartley continuum", *J. Phys. Chem.*, 86, 696-699, **1982**.

ASM, American Society for Metals, "*Corrosion in the Petrochemical Industry*", ASM International publisher, **1994**.

Atkinson, B., Brocklebank, M.P., Card, C.C.H., and Smith, J.M., "Low Reynolds number developing flows", *AIChE* 15, 548-553, **1969**.

Atkinson, R., Baulch, D.L., Cox, R.A., Crowley, J.N., Hampson, R.F., Hynes, R.G., Jenkin M.E., Rossi, M.J. and Troe, J., "Evaluated kinetic and photochemical data for atmospheric chemistry: Volume I – gas phase reactions of O_x, HO_x, NO_x and SO_x species", *Atmos. Chem. Phys.*, 4, 1461–1738, **2004**.

Atyabi, M., "Ultraviolet Degradation of BTX in Waste Gas: Effects of Photocatalysis and Ozone Premixing", M.Sc. thesis, University of Calgary, Canada, **2013**.

Bansal, R.K., "*A Textbook of Fluid Mechanics and Hydraulic Machines*", Laxmi Publications, **2005**.

Barrera, M., "Photochemical treatment of organic constituents and bacterial pathogens from synthetic slaughterhouse wastewater by combining vacuum UV and UV-C", M.Sc. thesis, *Ryerson University*, Canada, **2011**.

Bass, A.M., Ledford, A.E., and Laufer, A.H., "Extinction coefficients of NO_2 and N_2O_4*", J. Res. Natl. Bur. Stand.*, 80A, 143-166, **1976**.

Bird, R.B., Stewart, W.E., and Lightfoot, E.N., "*Transport Phenomena*", 2nd Ed., J. Wiley & Sons, **2002**.

Bott, R.D., "Flaring: Questions + Answers", 2nd Ed., Canadian Centre for Energy Information, **2007**.

Braslavsky, S.E., "Glossary of terms used in photochemistry", 3rd Ed., *Pure and Applied Chemistry*, **2007**, 293-465.

Burkholder, J.B., and McKeen, S., "UV absorption cross sections for SO_3", *Geophys. Res. Lett.*, 24, 3201-3204, **1997**.

Burkholder, J.B., Talukdar, R.K., Ravishankara, A.R., and Solomon, S., "Temperature Dependence of the HNO_3 UV Absorption Cross Sections", *J. Geophys. Res.*, **1993,** 98, 22937-22948.

Canela M.C., Alberici R.M., and Jardim W.F., "Gas-phase destruction of H_2S using TiO_2/UV-VIS", *J. Photochem. and Photobio. A: Chemistry*, 112, **1998**, 73-80.

CAPP, Canadian Association of Petroleum Producers, "Technical report of a National Inventory of Greenhouse Gas (GHG), Criteria Air Contaminant (CAC) and Hydrogen Sulphide (H_2S) Emissions by the Upstream Oil and Gas Industry", Vol. 2, **2005**.

CCOHS, Canadian Centre for Occupational on Health and Safety, *H_2S database*, Accessed on March **2013**. <http://www.ccohs.ca/products/databases/samples/CHEMINFO.html>

Chen, F., Yang, Q., and Pehkonen, S.O., Ray, M.B., "Modeling of Gas-Phase Photodegradation of Chloroform and Carbon Tetrachloride", *J. Air & Waste Manage. Assoc.*, **2004**, 54, 1281–1292.

Chung, C-Y., Chew, B-M., Cheng, M.B., and Lee, Y-P., "Temperature dependence of absorption cross-section of H_2O, HDO, and D_2O in the spectral region 140-193 nm", *Nucl. Instr. Meth. Phys. Res. A*, 467-468, 1572-1576, **2001**.

Cooper, C.D., Alley, F.C., "*Air Pollution Control: A Design Approach*", 4th Ed., Waveland Press Inc., **2010**.

Cussler, E.L., "*Diffusion, Mass Transfer in Fluid Systems*", 3rd Ed., Cambridge University Press, **2009**.

Danielache, S.O., Eskebjerg, C., Johnson, M.S., Ueno, Y., and Yoshida, N., "High-precision spectroscopy of 32S, 33S, and 34S sulfur dioxide: Ultraviolet absorption cross sections and isotope effects", *J. Geophys. Res. D* 113, D17314, **2008**.

De Visscher, A., "*Air Dispersion modeling, Foundations and Applications*", J. Wiley & Sons, in press, **2013**.

De Visscher, A., Dewulf, J., Van Durme, J., Leys, C., Morent, R., Van Langenhove, H., "Non-thermal plasma destruction of allyl alcohol in waste gas: kinetics and modeling", *Plasma Sources Sci. Eng. 17*, **2008**, 015004.

De Visscher, A., Rezaei, M., Mahmoudkhani, F., Langford, C.H., Vaisman, E. "Photochemical Degradation of BTEX in Waste Gas: Experiments and Modeling", *Proceedings 103rd Conference of the Air and Waste Management Association*, Calgary, 2010. Paper 2010-A-594-AWMA, **2010**.

Dean, J.A., "*Lang's Handbook of Chemistry*", 15th Ed., McGraw Hill Inc., **1999**.

Demeestere, K., Dewulf, J., and Van Langenhove, H., "Heterogeneous Photocatalysis as an Advanced Oxidation Process for the Abatement of Chlorinated, Monocyclic Aromatic and Sulfurous Volatile Organic Compounds in Air: State of the Art", *Crit. Rev. Environ. Sci. Technol.*, 37(6), **2007,** 489-538.

Driscoll, J.N., and Arneck, D.P., "Primary Processes in the Photolysis of SO_2, at 1849 Å", *J. Phys. Chem*., **1968**, 72 (11), 3736–3740.

EPA, "Advanced Photochemical Oxidation Processes Handbook", Office of Research and Development, Washington, DC, **1998**.

EPA, "Hydrogen Sulfide Corrosion: Its consequence, detection and control", Office of Water, Washington, DC, **1991**.

EPA, "National Air Quality and Emissions Trend report, 1998", Research Triangle Park, NC, **2000**.

EPA, "Report to Congress on Hydrogen Sulfide Emissions with the Extraction of Oil and Natural Gas", Research Triangle Park, NC, **1993**.

Fogler, H.S., "*Elements of Chemical Reaction Engineering*", 4th Ed., Prentice Hall, **2005**.

Froment, G.F., and Bischoff, K.B., "*Chemical Reactor Analysis and Design*", 2nd Ed., John Wiley & Sons, New York, **1993**.

Fuller, E.N., Ensley, K., and Giddings, J.C., "Diffusion of Halogenated Hydrocarbons in Helium. The Effect of Structure on Collision Cross Sections", *J. Phys. Chem.*, 73, 3679-3685, **1969**.

Gutierrez, R.L., Bourgeous, K.N., Salveson, A., Meir, J., and Slater, A., "Microwave UV: A New Wave Of Tertiary Disinfection", *Proceedings of the Water Environment Federation, WEFTEC*, **2006**: Session 31 through Session 40, 2853-2864.

Heicklen, J., Kelly, N., and Partymiller, K., "The photophysics and photochemistry of SO_2", *Rev. Chem. Intermed.*, **1980**, Vol. 3, 315-404.

Huang, L., Xia, L., Ge, X., Jing, H., Dong, W., and Hou, H., "Removal of H_2S from gas stream using combined plasma photolysis technique at atmospheric pressure", *Chemosphere*, 88, **2012**, 229–234.

Jayne, J.T., Pöschl, U., Chen, Y., Dai, D., Molina, L.T., Worsnop, D.R., Kolb, C.E., and Molina, M.J., "Pressure and Temperature Dependence of the Gas-Phase Reaction of SO_3 with H_2O and the Heterogeneous Reaction of SO_3 with H_2O/H_2SO_4 Surfaces", *J. Phys. Chem.* A, **1997,** 101, 10000-10011.

Jeong, J. Sekiguchi, K., and Sakamoto, K., "Photochemical and photocatalytic degradation of gaseous toluene using short-wavelength UV irradiation with TiO_2 catalyst: comparison of three UV", *Chemosphere*, 57, **2004**, 663-671.

Johnston, H.S., and Graham, R., "Photochemistry of No_x and HNO_x Compounds", *Can. J. Chem.*, 52, 1415, **1974**.

Kataoka, S., Lee, E., Tejedor-Tejedor, M.I., and Anderson, M.A., "Photocatalytic degradation of hydrogen sulfide and in situ FT-IR analysis of reaction products on surface of TiO_2", *Applied Catalysis B: Environmental*, 61, **2005**, 159–163.

Koda, S., Koga, K., Takizawa, K., Ihara, Y., and Takami, A., "Photodissociation of H_2S doped in low temperature rare gas solids under UV irradiation", *J. Chem. Phys*., 274, **2001**, 283-289.

Koteeswaran, F., "CO_2 and H_2S Corrosion in Oil Pipelines", MSc thesis, *University of Stavanger*, Norway, **2010**.

Kovalenko, O.N., Kundo, N.N., and Kalinkin, P.N., "Kinetics and Mechanism Of Low-Temperature Oxidation Of H_2S With Oxygen In The Gas Phase", *React. Kinet. Catal. Lett.*, Vol. 72, No. 1, 139-145, **2001**.

Kralik, P., Kusic, H., Koprivanac, N., and Bozic, A.L., "Degradation of chlorinated hydrocarbons by UV/H_2O_2: The application of experimental design and kinetic modeling approach", *Chem. Eng. J.*, 158, **2010,** 154–166.

Li, X., Zhang, G., and Pan, H., "Experimental study on ozone photolytic and photocatalytic degradation of H_2S using continuous flow mode", *J. Hazard. Mater.*, 199–200, **2012**, 255–261.

Liu, X., Hwang, D.W., Yang, X.F., Harich, S., Lin, J.J., and Yang, X., "Photodissociation of hydrogen sulfide at 157.6 nm: Observation of SH bimodal rotational distribution", *J. Chem. Phys*. 111, **1999**, 3940-3945.

Lovejoy, E.R., Hanson, D.R., and Huey, L.G., "Kinetics and Products of the Gas-Phase Reaction of SO_3 with Water", *J. Phys. Chem.*, **1996**, 100, 19911-19916.

Luo, Y.R., "*Comprehensive Handbook of Chemical Bond Energies*", Boca Raton, FL. CRC press, **2007**.

Mahmoudkhani, F., "Simulation of a Photochemical Reactor for Benzene Elimination from Waste Gas", M.Sc. thesis, *University of Calgary*, Canada, **2012**.

Mohseni, M., and Zhao, J.L., "Coupling ultraviolet photolysis and bilofiltration for enhanced degradation of aromatic air pollutants." *J. Chem. Technol. Biotechnol.* **2006**, *81*, 146-151.

NPRI (*National Pollutant Release Inventory*), Environment Canada, June **2012**, Accessed on March 2013. < http://www.ec.gc.ca/inrp-npri/ >

Obuka, N.S.P., Okoli, N.C., Ikwu, G.R., and Chukwumuanya, E.O., "Review of Corrosion Kinetics and Thermodynamics of CO_2 and H_2S Corrosion Effects and Associated Prediction/Evaluation on Oil and Gas Pipeline System", *Int. J. Sci. & Tec. Res.*, 1, May **2012**.

OHS, Occupational Health and Safety of Alberta, "Hydrogen Sulphide at the Work Site", Government of Alberta, **2010**.

Oilfield Glossary, Schlumberger, Accessed on March **2013**.
<http://www.glossary.oilfield.slb.com/ >

Oppenländer, T., "*Photochemical Purification of Water and Air, Advanced Oxidation Processes (AOPs): Principles, Reaction Mechanisms, Reactor Concepts*", Wiley-VCH, Weinheim, Germany, **2003**.

Osborne, B.A., Marston, G., Kaminski, L., Jones, N.C., Gingell, J.M., Mason, N., Walker, I.C., Delwiche, J., and Hubin-Franskin, M.J., "Vacuum ultraviolet spectrum of dinitrogen pentoxide" *J. Quant. Spectrosc. Radiat. Transf.*, 64, 67-74, **2000**.

Pereira, V.J., Weinberg, H.S., Linden, K.G., and Singer, P.C., "UV degradation kinetics and modeling of pharmaceutical compounds in laboratory grade and surface water via direct and indirect photolysis at 254 nm.", *Environ. Sci. Technol*., **2007**, 41, 1682- 1688.

Perry, R.H., Green, D.W., Maloney, J.O., "*Perry's Chemical Engineers' Handbook*", 7th Ed., McGraw-Hill, **1997**.

Portela, R., Sa´nchez, B., Coronado, J.M., Candal., R., and Sua´rez, S. "Selection of TiO_2-support: UV-transparent alternatives and long-term use limitations for H_2S removal", *Catal. Today*, 129, **2007**, 223–230.

Portela, R., Tessinari, R.F., Suárez, S., Rasmussen, S.B., Hernández-Alonso, M.D., Canela, M.C., Ávila, P., and Sánchez, B. "Photocatalysis for Continuous Air Purification in Wastewater Treatment Plants: From Lab to Reality", *Environ. Sci. Technol.* **2012**, 46, 5040−5048.

Rogers, L.J., Ashfold, M., Matsumi Y., Kawasaki, M., and Whitaker, B.J., "Photolysis of CH_3SH and H_2S at 243.1 nm studied by photofragment ion imaging", *J. Chem. Soc., Faraday Trans.*, **1996**, 92, 5181-518.

Sanches, S., Leitão, C., Penetra, A., Cardoso, V., Ferreira, E., Benoliel, M.J, Barreto Crespo, M.T., and Pereira, V.J. "Direct photolysis of polycyclic aromatic hydrocarbons in drinking water sources", *J. Hazard. Mater.*, 192, September **2011**, 1458–1465.

Sander, S.P., J. Abbatt, J.R. Barker, J.B. Burkholder, R.R. Friedl, D.M. Golden, R.E. Huie, C.E. Kolb, M.J. Kurylo, G.K. Moortgat, V.L. Orkin and P.H. Wine "Chemical Kinetics and Photochemical Data for Use in Atmospheric Studies, Evaluation No. 17," *JPL Publication 10-6, Jet Propulsion Laboratory,* Pasadena, **2011**.

Seader, J.D., Henley, E.J., and Roper, D.K., "*Separation Process Principles: Chemical and Biochemical Operations*", 3rd Ed., John Wiley & Sons, **2010**.

Sellami, M.H., Hassen, A., and Sifaoui, M.S., "Modelling of UV radiation field inside a photoreactor designed for wastewater disinfection, Experimental validation", *J. Quant. Spectr. Rad. Trans.*, 78, **2003**, 269 –287.

Shen, Y.S., and Ku, Y., "Decomposition of gas phase trichloroethane by the UV/TiO_2 process in the presence of ozone", *Chemosphere*, 46, **2002**, 101-107.

Skrtic, L, Hydrogen Sulfide, Oil and Gas, and People's Health", M.Sc. thesis, *University of California*, Berkeley, **2006**.

Sneep, M., and Ubachs, W., "Direct measurement of the Rayleigh scattering cross section in various gases", *J. Quant. Spectrosc. Radiat. Transf.*, 92, 293-310, **2005.**

Steijns, M., Derks, F., Verloop, A., and Mars, P., "The Mechanism of the Catalytic Oxidation of Hydrogen Sulfide", *J. Cata.*, 42, 87-95, **1976**.

Stockwell, W.R., Calvert, J.G., "The mechanism of the HO-SO_2 reaction", *Atmos. Environ.* **1983**, 17, 2231-2235.

Troe, J., "Predictive Possibilities of Unimolecular Rate Theory", *J. Phys. Chem.*, 83, No.7, **1979**.

Vandaele, A.C., Hermans, C., and Fally, S., "Fourier transforms measurements of SO_2 absorption cross sections: II. Temperature dependence in the 29000-44000 cm-1 (227-345 nm) region", *J. Quant. Spectrosc. Radiat. Transfer* 110, 2115-2126, **2009**.

Wang, J.H., and Ray M.B., "Application of ultraviolet photooxidation to remove organic pollutants in the gas phase", *Sep. Purif. Technol*. **2000**, 11-20.

Weiner, B.R., Levene, H.B., Valentini, J.J., and Baronavski, A.P., "Ultraviolet photodissociation dynamics of H_2S and D_2S", *J. Chem. Phys.*, 90, (3), **1989**.

White, F., "*Fluid Mechanics*", 5th Ed., McGraw Hill, **2003**.

Wine, P.H., Kreutter, N.M., Gump, C.A., and Ravishankara, A.R., "Kinetics of OH reactions with the atmospheric sulfur compounds H_2S, CH_3SH, CH_3SCH_3, and CH_3SSCH_3", *J. Phys. Chem.*, **1981**, 85 (18), 2660–2665.

Wu, C.Y.R., and Chen, F.Z., "Temperature-dependent photoabsorption cross sections of H_2S in the 1600-2600 Å region", *J. Quant Spectrosc. Radiat. Transfer*, 60, 17-23, **1998**.

Wu, C.Y.R., Yang, B.W., Chen, F.Z., Jude, D.L., Caldwell, J., and Trafton L.M., "Measurements of high-, room-, and low-temperature photoabsorption cross sections of SO_2 in the 2080- to 2950-Å region, with application to IO", *Icarus* 145, 289-296, **2000**.

Xia, L-Y, Gu, D-H, Tan, J., Dong, W-B, and Hou, H-Q, "Photolysis of low concentration H_2S under UV/VUV irradiation emitted from microwave discharge electrodeless lamps", *Chemosphere*, Vol.71, **2008**, 1774-1780.

Yoshino, K., Parkinson, W.H., Ito, K., and Matusi, T., "Absolute absorption cross-section measurements of Schumann–Runge continuum of O_2 at 90 and 295 K", *J. Molec Spectr.*, 229, **2005**, 238–243.

Yue, P.L. "Modelling of kinetics and reactor for water purification by photo-oxidation", *Chem. Eng. Sci.*, 48, January **1993,** 1-11.

Zhang, L., and Anderson, W.A., "Kinetic analysis of the photochemical decomposition of gas-phase chlorobenzene in a UV reactor: Quantum yield and photonic efficiency", *Chem. Eng. J.*, 218, **2013**, 247–252.

APPENDICES

Appendix A: Developed code for H_2S photolysis model

Data file:

```
length = 56;            % Reactor length in cm
dz = 1;
zspan = 0:dz:length;
Nnodes = 19;            % Number of internal nodes in the grid
Ncomp = 19;             % Number of compounds considered
P = 89000;              % Pressure in Pa
T = 310;                % Temperature in K
Ctot = P/1.38e-23/T;    % Concentration in molecules per m3
Ctot = Ctot/1e6;        % Concentration in molecules per cm3
MMh2s=34.08;
Cmh2s=1;                %Concentration in grams per m3
Ch2s=Cmh2s/MMh2s;       %Concentration in moles per m3
Ch2s=Ch2s*6.022e23;     %Concentration in molecules per m3
yh2s = Ch2s/Ctot/1e6;   % H2S mole fraction
yH2O = 0.002;           % Water mole fraction
yO3 = 0.00;
yO2 = 0.21*(1-yH2O-yh2s-yO3); % O2 mole fraction
yN2 = 0.79*(1-yH2O-yh2s-yO3); % N2 mole fraction
Ch2s = Ctot*yh2s;       % H2S concentration (molecules/cm3)
CH2O = Ctot*yH2O;
CO2 = Ctot*yO2;
CN2 = Ctot*yN2;
CO3 = Ctot*yO3;

% Initial concentrations:
%y0(i+(j-1)*Ncomp) is initial conc. of compound j in node point i from center
% j  Compound
% -- --------
% 1  H2S
% 2  O2
% 3  N2 + argon
% 4  H2O
% 5  O radical (O(3P))
% 6  OH radical
% 7  HO2 radical
% 8  O(1D) radical
% 9  O3
% 10 H2O2
% 11 HS radical
% 12 S radical
% 13 SO radical
% 14 SO2
% 15 SO3
% 16 HSO3 radical
% 17 HSO2 radical
```

```
% 18 HSO radical
% 19 H2SO4

for i = 1:Nnodes
    y0(i) = Ch2s;
    y0(i+Nnodes) = CO2;
    y0(i+2*Nnodes) = CN2;
    y0(i+3*Nnodes) = CH2O;
    for j = 4:Ncomp-1
        y0(i+j*Nnodes) = 0;
    end
    y0(i+8*Nnodes) = CO3;
end
r0 = 1.25;                % Internal diameter, cm
r1 = 2.1;                 % External diameter, cm
for j = 1:Ncomp
    for k = 1:2              % k is spectral line (1 = 185 nm, 2 = 254 nm)
        sig(j,k) = 0;
    end
end
sig(1,1) = 3.82e-18;      % Sigma h2s at 185 nm
sig(1,2) = 7.45e-21;
sig(2,1) = 2e-21;
sig(4,1) = 5.5e-20;
sig(7,1) = 324.8e-20;
sig(7,2) = 29.9e-20;
sig(9,1) = 66.1e-20;
sig(9,2) = 1148e-20;
sig(10,1) = 80.1e-20;
sig(10,2) = 6.99e-20;
sig(14,1) = 3.65e-18;
sig(14,2) = 1.35e-19;
sig(15,1) = 9.95e-19;
sig(15,2) = 1.34e-20;
power1 = 40*0.08;             % Emitted light at 185nm (W)
power2 = 40*0.30;             % Emitted light at 254nm (W)
nu1 = 299792458/185e-9;
nu2 = 299792458/254e-9;
photon1 = 6.626e-34*nu1;      % Photon energy at 185 nm
photon2 = 6.626e-34*nu2;      % Photon energy at 254 nm
E0(1) = power1/photon1/length/2/pi/r0; % Photons per cm2 per s leaving lamp
E0(2) = power2/photon2/length/2/pi/r0; % 1 = 185 nm, 2 = 254 nm

D = 0.7914*(T^1.75)/P;  %H2S diffusivity (cm2/s)
Q = 1000/60;            %Flow rate (cm3/s)
U = Q/pi/(r1*r1-r0*r0); %Mean gas velocity (cm/s)
reflamp = 0.7;          %Reflection at the lamp
reflamp2 = 0.7;         %Fraction of the received light at the lamp reflected
```

Function file:

```
function dydz = f(z,y,dz,Nnodes,Ncomp,r0,r1,sig,E0,D,U,P,T,reflamp,reflamp2)

dydz = zeros(Nnodes*Ncomp,1);

% j  Compound
% -- --------
% 1  H2S
% 2  O2
% 3  N2 + argon
% 4  H2O
% 5  O radical (O(3P))
% 6  OH radical
% 7  HO2 radical
% 8  O(1D) radical
% 9  O3
% 10 H2O2
% 11 HS radical
% 12 S radical
% 13 SO radical
% 14 SO2
% 15 SO3
% 16 HSO3 radical
% 17 HSO2 radical
% 18 HSO radical
% 19 H2SO4

dr = (r1-r0)/(Nnodes+1);   % Node distance

% User-friendly notation of concentrations: i = node number
%                                           j = compound number

for j = 1:Ncomp
    for i = 1:Nnodes
        C(j,i+1) = y(i+Nnodes*(j-1));        % concentration of j in node i,
                                             molecules/cm3
    end
    C(j,1)=C(j,2)-(C(j,3)-C(j,2))/3;   % boundary condition: zero radial flux
    C(j,Nnodes+2) = C(j,Nnodes+1) - (C(j,Nnodes) - C(j,Nnodes+1))/3;
end

% calculate radiation fields

Eref(1,1)=E0(1)/reflamp;    %Considering original radiation from the lamp
Eref(1,2)=E0(2)/reflamp;    %Considering original radiation from the lamp
for k = 1:2
    for i=1:Nnodes+1
        Etot(i+1,k)=0;
    end
    while (Eref(1,k)>0.01*E0(k))
    E(1,k) = reflamp*Eref(1,k);
    for i = 1:Nnodes+1
```

```
        Ei = E(i,k);
        r = r0 + dr*(i-0.5);
        alpha = 0;
        for j = 1:Ncomp
            Ci(j) = (C(j,i) + C(j,i+1))/2;
            alpha = alpha + Ci(j)*sig(j,k);
        end
        E(i+1,k) = (Ei/dr - alpha*Ei/2 - Ei/2/r)/(1/dr + alpha/2 + 1/2/r);
        if E(i+1,k) < 0
            E(i+1,k) = 0;
        end
    end
    Eref(Nnodes+2,k)=0.99*E(Nnodes+2,k);
    for i=Nnodes+1:-1:1
        Erefi=Eref(i+1,k);
        r=r0+dr*(i-0.5);
        alpha=0;
        for j=1:Ncomp
            Ci(j)=(C(j,i)+C(j,i+1))/2;
            alpha=alpha+Ci(j)*sig(j,k);
        end
        Eref(i,k)=(Erefi/dr+Erefi/2/r-alpha*Erefi/2)/(1/dr-1/2/r+alpha/2);
        if Eref(i,k)<0
            Eref(i,k)=0;
        end
    end
    for i=1:Nnodes+2
        Etot(i,k)=Etot(i,k)+E(i,k)+Eref(i,k);
    end
    end
end

for i = 2:Nnodes+1
    % Calculate reaction rates per reaction
    Ph2s = C(1,i)*1.38e-23*T*1e6;      % H2S partial pressure, Pa
    Pinert = (C(2,i)+C(3,i)+C(4,i))*1.38e-23*T*1e6;
    phih2s185 = 1;
    phih2s254 = 1;
    phiso2185 = 0.27;
    phiso2254 = 0;
    phiso3185 = 1;
    phiso3254 = 1;
    rp1(i) = C(1,i)*(phih2s185*sig(1,1)*Etot(i,1)+
             phih2s254*sig(1,2)*Etot(i,2));
    rp2(i) = C(4,i)*sig(4,1)*Etot(i,1);
    rp3(i) = C(9,i)*(sig(9,1)*Etot(i,1) + sig(9,2)*Etot(i,2));
    rp4(i) = C(7,i)*(sig(7,1)*Etot(i,1) + sig(7,2)*Etot(i,2));
    rp5a(i) = C(10,i)*(sig(10,1)*Etot(i,1)*0.75 + sig(10,2)*Etot(i,2));
    rp5b(i) = C(10,i)*sig(10,1)*Etot(i,1)*0.16;
    rp6(i) = C(14,i)*(phiso2185*sig(14,1)*Etot(i,1)+
             phiso2254*sig(14,2)*Etot(i,2));
    rp7(i) = C(15,i)*(phiso3185*sig(15,1)*Etot(i,1)+
             phiso3254*sig(15,2)*Etot(i,2));
```

```
% Oxygen atom reactions

ko1 = 2.3e-11*exp(110/T);
ko2 = 2.7e-11*exp(224/T);
ko3 = 1.4e-12*exp(-2000/T);
ko4 = 6e-34*(T/300)^(-2.8)*C(2,i) + 5.6e-34*(T/300)^(-2.8)*C(3,i);
ko5 = 2.7e-34*T^(-0.41)*(C(2,i)+C(3,i));
ko6 = 8e-12*exp(-2060/T);
ko7 = 7.9e-14*(T/298)^2.6*exp(945/T);
ko8 = 2.2e-10;
ko9 = 3.2e-11*exp(67/T);
ko10 = 2.15e-11*exp(110/T);

ro1(i) = ko1*C(5,i)*C(6,i);
ro2(i) = ko2*C(5,i)*C(7,i);
ro3(i) = ko3*C(5,i)*C(10,i);
ro4(i) = ko4*C(5,i)*C(2,i);
ro5(i) = ko5*C(5,i)*C(5,i);
ro6(i) = ko6*C(5,i)*C(9,i);
ro7(i) = ko7*C(6,i)*C(6,i);
ro8(i) = ko8*C(8,i)*C(4,i);
ro9(i) = ko9*C(8,i)*C(2,i);
ro10(i) = ko10*C(8,i)*C(3,i);

% Scavenging reactions

ks1 = 2.9e-12*exp(-160/T);
ks2 = 1.9e-12*exp(-1000/T);
ks3 = 1.4e-14*exp(-600/T);

rs1(i) = ks1*C(6,i)*C(10,i);
rs2(i) = ks2*C(6,i)*C(9,i);
rs3(i) = ks3*C(7,i)*C(9,i);

% Termination reactions

kt1 = 4.8e-11*exp(250/T);
kt2 = 2.2e-13*exp(600/T) + 1.9e-33*exp(980/T)*C(3,i) + 1.6e-
      33*exp(980/T)*C(2,i);
kt2 = kt2*(1 + 1.4e-21*exp(980/T)*C(4,i));
kt3zero = 6.9e-31*(T/300)^(-0.8)*C(3,i);
kt3inf = 2.6e-11;
kt3Fc = 0.5;
Nkt3 = 0.75 - 1.27*log10(kt3Fc);
kt3F = 10^((log10(kt3Fc))/(1+((log10(kt3zero/kt3inf))/Nkt3)^2));
kt3 = kt3zero*kt3inf*kt3F/(kt3zero + kt3inf);

rt1(i) = kt1*C(6,i)*C(7,i);
rt2(i) = kt2*C(7,i)*C(7,i);
rt3(i) = kt3*C(6,i)*C(6,i);
```

```
% Degradation reactions

kd1 = 6.1e-12*exp(-80/T);
kd2 = 2.3e-12*exp(0/T);
kd3 = 1.6e-10;
kd4 = 9.2e-12*exp(-1800/T);

kd5zero = 1.8e-33*(T/300)^(2)*C(3,i);
kd5inf = 4.2e-14*(T/300)^(1.8);
kd5Fc = 0.6;
Nkd5 = 0.75 - 1.27*log10(kd5Fc);
kd5F = 10^((log10(kd5Fc))/(1+((log10(kd5zero/kd5inf))/Nkd5)^2));
kd5 = kd5zero*kd5inf*kd5F/(kd5zero + kd5inf);

kd6 = 3.0e-12*exp(-7000/T);
kd7 = 6.6e-11;
kd8 = 2.7e-11*exp(335/T);
kd9 = 1.2e-11;
kd10 = 1.6e-13*exp(-2280/T);
kd11 = 4.5e-12*exp(-1170/T);

kd12zero = 4.5e-31*(T/300)^(-3.9)*C(3,i);
kd12inf = 1.3e-12*(T/300)^(-0.7);
kd12Fc = 0.525;
Nkd12 = 0.75 - 1.27*log10(kd12Fc);
kd12F = 10^((log10(kd12Fc))/(1+((log10(kd12zero/kd12inf))/Nkd12)^2));
kd12 = kd12zero*kd12inf*kd12F/(kd12zero + kd12inf);

kd13 = 1.3e-12*exp(-330/T);
kd14 = 8.5e-41*exp(6540/T)*(C(4,i))^2;
kd15 = 1.5e-15;
kd16 = 5.0e-19;
kd17 = 2.0e-19;
kd18 = 9.5e-12*exp(-280/T);
kd19 = 2.5e-15;
kd20 = 1.0e-17;
kd21a = 6.0e-14;
kd21b = 5.0e-14;
kd22 = 3.0e-13;

rd1(i) = kd1*C(1,i)*C(6,i);
rd2(i) = kd2*C(2,i)*C(12,i);
rd3(i) = kd3*C(5,i)*C(11,i);
rd4(i) = kd4*C(1,i)*C(5,i);
rd5(i) = kd5*C(5,i)*C(14,i);
rd6(i) = kd6*C(9,i)*C(14,i);
rd7(i) = kd7*C(6,i)*C(12,i);
rd8(i) = kd8*C(6,i)*C(13,i);
rd9(i) = kd9*C(12,i)*C(9,i);
rd10(i) = kd10*C(13,i)*C(2,i);
```

```
    rd11(i) = kd11*C(13,i)*C(9,i);
    rd12(i) = kd12*C(14,i)*C(6,i);
    rd13(i) = kd13*C(2,i)*C(16,i);
    rd14(i) = kd14*C(4,i)*C(15,i);
    rd15(i) = kd15*C(1,i)*C(7,i);
    rd16(i) = kd16*C(14,i)*C(7,i);
    rd17(i) = kd17*C(2,i)*C(11,i);
    rd18(i) = kd18*C(11,i)*C(9,i);
    rd19(i) = kd19*C(11,i)*C(10,i);
    rd20(i) = kd20*C(18,i)*C(2,i);
    rd21a(i) = kd21a*C(18,i)*C(9,i);
    rd21b(i) = kd21b*C(18,i)*C(9,i);
    rd22(i) = kd22*C(17,i)*C(2,i);

% Calculate reaction rates per species using stoichiometry

    react(1,i) = -rd1(i) - rd4(i) - rd15(i) + rd19(i) - rp1(i);
    react(2,i) = ro1(i) + ro2(i) - ro4(i) + ro5(i) + 2*ro6(i)+ rs2(i) +
2*rs3(i) + rt1(i) + rt2(i) - 3.75*rp1(i) - rp2(i) + rp3(i) - rd2(i) + rd6(i)
+ rd9(i) - rd10(i) + rd11(i) - rd13(i) + rd16(i) - rd17(i) + rd18(i) -
rd20(i) + 2*rd21a(i) + rd21b(i) - rd22(i);
    react(3,i) = 0;
    react(4,i) = ro7(i) + rs1(i) + rt1(i) - rp2(i) + rp5b(i) - ro8(i) +
rd1(i) - rd14(i);
    react(5,i) = - ro1(i) - ro2(i) - ro3(i) - ro4(i) - 2*ro5(i) - ro6(i) +
ro7(i) + 0.1*rp3(i) + rp4(i) + rp5b(i) + ro9(i) + ro10(i) + rd2(i) - rd3(i) -
rd4(i) - rd5(i) + rd10(i) + rp6(i) + rp7(i);
    react(6,i) = - ro1(i) + ro2(i) + ro3(i) - 2*ro7(i) - rs1(i) - rs2(i) +
rs3(i) - rt1(i) - 2*rt3(i) + rp2(i) + rp4(i) + 2*rp5a(i) + 2*ro8(i) - rd1(i)
+ rd4(i) - rd7(i) - rd8(i) - rd12(i) + rd17(i);
    react(7,i) = ro1(i) - ro2(i) + rs1(i) + rs2(i) - rs3(i) - rt1(i) -
2*rt2(i) + 2*rp1(i) + rp2(i) - rp4(i) + 2*rp6(i) + 2*rp7(i) + rd13(i) + -
rd15(i) - rd16(i) + rd19(i) + rd20(i) + rd22(i);
    react(8,i) = 0.9*rp3(i) - ro8(i) - ro9(i) - ro10(i);
    react(9,i) = ro4(i) - ro6(i) - rs2(i) - rs3(i) - rp3(i) - rd6(i) - rd9(i)
- rd11(i) - rd18(i) - rd21a(i) - rd21b(i);
    react(10,i) = -ro3(i) - rs1(i) + rt2(i) + rt3(i) - rp5a(i) - rp5b(i) +
rd15(i) - rd19(i);
    react(11,i) = rd1(i) - rd3(i) + rd4(i) + rd15(i) - rd17(i) - rd18(i) -
rd19(i) + rd21a(i) +rp1(i);
    react(12,i) = -rd2(i) - rd7(i) - rd9(i);
    react(13,i) = rd2(i) + rd3(i) + rd7(i) - rd8(i) + rd9(i) - rd10(i) -
rd11(i) + rd17(i) + rd20(i) + rp6(i);
    react(14,i) = -rd5(i) - rd6(i) + rd8(i) + rd10(i) + rd11(i) - rd12(i) -
rd16(i) + rd22(i) - rp6(i) + rp7(i);
    react(15,i) = rd5(i) + rd6(i) + rd13(i) - rd14(i) - rp7(i);
    react(16,i) = rd12(i) - rd13(i);
    react(17,i) = rd16(i) + rd21b(i) - rd22(i);
    react(18,i) = rd18(i) - rd20(i) - rd21a(i) - rd21b(i);
    react(19,i) = rd14(i);
```

```
% Assume velocity not homogeneous; laminar flow

    r(i) = r0 + dr*(i-1);
    denom = 2*r1*r1 - (r1*r1-r0*r0)/log(r1/r0) - (r1*r1-r0*r0);
    v(i) = 2*U*((r1*r1-r0*r0)*log(r(i)/r0)/log(r1/r0) - (r(i)*r(i)-
           r0*r0))/denom;

    % Build the differential equations
    for j = 1:Ncomp
        dcdr(j,i) = (C(j,i+1) - C(j,i-1))/2/dr;
        d2cdr2(j,i) = (C(j,i-1) - 2*C(j,i) + C(j,i+1))/dr/dr;
        dcdL(j,i) = (D*d2cdr2(j,i) + D/r(i)*dcdr(j,i)+react(j,i))/v(i);
    end
end

for j = 1:Ncomp
    for i = 1:Nnodes
        dydz(i+Nnodes*(j-1)) = dcdL(j,i+1);
    end
end
%Calculation of concentrations in the intersections
for j = 1:Ncomp
            Clamp(j) = (4*C(j,1)-C(j,2))/3; % Concentrations on the lamp
(considering a parabolic equation for Conc.)
end
```

Main file:

```
clear all
clc
tic %start a timer
format long
data
options = odeset('RelTol', 1e-6, 'AbsTol', 1e-8, 'InitialStep', 0.0001);
[Z,Y] = ode15s (@f,zspan, y0,options,dz,Nnodes,Ncomp, r0,r1,sig,E0,D,U,P,T,
        reflamp);
[s1,s2] = size(Z);
plot(Z,Y(1:s1,1:Nnodes))
ylabel 'H2S Concentration(molecules/cm3)'
xlabel 'Reactor Length(cm)'
figure
plot(Z,Y(1:s1,Nnodes+1:2*Nnodes))
title 'Oxygen Concentration(molecules/cm3)'

ncomp1=14; %Component number 1 (SO2)
figure
plot(Z,Y(1:s1,(ncomp1-1)*Nnodes+1:ncomp1*Nnodes))
ylabel 'SO2 Concentration(molecules/cm3)'
xlabel 'Reactor Length(cm)'
Z;
RS1=Y(1:s1,(ncomp1-1)*Nnodes+1:ncomp1*Nnodes);

ncomp2=19; %Component number 2 (H2SO4)
figure
plot(Z,Y(1:s1,(ncomp2-1)*Nnodes+1:ncomp2*Nnodes))
ylabel 'H2SO4 Concentration(molecules/cm3)'
xlabel 'Reactor Length(cm)'
Z;
RS2=Y(1:s1,(ncomp2-1)*Nnodes+1:ncomp2*Nnodes);

Y(1:s1,1:Nnodes);
toc %read the timer

%Efficiency Calculation
dr = (r1-r0)/(Nnodes+1);   % Node distance
for i = 2:Nnodes+1
    r(i) = r0 + dr*(i-1);
    denom = 2*r1*r1 - (r1*r1-r0*r0)/log(r1/r0) - (r1*r1-r0*r0);
    v(i) = 2*U*((r1*r1-r0*r0)*log(r(i)/r0)/log(r1/r0) - (r(i)*r(i)-
           r0*r0))/denom;
end

%Concentration SO2 at exit
F_mass1 = 0;
F_vol = 0;
for i = 1:(Nnodes-1)/2
    F_mass1 = F_mass1 + 2*pi*dr*(4*r(2*i)*v(2*i)*RS1(s1,2*i-1)+
              2*r(2*i+1)*v(2*i+1)*RS1(s1,2*i));
    F_vol  = F_vol + 2*pi*dr*(4*r(2*i)*v(2*i)+2*r(2*i+1)*v(2*i+1));
```

```
end
C_exit1 = F_mass1 / F_vol;
C_SO2_gm3 = C_exit1 * 64.066 * 1e6 / 6.0221412e23

%Concentration H2SO4 at exit
F_mass2 = 0;
F_vol = 0;
for i = 1:(Nnodes-1)/2
    F_mass2 = F_mass2 + 2*pi*dr*(4*r(2*i)*v(2*i)*RS2(s1,2*i-1)+
              2*r(2*i+1)*v(2*i+1)*RS2(s1,2*i));
    F_vol  = F_vol + 2*pi*dr*(4*r(2*i)*v(2*i)+2*r(2*i+1)*v(2*i+1));
end
C_exit2 = F_mass2 / F_vol;
C_H2SO4_gm3 = C_exit2 * 98.079 * 1e6 / 6.0221412e23

%Concentration H2S at exit
C_exit_H2S = (Ft/F_vol) * 34.08 * 1e6 / 6.0221412e23;


% Total flow rates at entrance and exit
Ft0 = 0;
Ft = 0;

for i = 1:(Nnodes-1)/2
    Ft0 = Ft0+2*pi*dr*(4*r(2*i)*v(2*i)*Y(1,2*i-1)+
          2*r(2*i+1)*v(2*i+1)*Y(1,2*i));
    Ft = Ft+2*pi*dr*(4*r(2*i)*v(2*i)*Y(s1,2*i-1)+
         2*r(2*i+1)*v(2*i+1)*Y(s1,2*i));
end
s1;
s2;
Efficiency = (1-(Ft/Ft0))*100
```

Appendix B: Developed code for photolysis of H_2S combined with NO_x

Data file:

```
length = 56;            % Reactor length in cm
dz = 1;
zspan = 0:dz:length;
Nnodes = 19;            % Number of internal nodes in the grid
Ncomp = 30;             % Number of compounds considered
P = 89000;              % Pressure in Pa
T = 310;                % Temperature in K
Ctot = P/1.38e-23/T;    % Concentration in molecules per m3
Ctot = Ctot/1e6;        % Concentration in molecules per cm3
MMh2s=34.08;
MMNO = 30.01;
Cmh2s=1;                %Concentration in grams per m3 of H2S
CmNO =1;               %Concentration in grams per m3 of NO
Ch2s=Cmh2s/MMh2s;        %Concentration in moles per m3 of H2S
CNO=CmNO/MMNO;           %Concentration in moles per m3 of NO
Ch2s=Ch2s*6.022e23;      %Concentration in molecules per m3 of H2S
CNO=CNO*6.022e23;        %Concentration in molecules per m3 of NO
yh2s = Ch2s/Ctot/1e6;    % H2S mole fraction
yNO = CNO/Ctot/1e6;      % NO mole fraction
yH2O = 0.02;             % Water mole fraction
yO3 = 0.00;
yO2 = 0.21*(1-yH2O-yh2s-yO3-yNO); % O2 mole fraction
yN2 = 0.79*(1-yH2O-yh2s-yO3-yNO); % N2 mole fraction
Ch2s = Ctot*yh2s;        % H2S concentration (molecules/cm3)
CNO =  Ctot*yNO;         % NO concentration (molecules/cm3)
CH2O = Ctot*yH2O;
CO2 = Ctot*yO2;
CN2 = Ctot*yN2;
CO3 = Ctot*yO3;

% Initial concentrations:
% y0(i+(j-1)*Ncomp) is initial concentration
% of compound j in node point i from the center
% j  Compound
% -- --------
% 1  H2S
% 2  O2
% 3  N2 + argon
% 4  H2O
% 5  O radical (O(3P))
% 6  OH radical
% 7  HO2 radical
% 8  O(1D) radical
% 9  O3
% 10 H2O2
% 11 HS radical
% 12 S radical
% 13 SO radical
% 14 SO2
```

```
% 15 SO3
% 16 HSO3 radical
% 17 HSO2 radical
% 18 HSO radical
% 19 H2SO4

% 20 N2O
% 21 NO
% 22 NO2
% 23 NO3
% 24 N2O4
% 25 HNO2
% 26 HNO3
% 27 HO2NO2
% 28 N2O3
% 29 N2O5
% 30 HSNO

for i = 1:Nnodes
    y0(i) = Ch2s;
    y0(i+Nnodes) = CO2;
    y0(i+2*Nnodes) = CN2;
    y0(i+3*Nnodes) = CH2O;
    for j = 4:Ncomp-1
        y0(i+j*Nnodes) = 0;
    end
    y0(i+8*Nnodes) = CO3;
    y0(i+20*Nnodes) = CNO;
end
r0 = 1.25;                % Internal diameter, cm
r1 = 2.1;                 % External diameter, cm
for j = 1:Ncomp
    for k = 1:2      % k is spectral line (1 = 185 nm, 2 = 254 nm)
        sig(j,k) = 0;
    end
end
sig(1,1) = 3.82e-18;     % Sigma h2s at 185 nm
sig(1,2) = 7.45e-21;
sig(2,1) = 2e-21;
sig(4,1) = 5.5e-20;
sig(7,1) = 324.8e-20;
sig(7,2) = 29.9e-20;
sig(9,1) = 66.1e-20;
sig(9,2) = 1148e-20;
sig(10,1) = 80.1e-20;
sig(10,2) = 6.99e-20;
sig(14,1) = 3.65e-18;
sig(14,2) = 1.35e-19;
sig(15,1) = 9.95e-19;
sig(15,2) = 1.34e-20;
sig(20,1) = 1.43e-19;
sig(20,2) = 0 ;
sig(22,1) = 6.88e-18;
sig(22,2) = 1.16e-20;
```

```
sig(25,1) = 9e-19;
sig(25,2) = 1.45e-19;
sig(26,1) = 1.63e-17;
sig(26,2) = 1.95e-20;
sig(27,1) = 1.24e-17;
sig(27,2) = 3.63e-19;
sig(29,1) = 1.85e-17;
sig(29,1) = 3.26e-19;

power1 = 40*0.08;              % Emitted light at 185nm (W)
power2 = 40*0.30;              % Emitted light at 254nm (W)
nu1 = 299792458/185e-9;
nu2 = 299792458/254e-9;
photon1 = 6.626e-34*nu1; % Photon energy at 185 nm
photon2 = 6.626e-34*nu2; % Photon energy at 254 nm
E0(1) = power1/photon1/length/2/pi/r0; % Photons per cm2 per s leaving lamp
E0(2) = power2/photon2/length/2/pi/r0; % 1 = 185 nm, 2 = 254 nm

D = 0.94152*(T^1.75)/P; %H2S - NO diffusivity (cm2/s)
Q = 1000/60;            %Flow rate (cm3/s)
U = Q/pi/(r1*r1-r0*r0); %Mean gas velocity (cm/s)
reflamp = 0.7;          %Reflection at the lamp
reflamp2 = 0.7;         %Fraction of the received light at the lamp reflected
```

Function file:

```
function dydz = f(z,y,dz,Nnodes,Ncomp,r0,r1,sig,E0,D,U,P,T,reflamp,reflamp2)

dydz = zeros(Nnodes*Ncomp,1);

% j  Compound
% -- --------
% 1  H2S
% 2  O2
% 3  N2 + argon
% 4  H2O
% 5  O radical (O(3P))
% 6  OH radical
% 7  HO2 radical
% 8  O(1D) radical
% 9  O3
% 10 H2O2
% 11 HS radical
% 12 S radical
% 13 SO radical
% 14 SO2
% 15 SO3
% 16 HSO3 radical
% 17 HSO2 radical
% 18 HSO radical
% 19 H2SO4

% 20 N2O
% 21 NO
% 22 NO2
% 23 NO3
% 24 N2O4
% 25 HNO2
% 26 HNO3
% 27 HO2NO2
% 28 N2O3
% 29 N2O5
% 30 HSNO

dr = (r1-r0)/(Nnodes+1);   % Node distance

% User-friendly notation of concentrations: i = node number
%                                           j = compound number

for j = 1:Ncomp
    for i = 1:Nnodes
        C(j,i+1) = y(i+Nnodes*(j-1));          % concentration of j in node i,
                                                 molecules/cm3
    end
    C(j,1) = C(j,2) - (C(j,3) - C(j,2))/3;     % boundary condition: zero
                                                 radial flux
    C(j,Nnodes+2) = C(j,Nnodes+1) - (C(j,Nnodes) - C(j,Nnodes+1))/3;
```

```
end
% Calculate radiation fields

Eref(1,1)=E0(1)/reflamp;    %Considering original radiation from the lamp
Eref(1,2)=E0(2)/reflamp;    %Considering original radiation from the lamp
for k = 1:2
    for i=1:Nnodes+1
        Etot(i+1,k)=0;
    end
    while (Eref(1,k)>0.01*E0(k))
    E(1,k) = reflamp*Eref(1,k);
    for i = 1:Nnodes+1
        Ei = E(i,k);
        r = r0 + dr*(i-0.5);
        alpha = 0;
        for j = 1:Ncomp
            Ci(j) = (C(j,i) + C(j,i+1))/2;
            alpha = alpha + Ci(j)*sig(j,k);
        end
        E(i+1,k) = (Ei/dr - alpha*Ei/2 - Ei/2/r)/(1/dr + alpha/2 + 1/2/r);
        if E(i+1,k) < 0
            E(i+1,k) = 0;
        end
    end
    Eref(Nnodes+2,k)=0.99*E(Nnodes+2,k);
    for i=Nnodes+1:-1:1
        Erefi=Eref(i+1,k);
        r=r0+dr*(i-0.5);
        alpha=0;
        for j=1:Ncomp
            Ci(j)=(C(j,i)+C(j,i+1))/2;
            alpha=alpha+Ci(j)*sig(j,k);
        end
        Eref(i,k)=(Erefi/dr+Erefi/2/r-alpha*Erefi/2)/(1/dr-1/2/r+alpha/2);
        if Eref(i,k)<0
            Eref(i,k)=0;
        end
    end
    for i=1:Nnodes+2
        Etot(i,k)=Etot(i,k)+E(i,k)+Eref(i,k);
    end
    end
end

for i = 2:Nnodes+1
    % Calculate reaction rates per reaction
        Ph2s = C(1,i)*1.38e-23*T*1e6;     % H2S partial pressure, Pa
    Pinert = (C(2,i)+C(3,i)+C(4,i))*1.38e-23*T*1e6;
    phih2s185 = 1;
    phih2s254 = 1;
    phiso2185 = 0.27;
    phiso2254 = 0;
    phiso3185 = 1;
    phiso3254 = 1;
```

```
rp1(i) = C(1,i)*(phih2s185*sig(1,1)*Etot(i,1)+
         phih2s254*sig(1,2)*Etot(i,2));
rp2(i) = C(4,i)*sig(4,1)*Etot(i,1);
rp3(i) = C(9,i)*(sig(9,1)*Etot(i,1) + sig(9,2)*Etot(i,2));
rp4(i) = C(7,i)*(sig(7,1)*Etot(i,1) + sig(7,2)*Etot(i,2));
rp5(i) = C(10,i)*(sig(10,1)*Etot(i,1)*0.75 + sig(10,2)*Etot(i,2));
rp_5(i) = C(10,i)*sig(10,1)*Etot(i,1)*0.16;
rp6(i) = C(14,i)*(phiso2185*sig(14,1)*Etot(i,1)+
         phiso2254*sig(14,2)*Etot(i,2));
rp7(i) = C(15,i)*(phiso3185*sig(15,1)*Etot(i,1)+
         phiso3254*sig(15,2)*Etot(i,2));

rp8(i) = C(22,i)*(1*sig(22,1)*Etot(i,1)+1*sig(22,2)*Etot(i,2));
rp9(i) = C(20,i)*(1*sig(20,1)*Etot(i,1));
rp10a(i) = C(29,i)*(0*sig(29,1)*Etot(i,1)+0.08*sig(29,2)*Etot(i,2));
rp10b(i) = C(29,i)*(1*sig(29,1)*Etot(i,1)+0.72*sig(29,2)*Etot(i,2));
rp11(i) = C(25,i)*(1*sig(25,1)*Etot(i,1)+1*sig(25,2)*Etot(i,2));
rp12(i) = C(26,i)*(1*sig(26,1)*Etot(i,1)+0.97*sig(26,2)*Etot(i,2));
rp13a(i) = C(27,i)*(0.7*sig(27,1)*Etot(i,1)+0.8*sig(27,2)*Etot(i,2));
rp13b(i) = C(27,i)*(0.3*sig(27,1)*Etot(i,1)+0.2*sig(27,2)*Etot(i,2));

% Oxygen atom reactions

ko1 = 2.3e-11*exp(110/T);
ko2 = 2.7e-11*exp(224/T);
ko3 = 1.4e-12*exp(-2000/T);
ko4 = 6e-34*(T/300)^(-2.8)*C(2,i) + 5.6e-34*(T/300)^(-2.8)*C(3,i);
ko5 = 2.7e-34*T^(-0.41)*(C(2,i)+C(3,i));
ko6 = 8e-12*exp(-2060/T);
ko7 = 7.9e-14*(T/298)^2.6*exp(945/T);
ko8 = 2.2e-10;
ko9 = 3.2e-11*exp(67/T);
ko10 = 2.15e-11*exp(110/T);

ro1(i) = ko1*C(5,i)*C(6,i);
ro2(i) = ko2*C(5,i)*C(7,i);
ro3(i) = ko3*C(5,i)*C(10,i);
ro4(i) = ko4*C(5,i)*C(2,i);
ro5(i) = ko5*C(5,i)*C(5,i);
ro6(i) = ko6*C(5,i)*C(9,i);
ro7(i) = ko7*C(6,i)*C(6,i);
ro8(i) = ko8*C(8,i)*C(4,i);
ro9(i) = ko9*C(8,i)*C(2,i);
ro10(i) = ko10*C(8,i)*C(3,i);

% Scavenging reactions

ks1 = 2.9e-12*exp(-160/T);
ks2 = 1.9e-12*exp(-1000/T);
ks3 = 1.4e-14*exp(-600/T);

rs1(i) = ks1*C(6,i)*C(10,i);
```

```
rs2(i) = ks2*C(6,i)*C(9,i);
rs3(i) = ks3*C(7,i)*C(9,i);

% Termination reactions

kt1 = 4.8e-11*exp(250/T);
kt2 = 2.2e-13*exp(600/T)+ 1.9e-33*exp(980/T)*C(3,i) + 1.6e-33*
      exp(980/T)*C(2,i);
kt2 = kt2*(1 + 1.4e-21*exp(980/T)*C(4,i));
kt3zero = 6.9e-31*(T/300)^(-0.8)*C(3,i);
kt3inf = 2.6e-11;
kt3Fc = 0.5;
Nkt3 = 0.75 - 1.27*log10(kt3Fc);
kt3F = 10^((log10(kt3Fc))/(1+((log10(kt3zero/kt3inf))/Nkt3)^2));
kt3 = kt3zero*kt3inf*kt3F/(kt3zero + kt3inf);

rt1(i) = kt1*C(6,i)*C(7,i);
rt2(i) = kt2*C(7,i)*C(7,i);
rt3(i) = kt3*C(6,i)*C(6,i);

% Degradation reactions

kd1 = 6.1e-12*exp(-80/T);
kd2 = 2.3e-12*exp(0/T);
kd3 = 1.6e-10;
kd4 = 9.2e-12*exp(-1800/T);

kd5zero = 1.8e-33*(T/300)^(2)*C(3,i);
kd5inf = 4.2e-14*(T/300)^(1.8);
kd5Fc = 0.6;
Nkd5 = 0.75 - 1.27*log10(kd5Fc);
kd5F = 10^((log10(kd5Fc))/(1+((log10(kd5zero/kd5inf))/Nkd5)^2));
kd5 = kd5zero*kd5inf*kd5F/(kd5zero + kd5inf);

kd6 = 3.0e-12*exp(-7000/T);
kd7 = 6.6e-11;
kd8 = 2.7e-11*exp(335/T);
kd9 = 1.2e-11;
kd10 = 1.6e-13*exp(-2280/T);
kd11 = 4.5e-12*exp(-1170/T);

kd12zero = 4.5e-31*(T/300)^(-3.9)*C(3,i);
kd12inf = 1.3e-12*(T/300)^(-0.7);
kd12Fc = 0.525;
Nkd12 = 0.75 - 1.27*log10(kd12Fc);
kd12F = 10^((log10(kd12Fc))/(1+((log10(kd12zero/kd12inf))/Nkd12)^2));
kd12 = kd12zero*kd12inf*kd12F/(kd12zero + kd12inf);

kd13 = 1.3e-12*exp(-330/T);
kd14 = 8.5e-41*exp(6540/T)*(C(4,i))^2;
kd15 = 1.5e-15;
kd16 = 5.0e-19;
```

```
    kd17 = 2.0e-19;
    kd18 = 9.5e-12*exp(-280/T);
    kd19 = 2.5e-15;
    kd20 = 1.0e-17;
    kd21a = 6.0e-14;
    kd21b = 5.0e-14;
    kd22 = 3.0e-13;

    % Added for NOx Reactions

    kd23 = 2.8e-36*(T/300)^(-0.9)*C(3,i);
    kd24a = 5.0e-13;
    kd24b = 4.64e-11*exp(20/T);
    kd24c = 7.25e-11*exp(20/T);

    kd25zero = 9e-32*(T/300)^(-1.5)*C(3,i);
    kd25inf = 3e-11*(T/300);
    kd25 =
(kd25zero/(1+(kd25zero/kd25inf)))*0.6^((1+(log10(kd25zero/kd25inf))^2)^(-1));

    kd26 = 5.15e-12*exp(210/T);

    kd27zero = 1.3e-31*(T/300)^(-1.5)*C(3,i);
    kd27inf = 2.3e-11*(T/300)^(0.24);
    kd27Fc = 0.6;
    Nkd27 = 0.75 - 1.27*log10(kd27Fc);
    kd27F = 10^((log10(kd27Fc))/(1+((log10(kd27zero/kd27inf))/Nkd27)^2));
    kd27 = kd27zero*kd27inf*kd27F/(kd27zero + kd27inf);

    kd28 = 1e-11;

    kd29zero = 1.4e-33*(T/300)^(-3.8)*C(3,i);
    kd29inf = 1e-12;
    kd29Fc = 0.4;
    Nkd29 = 0.75 - 1.27*log10(kd29Fc);
    kd29F = 10^((log10(kd29Fc))/(1+((log10(kd29zero/kd29inf))/Nkd29)^2));
    kd29 = kd29zero*kd29inf*kd29F/(kd29zero + kd29inf);

    kd30zero = 1.3e-5*(T/300)^(-3.8)*exp(-6400/T)*C(3,i);
    kd30inf = 1.15e16*exp(-6400/T);
    kd30Fc = 0.4;
    Nkd30 = 0.75 - 1.27*log10(kd30Fc);
    kd30F = 10^((log10(kd30Fc))/(1+((log10(kd30zero/kd30inf))/Nkd30)^2));
    kd30 = kd30zero*kd30inf*kd30F/(kd30zero + kd30inf);

    kd31 = 4e-10*exp(-340/T);

    kd32zero = 7.4e-31*(T/300)^(-2.4)*C(3,i);
    kd32inf = 3.3e-11*(T/300)^(-0.3);
    kd32Fc = exp(-T/1420);
    Nkd32 = 0.75 - 1.27*log10(kd32Fc);
    kd32F = 10^((log10(kd32Fc))/(1+((log10(kd32zero/kd32inf))/Nkd32)^2));
```

```
kd32 = kd32zero*kd32inf*kd32F/(kd32zero + kd32inf);

kd33zero = 3.3e-30*(T/300)^(-3)*C(3,i);
kd33inf = 4.1e-11;
kd33Fc = 0.4;
Nkd33 = 0.75 - 1.27*log10(kd33Fc);
kd33F = 10^((log10(kd33Fc))/(1+((log10(kd33zero/kd33inf))/Nkd33)^2));
kd33 = kd33zero*kd33inf*kd33F/(kd33zero + kd33inf);

kd34 = 2e-11;
kd35 = 1.8e-11*exp(-390/T);
kd36 = 8.3e-15*exp(850/T);
kd37 = 1.3e-12*exp(380/T);
kd38 = 3.3e-12*exp(270/T);

kd39zero = 1.8e-31*(T/300)^(-3.2)*C(3,i);
kd39inf = 4.7e-12;
kd39Fc = 0.6;
Nkd39 = 0.75 - 1.27*log10(kd39Fc);
kd39F = 10^((log10(kd39Fc))/(1+((log10(kd39zero/kd39inf))/Nkd39)^2));
kd39 = kd39zero*kd39inf*kd39F/(kd39zero + kd39inf);

kd40zero = 4.1e-5*exp(-10650/T)*C(3,i);
kd40inf = 4.8e15*exp(-11070/T);
kd40Fc = 0.6;
Nkd40 = 0.75 - 1.27*log10(kd40Fc);
kd40F = 10^((log10(kd40Fc))/(1+((log10(kd40zero/kd40inf))/Nkd40)^2));
kd40 = kd40zero*kd40inf*kd40F/(kd40zero + kd40inf);

kd41 = 2.3e-12*exp(170/T);
kd42 = 3.0e-12*exp(-1500/T);
kd43 = 3.3e-39*exp(530/T);
kd44 = 1.5e-11*exp(170/T);

kd45zero = 3.1e-34*(T/300)^(-7.7)*C(3,i);
kd45inf = 7.9e-12*(T/300)^(1.4);
kd45Fc = 0.6;
Nkd45 = 0.75 - 1.27*log10(kd45Fc);
kd45F = 10^((log10(kd45Fc))/(1+((log10(kd45zero/kd45inf))/Nkd45)^2));
kd45 = kd45zero*kd45inf*kd45F/(kd45zero + kd45inf);

kd46zero = 1.9e-7*(T/300)^(-8.7)*exp(-4880/T)*C(3,i);
kd46inf = 4.7e15*(T/300)^(0.4)*exp(-4880/T);
kd46Fc = 0.6;
Nkd46 = 0.75 - 1.27*log10(kd46Fc);
kd46F = 10^((log10(kd46Fc))/(1+((log10(kd46zero/kd46inf))/Nkd46)^2));
kd46 = kd46zero*kd46inf*kd46F/(kd46zero + kd46inf);

kd47zero = 3.6e-30*(T/300)^(-4.1)*C(3,i);
kd47inf = 1.9e-12*(T/300)^(0.2);
kd47Fc = 0.35;
Nkd47 = 0.75 - 1.27*log10(kd47Fc);
kd47F = 10^((log10(kd47Fc))/(1+((log10(kd47zero/kd47inf))/Nkd47)^2));
```

```
    kd47 = kd47zero*kd47inf*kd47F/(kd47zero + kd47inf);

    kd48zero = 1.3e-3*(T/300)^(-3.5)*exp(-11000/T)*C(3,i);
    kd48inf = 9.7e14*(T/300)^(0.1)*exp(-11080/T);
    kd48Fc = 0.35;
    Nkd48 = 0.75 - 1.27*log10(kd48Fc);
    kd48F = 10^((log10(kd48Fc))/(1+((log10(kd48zero/kd48inf))/Nkd48)^2));
    kd48 = kd48zero*kd48inf*kd48F/(kd48zero + kd48inf);

    kd49 = 2.5e-19;
    kd50 = 1.2e-13*exp(-2450/T);
    kd51 = 2.5e-19;
    kd52 = 1.4e-11;

    kd53zero = 2.4e-31*(T/300)^(-2.5)*C(3,i);
    kd53inf = 2.7e-11;
    kd53 =
(kd53zero/(1+(kd53zero/kd53inf)))*0.6^((1+(log10(kd53zero/kd53inf))^2)^(-1));

    kd54 = 3e-11*exp(250/T);
    kd55 = 2.5e-16;
    kd56 = 9.6e-12;

     % Added for NOx Reactions

    rd1(i) = kd1*C(1,i)*C(6,i);
    rd2(i) = kd2*C(2,i)*C(12,i);
    rd3(i) = kd3*C(5,i)*C(11,i);
    rd4(i) = kd4*C(1,i)*C(5,i);
    rd5(i) = kd5*C(5,i)*C(14,i);
    rd6(i) = kd6*C(9,i)*C(14,i);
    rd7(i) = kd7*C(6,i)*C(12,i);
    rd8(i) = kd8*C(6,i)*C(13,i);
    rd9(i) = kd9*C(12,i)*C(9,i);
    rd10(i) = kd10*C(13,i)*C(2,i);
    rd11(i) = kd11*C(13,i)*C(9,i);
    rd12(i) = kd12*C(14,i)*C(6,i);
    rd13(i) = kd13*C(2,i)*C(16,i);
    rd14(i) = kd14*C(4,i)*C(15,i);
    rd15(i) = kd15*C(1,i)*C(7,i);
    rd16(i) = kd16*C(14,i)*C(7,i);
    rd17(i) = kd17*C(2,i)*C(11,i);
    rd18(i) = kd18*C(11,i)*C(9,i);
    rd19(i) = kd19*C(11,i)*C(10,i);
    rd20(i) = kd20*C(18,i)*C(2,i);
    rd21a(i) = kd21a*C(18,i)*C(9,i);
    rd21b(i) = kd21b*C(18,i)*C(9,i);
    rd22(i) = kd22*C(17,i)*C(2,i);


    rd23(i) = kd23*C(8,i)*C(3,i);
    rd24a(i) = kd24a*C(8,i)*C(20,i);
    rd24b(i) = kd24b*C(8,i)*C(20,i);
```

```
    rd24c(i) = kd24c*C(8,i)*C(20,i);
    rd25(i) = kd25*C(5,i)*C(21,i);
    rd26(i) = kd26*C(5,i)*C(22,i);
    rd27(i) = kd27*C(5,i)*C(22,i);
    rd28(i) = kd28*C(5,i)*C(23,i);
    rd29(i) = kd29*C(22,i)*C(22,i);
    rd30(i) = kd30*C(24,i);
    rd32(i) = kd32*C(6,i)*C(21,i);
    rd33(i) = kd33*C(6,i)*C(22,i);
    rd34(i) = kd34*C(6,i)*C(23,i);
    rd35(i) = kd35*C(6,i)*C(25,i);
    rd36(i) = kd36*C(6,i)*C(26,i);
    rd37(i) = kd37*C(6,i)*C(27,i);
    rd38(i) = kd38*C(7,i)*C(21,i);
    rd39(i) = kd39*C(7,i)*C(22,i);
    rd40(i) = kd40*C(27,i);
    rd41(i) = kd41*C(7,i)*C(23,i);
    rd42(i) = kd42*C(9,i)*C(21,i);
    rd43(i) = kd43*C(2,i)*C(21,i)*C(21,i);
    rd44(i) = kd44*C(21,i)*C(23,i);
    rd45(i) = kd45*C(21,i)*C(22,i);
    rd46(i) = kd46*C(28,i);
    rd47(i) = kd47*C(22,i)*C(23,i);
    rd48(i) = kd48*C(29,i);
    rd49(i) = kd49*C(4,i)*C(29,i);
    rd50(i) = kd50*C(9,i)*C(22,i);
    rd51(i) = kd51*C(9,i)*C(25,i);
    rd52(i) = kd52*C(13,i)*C(22,i);
    rd53(i) = kd53*C(11,i)*C(21,i);
    rd54(i) = kd54*C(11,i)*C(22,i);
    rd55(i) = kd55*C(11,i)*C(20,i);
    rd56(i) = kd56*C(18,i)*C(22,i);


    % Calculate reaction rates per species using stoichiometry

    react(1,i) = -rd1(i) - rd4(i) - rd15(i) + rd19(i) - rp1(i);
    react(2,i) = ro1(i) + ro2(i) - ro4(i) + ro5(i) + 2*ro6(i)+ rs2(i) +
2*rs3(i) + rt1(i) + rt2(i) - 3.75*rp1(i) - rp2(i) + rp3(i) - rd2(i) + rd6(i)
+ rd9(i) - rd10(i) + rd11(i) - rd13(i) + rd16(i) - rd17(i) + rd18(i) -
rd20(i) + 2*rd21a(i) + rd21b(i) - rd22(i)+ rd24b(i) + rd26(i) + rd28(i) +
rd37(i) + rd41(i) + rd42(i) - rd43(i) + rd50(i) + rd51(i);
    react(3,i) = 0 - rd23(i) + rd24b(i) + rd55(i) + rp9(i);
    react(4,i) = ro7(i) + rs1(i) + rt1(i) - rp2(i) + rp_5(i) - ro8(i) +
rd1(i) - rd14(i) + rd35(i) + rd36(i) + rd37(i) - rd49(i);
    react(5,i) = - ro1(i) - ro2(i) - ro3(i) - ro4(i) - 2*ro5(i) - ro6(i) +
ro7(i) + 0.1*rp3(i) + rp4(i) + rp_5(i) + ro9(i) + ro10(i) + rd2(i) - rd3(i) -
rd4(i) - rd5(i) + rd10(i) + rp6(i) + rp7(i)+ rd24a(i) - rd25(i) - rd26(i) -
rd27(i) - rd28(i) + rp8(i) + rp10b(i);
    react(6,i) = - ro1(i) + ro2(i) + ro3(i) - 2*ro7(i) - rs1(i) - rs2(i) +
rs3(i) - rt1(i) - 2*rt3(i) + rp2(i) + rp4(i) + 2*rp5(i) + 2*ro8(i) - rd1(i) +
rd4(i) - rd7(i) - rd8(i) - rd12(i) + rd17(i) + rd31(i) - rd32(i) - rd33(i) -
rd34(i) - rd35(i) - rd36(i) - rd37(i) + rd38(i) + rd41(i) + rp11(i) + rp12(i)
+ rp13b(i);
```

```
    react(7,i) = ro1(i) - ro2(i) + rs1(i) + rs2(i) - rs3(i) - rt1(i) -
2*rt2(i) + 2*rp1(i) + rp2(i) - rp4(i) + 2*rp6(i) + 2*rp7(i) + rd13(i) + -
rd15(i) - rd16(i) + rd19(i) + rd20(i) + rd22(i) + rd34(i) - rd38(i) - rd39(i)
+ rd40(i) - rd41(i) + rp13a(i);
    react(8,i) = 0.9*rp3(i) - ro8(i) - ro9(i) - ro10(i)- rd23(i)- rd24a(i)-
rd24b(i)- rd24c(i) + rp9(i);
    react(9,i) = ro4(i) - ro6(i) - rs2(i) - rs3(i) - rp3(i) - rd6(i) - rd9(i)
- rd11(i) - rd18(i) - rd21a(i) - rd21b(i) - rd42(i) - rd50(i) - rd51(i);
    react(10,i) = -ro3(i) - rs1(i) + rt2(i) + rt3(i) - rp5(i) - rp_5(i) +
rd15(i) - rd19(i);
    react(11,i) = rd1(i) - rd3(i) + rd4(i) + rd15(i) - rd17(i) - rd18(i) -
rd19(i) + rd21a(i) +rp1(i) - rd53(i) - rd54(i) - rd55(i);
    react(12,i) = -rd2(i) - rd7(i) - rd9(i);
    react(13,i) = rd2(i) + rd3(i) + rd7(i) - rd8(i) + rd9(i) - rd10(i) -
rd11(i) + rd17(i) + rd20(i) + rp6(i) - rd52(i);
    react(14,i) = -rd5(i) - rd6(i) + rd8(i) + rd10(i) + rd11(i) - rd12(i) -
rd16(i) + rd22(i) - rp6(i) + rp7(i) + rd52(i);
    react(15,i) = rd5(i) + rd6(i) + rd13(i) - rd14(i) - rp7(i);
    react(16,i) = rd12(i) - rd13(i);
    react(17,i) = rd16(i) + rd21b(i) - rd22(i) + rd56(i);
    react(18,i) = rd18(i) - rd20(i) - rd21a(i) - rd21b(i) + rd54(i) + rd55(i)
- rd56(i);
    react(19,i) = rd14(i);

    react(20,i) = rd23(i)- rd24a(i)+ rd24a(i)- rd24b(i)- rd24c(i) - rd55(i) -
rp9(i);
    react(21,i) = 2*rd24c(i) - rd25(i) + rd26(i) + rd31(i) - rd32(i) -
rd38(i) - rd42(i) - 2*rd43(i) - rd44(i) - rd45(i) + rd46(i) + rd52(i) -
rd53(i) + rd54(i) + rd56(i) + rp8(i) + rp10b(i) + rp11(i);
    react(22,i) = rd25(i) - rd26(i) - rd27(i) + rd28(i) - 2*rd29(i) +
2*rd30(i) - rd31(i) - rd33(i) + rd34(i) + rd35(i) + rd37(i) + rd38(i) -
rd39(i) + rd40(i) + rd41(i) + rd42(i) + 2*rd43(i) + 2*rd44(i) - rd45(i) +
rd46(i) - rd47(i) + rd48(i) - rd50(i) - rd52(i) - rd54(i) - rd56(i) - rp8(i)
+ rp10a(i) + rp12(i) + rp13a(i);
    react(23,i) = rd27(i) - rd28(i) - rd34(i) + rd36(i) - rd41(i) - rd44(i) -
rd47(i) + rd48(i) + rd50(i) + rp10a(i) + rp10b(i) + rp13b(i);
    react(24,i) = rd29(i) - rd30(i);
    react(25,i) = rd32(i) - rd35(i) - rd51(i) - rp11(i);
    react(26,i) = rd33(i) - rd36(i) + 2*rd49(i) + rd51(i) - rp12(i);
    react(27,i) = -rd37(i) + rd39(i) - rd40(i) - rp13a(i) - rp13b(i);
    react(28,i) = rd45(i) - rd46(i);
    react(29,i) = rd47(i) - rd48(i) - rd49(i) - rp10a(i) - rp10b(i);
    react(30,i) = rd53(i);

  % Assume velocity not homogeneous; laminar flow

    r(i) = r0 + dr*(i-1);
    denom = 2*r1*r1 - (r1*r1-r0*r0)/log(r1/r0) - (r1*r1-r0*r0);
    v(i) = 2*U*((r1*r1-r0*r0)*log(r(i)/r0)/log(r1/r0) - (r(i)*r(i)-
           r0*r0))/denom;

    % Build the differential equations
    for j = 1:Ncomp
```

```
        dcdr(j,i) = (C(j,i+1) - C(j,i-1))/2/dr;
        d2cdr2(j,i) = (C(j,i-1) - 2*C(j,i) + C(j,i+1))/dr/dr;
        dcdL(j,i) = (D*d2cdr2(j,i) + D/r(i)*dcdr(j,i)+react(j,i))/v(i);
    end
end

for j = 1:Ncomp
    for i = 1:Nnodes
        dydz(i+Nnodes*(j-1)) = dcdL(j,i+1);
    end
end
%Calculation of concentrations in the intersections
for j = 1:Ncomp
            Clamp(j) = (4*C(j,1)-C(j,2))/3; % Concentrations on the lamp
(considering a parabolic equation for Conc.)
end
```

Main File:

```
clear all
tic %start a timer
format long
data
options = odeset('RelTol', 1e-6, 'AbsTol', 1e-8, 'InitialStep', 0.0001);
[Z,Y] = ode15s (@f,zspan, y0,options,dz,Nnodes,Ncomp, r0,r1,sig,E0,D,U,P,T,
        reflamp);
[s1,s2] = size(Z);
plot(Z,Y(1:s1,1:Nnodes))
ylabel 'H2S Concentration(molecules/cm3)'
xlabel 'Reactor Length(cm)'
plot(Z,Y(1:s1,Nnodes+1:2*Nnodes))
title 'Oxygen Concentration(molecules/cm3)'

ncomp1=14; %Component number (SO2)
plot(Z,Y(1:s1,(ncomp1-1)*Nnodes+1:ncomp1*Nnodes))
ylabel 'SO2 Concentration(molecules/cm3)'
xlabel 'Reactor Length(cm)'
Z;
RS1=Y(1:s1,(ncomp1-1)*Nnodes+1:ncomp1*Nnodes);

ncomp2=19; %Component number (H2SO4)
plot(Z,Y(1:s1,(ncomp2-1)*Nnodes+1:ncomp2*Nnodes))
ylabel 'H2SO4 Concentration(molecules/cm3)'
xlabel 'Reactor Length(cm)'
Z;
RS2=Y(1:s1,(ncomp2-1)*Nnodes+1:ncomp2*Nnodes);

ncompNO=21; %Component number NO
plot(Z,Y(1:s1,(ncompNO-1)*Nnodes+1:ncompNO*Nnodes))
ylabel 'NO Concentration(molecules/cm3)'
xlabel 'Reactor Length(cm)'
Z;
RSNO=Y(1:s1,(ncompNO-1)*Nnodes+1:ncompNO*Nnodes);

ncomp3=30; %Component number (HSNO)
plot(Z,Y(1:s1,(ncomp3-1)*Nnodes+1:ncomp3*Nnodes))
ylabel 'HSNO Concentration(molecules/cm3)'
xlabel 'Reactor Length(cm)'
Z;
RS3=Y(1:s1,(ncomp3-1)*Nnodes+1:ncomp3*Nnodes);

Y(1:s1,1:Nnodes);
toc %read the timer

%Efficiency Calculation
dr = (r1-r0)/(Nnodes+1);   % Node distance
for i = 2:Nnodes+1
    r(i) = r0 + dr*(i-1);
    denom = 2*r1*r1 - (r1*r1-r0*r0)/log(r1/r0) - (r1*r1-r0*r0);
```

```
    v(i) = 2*U*((r1*r1-r0*r0)*log(r(i)/r0)/log(r1/r0) - (r(i)*r(i)-
           r0*r0))/denom;
end

%Concentration SO2 at exit
F_mass1 = 0;
F_vol = 0;
for i = 1:(Nnodes-1)/2
    F_mass1 = F_mass1 + 2*pi*dr*(4*r(2*i)*v(2*i)*RS1(s1,2*i-1)+
              2*r(2*i+1)*v(2*i+1)*RS1(s1,2*i));
    F_vol  = F_vol + 2*pi*dr*(4*r(2*i)*v(2*i)+2*r(2*i+1)*v(2*i+1));
end
C_exit1 = F_mass1 / F_vol;
C_SO2_gm3 = C_exit1 * 64.066 * 1e6 / 6.0221412e23

%Concentration H2SO4 at exit
F_mass2 = 0;
F_vol = 0;
for i = 1:(Nnodes-1)/2
    F_mass2 = F_mass2 + 2*pi*dr*(4*r(2*i)*v(2*i)*RS2(s1,2*i-1)+
              2*r(2*i+1)*v(2*i+1)*RS2(s1,2*i));
    F_vol  = F_vol + 2*pi*dr*(4*r(2*i)*v(2*i)+2*r(2*i+1)*v(2*i+1));
end
C_exit2 = F_mass2 / F_vol;
C_H2SO4_gm3 = C_exit2 * 98.079 * 1e6 / 6.0221412e23

%Concentration NO at exit
F_massNO = 0;
F_vol = 0;
for i = 1:(Nnodes-1)/2
    F_massNO = F_massNO + 2*pi*dr*(4*r(2*i)*v(2*i)*RSNO(s1,2*i-1)+
               2*r(2*i+1)*v(2*i+1)*RSNO(s1,2*i));
    F_vol  = F_vol + 2*pi*dr*(4*r(2*i)*v(2*i)+2*r(2*i+1)*v(2*i+1));
end
C_exitNO = F_massNO / F_vol;
C_NO_gm3 = C_exitNO * 30.01 * 1e6 / 6.0221412e23 ;

%Concentration HSNO at exit
F_mass3 = 0;
F_vol = 0;
for i = 1:(Nnodes-1)/2
    F_mass3 = F_mass3 + 2*pi*dr*(4*r(2*i)*v(2*i)*RS3(s1,2*i-1)+
              2*r(2*i+1)*v(2*i+1)*RS3(s1,2*i));
    F_vol  = F_vol + 2*pi*dr*(4*r(2*i)*v(2*i)+2*r(2*i+1)*v(2*i+1));
end
C_exit3 = F_mass3 / F_vol;
C_HSNO_gm3 = C_exit3 * 63.079 * 1e6 / 6.0221412e23

% Total flow rates at entrance and exit
Ft0 = 0;
Ft = 0;

for i = 1:(Nnodes-1)/2
```

```
    Ft0 = Ft0+2*pi*dr*(4*r(2*i)*v(2*i)*Y(1,2*i-1) +
          2*r(2*i+1)*v(2*i+1)*Y(1,2*i));
    Ft = Ft+2*pi*dr*(4*r(2*i)*v(2*i)*Y(s1,2*i-1)+
         2*r(2*i+1)*v(2*i+1)*Y(s1,2*i));
end

Efficiency_H2S = (1-(Ft/Ft0))*100
Efficiency_NO = (1-(C_NO_gm3/CmNO))*100
```